Universidad de Huelva

Departamento de Ciencias Integradas

Equilibrio de fases y propiedades interfaciales de sistemas moleculares de interés industrial

Memoria para optar al grado de doctora
presentada por:

Esther Feria Delgado

Fecha de lectura: 10 de junio de 2022

Bajo la dirección de los doctores:

Felipe Jiménez Blas

José Manuel Míguez Díaz

Jesús Algaba Fernández

Huelva, 2022

Universidad de Huelva

Facultad de Ciencias Experimentales
Departamento de Ciencias Integradas (Física Aplicada)
Centro de Investigación en Química Sostenible (CIQSO)

Equilibrio de fases y propiedades interfaciales de sistemas moleculares de interés industrial

Memoria para optar al grado de Doctor

Esther Feria Delgado

Directores: Dr. Felipe Jiménez Blas, Dr. José Manuel Míguez Díaz y Dr. Jesús Algaba Fernández

Huelva, Abril 2022

Para que surja lo posible es preciso intentar una y otra vez lo imposible

Hermann Hesse

Agradecimientos

Llegué a este grupo de investigación en parte por curiosidad, en parte casualidad y en parte porque la vida a veces te lleva donde debes estar. Han sido años de aprendizaje, trabajo, risas, lágrimas y cafés.

Esta tesis es el resultado del sacrificio y la dedicación de muchas personas, sin las cuales yo no habría podido llegar hasta aquí. Para empezar, dar las gracias a mi director de tesis, Felipe Jiménez Blas, quién me animó a descubrir un mundo nuevo para mí, la simulación molecular. En segundo lugar a mis directores de tesis, José Manuel Míguez Díaz y Jesús Algaba Fernández, con quienes he trabajado codo con codo, apurando siempre los deadlines. En tercer lugar a todo el grupo de FILICO, y en especial a mis compañeros de laboratorio, por ser compañeros de dramas, sueño, proyectos y aspiraciones.

En el ámbito personal tengo que agradecer a mi familia, especialmente a mi hermana y mis padres, y amigos el apoyo constante a mis proyectos y el ánimo, incluso en los momentos más duros.

A todas esas personas que han sido y son calma dentro de mi tormenta, a todos, gracias. Os llevaré conmigo allá donde la vida me lleve porque sois energía.

Resumen

Desde finales del siglo XX ha crecido el interés por el estudio del biodiesel como alternativa a los combustibles fósiles y como una forma de reducir la emisión de gases de efecto invernadero. Esto es debido a que el biodiesel es una energía renovable, biodegradable, no tóxica y compatible con numerosos motores que se comercializan actualmente. Además el transporte, almacenaje y manipulación del biodiesel tienen menor riesgo que en el caso del diesel. El biodiesel se compone mayoritariamente de metil ésteres (FAMEs) a diferencia del diesel derivado del petróleo, cuyos componentes principales son n-alcanos e hidrocarburos aromáticos [1]. La investigación presentada estudia, mediante la técnica de simulación molecular, sistemas basados en n-alcanos y sistemas basados en metil ésteres. Concretamente se ha empleado la técnica de simulación molecular denominada Dinámica Molecular, utilizando el programa GROMACS (versión 4.6.1) en el colectivo canónico (NVT). Por una parte se estudiaron sistemas de mezclas binarias de metano con n-alcanos (n-decano, n-dodecano, n-tetradecano and n-hexadecano) a una temperatura de 344.15 K y en un rango de presión entre 0.1 y 30 MPa. Por otra parte, se han estudiado el equilibrio de fases y las propiedades interfaciales de una familia de metil ésteres (metil acetato, metil propionato, metil butirato, metil valerato, metil hexanoato y metil heptanoato), tanto para las sustancias puras como para sus respectivas mezclas con agua a distintas temperaturas. Los modelos moleculares para n-alcanos se describen como átomos Coarse Grained (CG), empleando un potencial de tipo Mie. Mientras que en el caso de los metil ésteres se emplearon modelos TraPPE-UA (Transferable Potentials for Phase Equilibria-United Atoms), donde la parametrización de los distintos grupos se ha desarrollado en base a trabajos llevados a cabo para sustancias similares [2–7]. En este último caso donde se utilizan modelos cuya eficacia se había comprobado en sistemas similares, como cetonas y éteres, nunca habían sido combinados para describir el comportamiento de los metil ésteres presentados.

El estudio de estos modelos mediante simulación molecular permite estudiar el equilibrio de fases y propiedades interfaciales de los distintos sistemas, y compararlos con datos experimentales existentes. En el caso de los n-alcanos se observa un descenso de la densidad de fase líquida y tensión interfacial a medida que aumenta la presión, un aumento de la densidad de fase líquida y tensión interfacial al aumentar la longitud de la cadena del n-alcano y adsorción de metano en la región interfacial que aumenta con la presión hasta alcanzar su límite de saturación. Para los sistemas puros de metil ésteres se observa una predicción correcta tanto de la coexistencia de fases como las densidades de coexistencia, presión de vapor, tensión interfacial, entropía interfacial y entalpía interfacial; comparando los datos simulados con datos experimentales existentes. En el caso de mezclas de metil ésteres con agua, se obtienen datos excelentes para las densidades de coexistencia y las fracciones molares, siendo mejores a medida que aumenta la longitud de la cadena alquílica. En los perfiles de densidad se puede observar el efecto de adsorción esperado. Sin embargo, en la tensión interfacial los valores se sobrestiman y no se observa el máximo esperado.

Palabras claves: n-alcanos, metil ésteres, dinámica molecular, densidades de coexistencia,

propiedades interfaciales.

Bibliography

[1] K. S. Tyson, R. McCormick, *et al.*, "2006 biodiesel handling and use guidelines," 2004.

[2] G. Kamath, F. Cao, and J. J. Potoff, "An improved force field for the prediction of the vapor-liquid equilibria for carboxylic acids," *The Journal of Physical Chemistry B*, vol. 108, no. 37, pp. 14130–14136, 2004.

[3] G. Kamath, J. Robinson, and J. J. Potoff, "Application of trappe-ua force field for determination of vapor–liquid equilibria of carboxylate esters," *Fluid phase equilibria*, vol. 240, no. 1, pp. 46–55, 2006.

[4] J. J. Potoff and J. I. Siepmann, "Vapor–liquid equilibria of mixtures containing alkanes, carbon dioxide, and nitrogen," *AIChE journal*, vol. 47, no. 7, pp. 1676–1682, 2001.

[5] B. Chen, J. J. Potoff, and J. I. Siepmann, "Monte carlo calculations for alcohols and their mixtures with alkanes. transferable potentials for phase equilibria. 5. united-atom description of primary, secondary, and tertiary alcohols," *The Journal of Physical Chemistry B*, vol. 105, no. 15, pp. 3093–3104, 2001.

[6] J. M. Stubbs, J. J. Potoff, and J. I. Siepmann, "Transferable potentials for phase equilibria. 6. united-atom description for ethers, glycols, ketones, and aldehydes," *The Journal of Physical Chemistry B*, vol. 108, no. 45, pp. 17596–17605, 2004.

[7] J. M. Briggs, T. B. Nguyen, and W. L. Jorgensen, "Monte carlo simulations of liquid acetic acid and methyl acetate with the opls potential functions," *The Journal of Physical Chemistry*, vol. 95, no. 8, pp. 3315–3322, 1991.

Índice de contenidos

Parte I

Introducción y Objetivos

Capítulo 1

Introducción

1.1 Motivaciones

El combustible fósil es la energía que procede de la descomposición de la materia orgánica de animales, plantas y microrganismos que después de haber sufrido un proceso de transformación por la acción de la propia naturaleza, a través de las uniones que se producen entre el carbono y el hidrógeno, da lugar a sustancias de gran contenido energético, como el carbón, el petróleo, o el gas natural. Concretamente, estas tres sustancias se han formado a partir de la acumulación de grandes cantidades de biomasa provenientes de plantas y de animales en depresiones como fondos marinos o lacustres, donde quedaron fuera del alcance de los microorganismos descomponedores aerobios, y fueron cubiertos por capas de sedimento donde la presión y la temperatura crecientes transforman progresivamente esos restos orgánicos en petróleo, carbón y gas, las tres fuentes de combustible fósil. Los combustibles fósiles son recursos no renovables, ya que al contrario que otros recursos de origen biológico, no se pueden reponer a corto plazo.

La *Energy Information Administration* estimó en 2006 que las principales fuentes primarias de energía en el mundo eran: el petróleo en un 35,9%, el carbón en un 27,4% y el gas natural en un 22,8%. Por lo tanto, con un 86%, los combustibles fósiles son la principal fuente de energía en el mundo. Tan solo un 14% de la energía total era producida a partir de energía no fósil en el mundo en el año 2006, y se distribuía de la siguiente forma: un 6,3% energía hidroeléctrica, un 5,9% energía nuclear y en menor grado las energías solar, eólica, geotérmica, etc. que solo sumaban un 1,0% de la producción mundial total.

Concretamente, el petróleo tiene su origen en los restos de microorganismos marinos que se acumulan en rocas en el fondo de los océanos a profundidades que varían entre los 600 y los 5000 metros, que mediante un proceso lento pero constante termina transformando estos materiales en petróleo que puede extraerse directamente del yacimiento mediante plataformas de explotación y se denomina petróleo crudo. Para poder utilizar esta energía que aporta tiene que pasar por un proceso de transformación, llamado refinamiento. El refinado del petróleo se realiza en las plantas petroquímicas, también llamadas refinerías. Antes que nada hay que limpiar el petróleo crudo de los restos de agua y arena para poder empezar el proceso de destilación fraccionada, donde el crudo se calienta a unos $320 - 340^{\circ}$ C

y se convierte en gas para poder separar todos sus componentes a medida que llegan a su punto de ebullición. Una vez condensados se van recogiendo los siguientes productos: butano y otros gases licuados del petróleo (GLP), gasolina, queroseno, gasóleo y subproductos utilizados para fabricar fuel, aceites lubricantes y alquitrán. El petróleo y sus derivados tienen múltiples y variadas aplicaciones. Además de ser un combustible de primer orden, también constituye una materia prima fundamental en la industria, pues a partir del petróleo se pueden elaborar fibras, caucho artificial, plásticos, jabones, asfalto, tintas de imprenta, caucho para la fabricación de neumáticos etc.

El petróleo es un líquido oleoso compuesto por una mezcla de hidrocarburos desde el más sencillo (CH_4) hasta especies complejas con 40 átomos de carbono. Los hidrocarburos son moléculas orgánicas conformados únicamente por átomos de hidrógeno y carbono. Éstos se pueden clasificar en dos tipos: alifáticos y aromáticos. Concretamente, los alifáticos se pueden clasificar a su vez en alcanos, alquenos y alquinos según los tipos de enlace que unen entre sí los átomos de carbono. Las fórmulas generales de los alcanos, alquenos y alquinos son C_nH_{2n+2}, C_nH_{2n} y C_nH_{2n-2}, respectivamente, donde n es el número de carbonos del compuesto. La molécula más simple de los alcanos es el metano, CH_4, un gas a temperatura ambiente. Eliminando un átomo de hidrógeno del metano se forma un radical: el grupo metilo (representado por $–CH_3$). Dada la capacidad de los átomos de carbono para formar cadenas, se pueden unir dos grupos metilo para formar un compuesto consistente en dos átomos de carbono y seis de hidrógeno: el etano $CH_3–CH_3$. Del mismo modo en que el etano se deriva del metano, uno de los átomos de hidrógeno de la molécula de etano puede ser sustituido por un grupo metilo, lo que da lugar a una cadena de tres átomos de carbono con ocho átomos de hidrógeno, que constituye el compuesto propano (C_3H_8). Repitiendo el proceso de sustituir un átomo de hidrógeno por un grupo metilo, la serie de los alcanos puede seguir extendiéndose al butano (C_4H_{10}), al pentano (C_5H_{12}), al hexano (C_6H_{14}) y a moléculas aún mayores. Se pueden obtener moléculas de hidrocarburos muy largas, de cadenas de cientos en incluso miles de átomos de carbono.

Por tanto, los n-alcanos son moléculas orgánicas simples, basadas en cadenas lineales de grupos CH_3 y CH_2 unidos mediante enlaces simples. Actualmente, por lo explicado anteriormente, son moléculas de interés por su presencia en el petróleo y procesos industriales como refinado aceites, licuefacción de gas natural o control del medio ambiente [1]. Existe un especial interés por estudiar sus mezclas con metano debido a que presentan un comportamiento de fases e interfacial muy complejo pero a la vez fascinante, debido principalmente a la diferencia de peso molecular entre ambos componentes. Específicamente, las mezclas de metano + n-alcano hasta n-pentano presentan un comportamiento tipo I en la clasificación de van Konynenburg y Scott, es decir, únicamente una línea crítica continua (VLE)que une los puntos críticos de ambas sustancias puras. A partir del metano + n-hexano, el diagrama de fases cambia completamente y se diferencia una línea de coexistencia trifásica, es decir, un equilibrio líquido-líquido-vapor (VLLE) cerca del punto crítico del metano. Esta VLLE provoca que la línea crítica VLE se separe en dos ramas y presente un punto crítico final inferior (LCEP) y superior (UCEP). Para el caso de la mezcla metano + n-heptano, la VLLE se interrumpe por otra línea trifásica: n-heptano sólido + L+V (SLVE). Esta intercepción genera un punto cuádruple n-heptano sólido + L_1+L_2+V (SLLVE). Finalmente para n-alcanos superiores, el VLLE desaparece y las mezclas muestran dos puntos críticos finales (CEPs). Estos tipos de equilibrio de fases fueron descritos inicialmente de forma general por Davenport y Rowlinson [2] y completados, posteriormente, por Rijkers [3].

La demanda de combustibles fósiles se ha incrementado notablemente en las últimas décadas debido al aumento de la población mundial y a la industrialización de países emergentes. La merma de reservas de petróleo junto a los crecientes problemas medioambientales hace necesaria la búsqueda de combustibles alternativos. El biodiesel se define como una mezcla de mono-alquil ésteres metílicos

(FAMEs) obtenidos a partir de aceites vegetales o grasas animales y constituye un combustible renovable [4, 4] y uno de los mejores candidatos para sustituir el diesel al ser ambientalmente más amigable respecto del diesel, ya que es biodegradable y no es tóxico.

Los ésteres son los compuestos químicos que se obtienen cuando se hace reaccionar un ácido orgánico (fórmula general: R-COOH) con un alcohol. Cuando el alcohol es el metílico (metanol: CH_3OH) se obtienen los metil ésteres a través de la siguiente reacción:

$$R–COOH + CH_3–OH \rightarrow R–COO–CH_3 + H_2O$$

También se pueden obtener ésteres metílicos tratando una grasa directamente con metanol (en las condiciones apropiadas). Como las grasas están compuestas mayormente por glicéridos (ésteres del glicerol con ácidos grasos), en la reacción de transesterificación se obtiene glicerina además de biodiesel.

Las principales ventajas del biodiesel estriban en que no produce SO_2 y que es una fuente de energía renovable. Sus principales objeciones son que la demanda de biodiesel puede desviar hacia su producción materias primas alimentarias y que no hay actualmente mercado para toda la glicerina que se libera. La mayoría del biodiesel producido en el mundo es proveniente de aceites vegetales principalmente del aceite de colza en Europa y Canadá, y aceite de soya en Estados Unidos. Es destacable la obtención de biodiesel a partir de materias primas alternativas, como los residuos grasos animales, aunque cabe mencionar que las grasas animales son altamente viscosas y en su mayoría sólida a temperatura ambiente, debido a su alto contenido de ácidos grasos saturados, por lo que su uso como combustibles puede conducir a mala atomización del mismo, y en consecuencia una combustión incompleta. Más del 95% de los tipos de aceite empleados en la actualidad para la producción de biodiesel son comestibles (palma, canola, soya, girasol, coco, alazor, colza, algodón, jatropha, karanja, ricino, lesquerella, cacahuate), lo que genera desequilibrios en el mercado de materias primas, aumentado el coste de éstos y del biodiesel, además de generar problemas medioambientales derivados del cultivo intensivo. El uso de aceites no comestibles permite aliviar estos inconvenientes, siendo los aceites de jatropha y karanja dos de los tipos de aceites no comestibles más utilizados para la producción de biodiesel. Por citar un ejemplo, el metil ester de karanja (KME) presenta una eficiencia térmica ligeramente inferior al diésel [5] pero a la vez una reducción significativa de las emisiones de CO y NO_x, lo que determina que sea es un sustituto adecuado del combustible diésel de petróleo.

Por todo ello, en este trabajo se han elaborado y desarrollado modelos moleculares para el estudio de sistemas tan complejos como: n-alcanos+metano, metil ésteres puros y metil ésters con agua. Con estos modelos se han realizado simulaciones mediante la técnica de dinámica molecular para predecir propiedades macroscópicas y microscópicas que presentan estos sistemas como, equilibrios de fases y propiedades interfaciales y que determinan su comportamiento a unas determinadas condiciones de presión y temperatura. Los datos obtenidos a partir de ellas son de especial interés debido a la escasez de datos experimentales disponibles en las bases de datos más prestigiosas internacionalmente, como son DECHEMA o NIST. Además, la aportación de la técnica de simulación molecular no es solo especialmente relevante para conocer detalles microscópicos de su comportamiento interfacial, inaccesibles desde cualquier otra técnica de investigación, información clave que puede ser clave para comprender y mejorar sus ya excelentes aplicaciones industriales sino que además permite predecir el comportamiento de estos sistemas moleculares en condiciones de presión y temperatura inexplorables a nivel experimental. En el caso de los n-alcanos se describen equilibrios de fase y propiedades interfaciales para mezclas binarias de metano con decano, dodecano, tetradecano y hexadecano a 344.15K y para distintas presiones. La temperatura y el rango de presiones han sido seleccionados en base a las condiciones habituales que se dan en reservas de petróleo. Las simulaciones se han llevado a cabo

mediante dinámica molecular, empleando un campo SAFT-VR-Mie y parámetros Coarse-Grained. Los datos obtenidos mediante simulación son comparados con datos experimentales existentes, como los del grupo Delft [3, 6–10] y con datos obtenidos mediante experimentación. En el caso de los metil ésteres puros se estudió el equilibrio líquido-vapor para sistemas puros de metil acetato, metil propionato, metil butirato, metil valerato, metil hexanoato y metil heptanoato. El estudio se llevó a cabo mediante simulaciones de Dinámica Molecular por el método de coexistencia directa a distintas temperaturas entre 300K y 550K. Se obtuvieron densiades de coexistencia, presiones de vapor, tensión interfacial, entropía y entalpía interfacial. Los datos obtenidos mediante simulación se comparan con resultados experimentales pertenecientes a la base de datos del NIST. Por último, el estudio de mezclas de metil ésteres con agua se realizó para un equilibrio líquido-líquido a presión atmosférica y en un rago de temperatura entre 278 y 358K. También se empleó la técnica de dinámica molecular combinándola con coexistencia directa para obtener propiedades interfaciales.

1.2 Organización de la Tesis y Objetivos

Esta tesis se organiza en un total de 7 capítulos. En este primer capítulo, se realiza una breve introducción que presenta las principales motivaciones al realizar dicho trabajo y una descripción de la estructura de la tesis. En los **Capítulo 2–3** se introducen conceptos relacionados con la Mecánica Estadística (**Capítulo 2**), con la Dinámica Molecular y técnicas empleadas en las simulaciones (**Capítulo 3**). En los **Capítulo 4–6** se presentan los resultados obtenidos y publicados durante el desarrollo de este trabajo. Cada capítulo consiste en un artículo publicado, como se explica a continuación:

Capítulo 4: Phase equilibria and interfacial properties of selected methane + n-alkane binary mixtures. A. Mejía, M. Cartes, G. Chaparro, E. Feria, F. J. Blas, J. M. Míguez, E. A. Müller. *Journal of Molecular Liquids*, **341**, 116918 (2021). En esta primera publicación, se estudiaron mezclas de metano y n-alcanos de forma experimental y mediante simulación molecular para describir el equilibrio de fase y propiedades interfaciales de mezclas de metano+n-decano, metano+n-dodecano, metano+n-tetradecano y metano+n-hexadecano a una temperatura de 344.15K y en un rango de presiones entre 0.1 y 30 MPa. Las determinaciones experimentales fueron realizadas con distintos equipos. Por otro lado, las simulaciones se realizaron mediante dinámica molecular, describiendo las moléculas como átomos Coarse Grained (CG) y empleando un potencial de Mie. Los datos obtenidos mediante las distintas técnicas se compararon, mostrando gran correlación.

Capítulo 5: Vapour–liquid phase equilibria and interfacial properties of fatty acid methyl esters from molecular dynamics simulations. E. Feria, J. Algaba, J. M. Míguez, A. Mejía, P. Gómez-Álvarez, F. J. Blas. *Physical Chemistry Chemical Physics*, **22(9)**, 4974-4983 (2020). En este segundo trabajo se determinaron en equilibrio de fases y propiedades interfaciales para una familia de metil ésteres, desde metil acetato hasta metil heptanoato, mediante simulaciones líquido-vapor. Los metil ésteres fueron modelados mediante modelos TraPPE-UA y estudiados en el colectivo NVT empleando simulaciones de dinámica molecular. Se obtuvieron perfiles de densidad, densidades de coexistencia, presiones de vapor, entropías, entalpías, tensiones interfaciles y parámetros críticos para los distintos metil ésteres. Estos resultados obtenidos mediante simulación fueron comparados con datos experimentales, mostrando gran concordancia.

Capítulo 6: Molecular dynamics of liquid-liquid equilibrium and interfacial properties of aqueous solutions of methyl esters. E. Feria, J. Algaba, J. M. Míguez, A. Mejía, F. J. Blas. *Physical Chemistry Chemical Physics*, **22(9)**, 4974-4983 (2020). Este tercer trabajo estudia el equilibrio de fases y propiedades interfaciales para mezclas binarias de agua y distintos metil ésteres, desde metil acetato hasta metil heptanoato. Por una parte, los metil ésteres fueron modelados según el trabajo previo, mientras que el agua se modeló con el conocido modelo TIP4P/2005. Se realizaron simulaciones de dinámica molecular con coexistencia directa en el colectivo isotérmico-isobárico (NPzT). A partir de estas simulaciones se obtuvieron perfiles de densidad, diagramas de fase, fracciones molares y tensión interfacial. Los datos obtenidos mediante simulación fueron comparados con datos experimentales existentes.

Finalmente, en el **Capítulo 7** se presenta un resumen de los principales resultados obtenidos y así las conclusiones más relevantes obtenidas a lo largo del desarrollo de estos trabajos de investigación que constituyen en su conjunto esta Tesis Doctoral.

Bibliography

[1] J. Speight, "The chemistry and technology of crude oil 5th edition," 2014.

[2] A. Davenport and J. Rowlinson, "The solubility of hydrocarbons in liquid methane," *Transactions of the Faraday Society*, vol. 59, pp. 78–84, 1963.

[3] R. Rijkers, "Retrograde condensation of lean natural gas," 1991.

[4] N. Nagle and P. Lemke, "Production of methyl ester fuel from microalgae," *Applied Biochemistry and Biotechnology*, vol. 24, no. 1, pp. 355–361, 1990.

[5] H. Raheman and A. Phadatare, "Diesel engine emissions and performance from blends of karanja methyl ester and diesel," *Biomass and bioenergy*, vol. 27, no. 4, pp. 393–397, 2004.

[6] M. Glaser, C. Peters, H. Van Der Kool, and R. Lichtenthaler, "Phase equilibria of (methane+ n-hexadecane) and (p, vm, t) of n-hexadecane," *The Journal of Chemical Thermodynamics*, vol. 17, no. 9, pp. 803–815, 1985.

[7] M. Rijkers, M. Malais, C. Peters, and J. d. de Swaan Arons, "Measurements on the phase behavior of binary hydrocarbon mixtures for modelling the condensation behavior of natural gas: Part i. the system methane+ decane," *Fluid phase equilibria*, vol. 71, no. 1-2, pp. 143–168, 1992.

[8] M. Rijkers, V. Maduro, C. Peters, and J. de Swaan Arons, "Measurements on the phase behavior of binary mixtures for modeling the condensation behavior of natural gas: Part ii. the system methane+ dodecane," *Fluid Phase Equilibria*, vol. 72, pp. 309–324, 1992.

[9] V. De Leeuw, T. W. de Loos, H. Kooijman, and J. de Swaan Arons, "The experimental determination and modelling of vle for binary subsystems of the quaterhary system n2+ ch4+ c4h10+ c14h30 up to 1000 bar and 440 k," *Fluid phase equilibria*, vol. 73, no. 3, pp. 285–321, 1992.

[10] M. Rijkers, C. Peters, and J. de Swaan Arons, "Measurements on the phase behavior of binary mixtures for modeling the condensation behavior of natural gas: Part iii. the system methane+ hexadecane," *Fluid phase equilibria*, vol. 85, pp. 335–345, 1993.

Parte II

Metodología

Capítulo 2

Mecánica Estadística

La Mecánica Estadística tiene como objetivo entender y describir el comportamiento de sistemas macroscópicos partiendo del estudio de sistemas microscópicos [1–4]. El comportamiento de un sistema macroscópico se describe en base a las leyes de la Termodinámica, mientras que el comportamiento de un sistema microscópico se describe según las leyes de la Mecánica Clásica y/o Cuántica. La Mecánica Cuántica tiene una aplicación general en cuanto a los sistemas microscópicos mientras que la Mecánica Clásica solo es aplicable bajo ciertas circunstancias, como altas temperaturas o densidades bajas y moderadas. En el caso de los sistemas macroscópicos, el número de variables necesarias para definir el macroestado de un sistema cerrado está definido por la regla de las fases de Gibbs, esta establece que el número de variables termodinámicas independientes (L) depende del número de componentes químicos (C) y de la cantidad de fases en equilibrio (F) como se indica a continuación:

$$L = C - F + 2 \tag{2.1}$$

Por otro lado, para los sistemas microscópicos considerados según la Mecánica Clásica, se requiere especificar la posición y velocidad de cada una de las partículas que componen el microestado. Por ello tendremos un número de parámetros mucho mayor respecto al necesario para describir macroestados. La Mecánica Estadística posibilita el conocimiento del comportamiento macroscópico de un sistema a partir de la descripción microscópica detallada del mismo.

2.1 Postulados Básicos de la Mecánica Estadística

Todo sistema macroscópico se compone de un número de constituyentes microscópicos del orden del número de Avogadro. Si consideramos que estos componentes microscópicos no tienen grados internos de libertad y que su comportamiento se ajusta a las condiciones de la Mecánica Clásica, la dinámica de cada constituyente queda definida en base a los momentos lineales y las coordenadas. En base a esto, la dinámica del sistema completo quedará definida por el conjunto de momentos lineales y coordenadas, es decir, tendremos un punto en un espacio de $6N$ dimensiones. Dicho espacio

se conoce como espacio de fases. La dinámica de las partículas dependerá del modelo elegido para describir el sistema y suele depender en gran medida de las condiciones iniciales. En contraposición, el sistema macroscópico se describe mediante las leyes de la Termodinámica. Estas leyes son aplicables a numerosos sistemas y son independientes de sus condiciones inicales. Además, como ya se ha dicho, se necesita un número de magnitudes físicas relativamente pequeño para describir el sistema. Debido a estas diferencias las relación entre ambas escalas es compleja, ya que la descripción macroscópica no es suficiente para estudiar el estado microscópico. Si consideramos un sistema en equilibrio, siendo un sistema en equilibrio aquel cuyas propiedades macroscópicas se mantienen constantes a lo largo del tiempo y el sistema podría definirse en base a este reducido número de variables que se mentienen constantes, se observa que ese macroestado puede relacionarse con numerosos microestados compatibles. La Mecánica Estadística nos dice que cada microestado compatible será accesible con una cierta probabilidad. Al utilizar una descripción clásica del sistema las coordenadas generalizadas q_i y los momentos generalizados p_i serán variables continuas y la Mecánica Estádistica postulará que a cada macrosistema le corresponde una función de densidad de probabilidad para dichas variables continuas. Así se obtiene una función *densidad de probabilidad* en el espacio de las fases [1–4], que para el caso más general corresponde a una función de la forma:

$$\rho(q_i, p_i; t) = \rho(q, p; t) \tag{2.2}$$

que según la definición de densidad de probabilidad,

$$\rho(q_i, p_i; t) dq_1 \cdots dq_f \; dp_1 \cdots dp_f \equiv \rho(q, p; t) dq dp \tag{2.3}$$

representa la probabilidad, para un instante t dado, de que el sistema se encuentre en un volumen infinitesimal del espacio fásico centrado en (q, p), correspondiendo $dqdp$ a

$$dpdq \equiv dq_1 \cdots dq_f \; dp_1 \cdots dp_f \tag{2.4}$$

En base a esta definición, $\rho(q, p; t)$ debe cumplir, en todo instante, la condición de normalización

$$\int dpdq \; \rho(q, p; t) = 1 \tag{2.5}$$

Hay que tener en cuenta que $\rho(q, p; t)$ debe de ser nula para los valores de q, p y t que lleven a un microestado no compatible con el sistema macroscópico.

Para tener en cuenta los posibles microestados compatibles con el sistema se considerará una variable, $A(q, p)$, que sea función de las coordenadas generalizadas$q$ y los momentos generalizados$p$. Así para cada microestado se obtiene un valor de $A(q, p)$. LLegamos así al primer postulado de la Mecánica Estadística [1–4]. Este primer postulado relaciona el valor de $A(q, p)$ de cada microestado con el valorde A en el sistema macroscópico.

Primer Postulado o postulado de equiprobabilidad a priori: los valores de las magnitudes macroscópicas que definen el estado del sistema son iguales al promedio en el colectivo correspondiente del valor que toma la magnitud análoga microscópica en todos los microestados accesibles, ponderado por la densidad de probabilidad.

$$\langle A(t)\rangle = \int dpdq\ \rho(q,p;t)\ A(q,p) \tag{2.6}$$

La variable $A(q,p)$ de un microestado tendrá mayor o menor peso en función de la probabilidad de que el sistema macroscópico se encuentre en dicho microestado. Cuando la función de distribución de probabilidades es independiente del tiempo, estado de equilibrio, y no intercambia materia ni energía con su entorno, es decir, tenemos un estado aislado, la probabilidad de que se encuentre en un cierto microestado viene dada por *el postulado de igualdad de probabilidades a priori* de la Mecánica Estadística [1–4].De esto se deduce que todos los microestados accesibles contribuirán de la misma forma en el promedio de la variable macroscópica A del sistema. Además este postulado implica que si la igualdad se cumple para un instante dado también se cumplirá en cualquier otro instante de tiempo. Se establece de esta forma la igualdad entre numerosas medidas en distintos instantes de tiempo sobre el mismo sistema y la medición en un instante dado sobre numerosos sistemas idénticos. Es decir, se establece una relación de igualdad entre el valor de una propiedad promediado sobre los diversos microestados accesibles para el sistema y el promedio temporal de dicha propiedad a escala macroscópica, ver ecuación (2.6).

El segundo postulado de la Mecánica estadística también se basa en la Hipótesis Ergódica, establecida por Paul y Tania Ehrenfest [5].

Segundo Postulado: la media temporal de una variable A para un sistema macroscópico en equilibrio será igual al promedio del colectivo en el límite termodinámico, siempre y cuando los sistemas del colectivo reproduzcan el estado termodinámico del sistema y su entorno.

$$\overline{A(t)} = \lim_{x\to\infty} \frac{1}{t} \int A(t')dt' \tag{2.7}$$

Esta equivalencia no puede demostrarse y ha sufrido numerosas reformulaciones, como su versión moderna en el teorema de Birkhoff [6]. Por ello, establecer si un sistema es ergódico o no es complejo, pero es aceptada por conducir a resultados correctos y debido a las diferencias de tiempo para poder realizar medidas macroscópicas en comparación con medidas microscópicas. Es decir, se puede suponer que durante la medición macroscópica el sistema ha transitado por todos los microestados compatibles, permanecienco en cada uno de ellos un tiempo proporcional a su probabilidad de ocupación, que será la misma para sistemas en equilibrio. En la práctica, un sistema se considera ergódico cuando cada punto accesible (o microestado) se alcanza en un número de pasos finito desde cualquier otro punto del espacio de fases. La Hipótesis Ergódica consigue eliminar la variable temporal y es utilizada para estudiar sistemas en equilibrio, mediante simulación molecular, dentro de la Mecánica Estadística del equilibrio [1–4, 7].

2.2 Colectivos de Gibbs

Un colectivo se define como el conjunto de microestados compatibles con un macroestado dado y su correspondiente densidad de probabilidad. Además, si el macroestado asociado al colectivo es un estado de equilibrio, se conoce como *conjunto o colectivo de Gibbs* . El concepto de colectivo relaciona las ideas de macroestado y microestado mediante una descripción probabilística, ya que no se puede, desde el estado macroscópico, definir unívocamente el estado microscópico del mismo instante dado. Para establecer la conexión entre una propiedad macroscópica con su análoga microscópica, la Mecánica

Estadística establece que una propiedad macroscópica es un promedio sobre el colectivo de Gibbs o promedio de la propiedad microscópica. Este postulado solo es válido cuando la propiedad macroscópica tiene un análogo microscópico. Para simplificar la situación, se considerarán solo sistemas en equillibrio termodinámico a los que corresponderá una función de distribución de probabilidades independiente del tiempo. Gibbs desarrolló un conjunto de formalismos que permiten el cálculo del conjunto de variables de un sistema dado, partiendo de propiedades mecánicas de los componenetes microscópicos. Las variables termodinámicas determinan los formalismos con que se definirá el macroestado. Con tan solo tres variables termodinámicas se puede establecer el estado termodinámico de un sistema simple, las tres variables deben ser elegidas una por cada pareja, una variable extensiva y otra intensiva, de las mostradas a continuación: $\{N, \mu\}$ (número de partículas o potencial químico), $\{V, p\}$ (volumen o presión), y $\{E, T\}$ (energía interna o temperatura). En base a estas parejas podemos encontrar ocho formas de definir el estado termodinámico. Los colectivos más importantes, empleados en esta Tesis, para describir el comportamiento de sistemas reales son los colectivos canónico, NVT, e isotérmico-isobárico,NPT.

2.2.1 Colectivo Canónico (NVT)

El colectivo canónico se compone de todos los microestados compatibles con el macroestado caracterizado por valores constantes de número de partículas N, volumen V y temperatura T. Se utiliza para estudiar sistemas cerrados en equilibrio térmico, el sistema de estudio estará aislado por una pared rígida e impermeable en contacto con un baño térmico a temperatura T, lo que garantiza valores constantes para la temperatura y el volumen del sistema. Este colectivo es importante debido a que numerosos experimentos con sistemas reales se realizan en estas condiciones. En este caso cada microestado se describe mediante las variables canónicas, es decir, coordenadas y momentos generalizados. La densidad de probabilidad para este colectivo viene dado por:

$$\rho(\mathbf{r}^N, \mathbf{p}^N) = \frac{\exp\left[-\beta\mathcal{H}(\mathbf{p}^N, \mathbf{r}^N)\right]}{N!h^{3N}} \, {Q_{NVT}}^{-1} \tag{2.8}$$

donde $\beta = (k_B T)^{-1}$, siendo k_B la constante de Boltzmann, el factor h es la constante de Planck, y $\mathcal{H}$ es el Hamiltoniano del sistema, que puede expresarse como:

$$\mathcal{H}(p, q) = \sum_{i=1}^{f} \frac{p_i^2}{2m} + \mathcal{U}(q) \tag{2.9}$$

Por otro lado Q_{NVT} es la función de partición del colectivo NVT, que se define como:

$$Q_{NVT} = \frac{1}{N!h^{3N}} \int d\mathbf{p}^N d\mathbf{r}^N \exp\left[-\beta\mathcal{H}(\mathbf{p}^N, \mathbf{r}^N)\right] \tag{2.10}$$

La constante de Planck aparece como consecuencia del principio de incertidumbre de Heisenberg, que indica la imposibilidad de determinar la posición y la cantidad de movimiento de una partícula de forma simultánea y exacta ($\Delta p_i \Delta q_i \geq h$). Debido a ello la mayor precisión con la que se puede describir un sistema semiclásico se encuentra en un volumen del espacio fásico que se corresponde con h^{3N}, siendo $3N$ el grado de números de libertad del sistema. La función de partición permite obtener las propiedades macroscópicas del sistema, es decir, podemos considerar una variable, $A(q, p)$, que sea

función de las coordenadas generalizadas q y de los momentos generalizados p, que podríamos expresar como:

$$\langle A\rangle_{NVT} = \frac{\int d\mathbf{p}^N d\mathbf{r}^N A(\mathbf{p}^N,\mathbf{r}^N)\exp\left[-\beta\mathcal{H}(\mathbf{p}^N,\mathbf{r}^N)\right]}{\int d\mathbf{p}^N d\mathbf{r}^N \exp\left[-\beta\mathcal{H}(\mathbf{p}^N,\mathbf{r}^N)\right]} \tag{2.11}$$

Si usamos la función de partición se puede obtener una forma más compacta de la expresión (2.11).

$$\langle A\rangle_{NVT} = -\frac{1}{Q_{NVT}}\frac{\partial Q_{NVT}}{\partial\beta} = -\frac{\partial \ln Q_{NVT}}{\partial\beta} \tag{2.12}$$

Para el colectivo canónico la función de estado natural que relaciona las descripciones microscópica y macroscópica del sistema es la energía libre de Helmholtz *F(N,V,T)*.

$$F(N,V,T) = -k_B T \ln Q_{NVT} \tag{2.13}$$

Las propiedades termodinámicas de equilibrio pueden calcularse a partir de las derivadas parciales de la energía libre de Helmholtz sobre los distintos parámetros, haciendo uso de las relaciones de Maxwell

$$\left(\frac{\partial F}{\partial V}\right)_{T,N} = -P,\ \left(\frac{\partial F}{\partial T}\right)_{V,N} = -S,\ \left(\frac{\partial F}{\partial N}\right)_{V,T} = \mu \tag{2.14}$$

2.2.2 Colectivo Isotérmico-Isobárico (NPT)

El colectivo isotérmico-isobárico, o NPT, se compone de todos los microestados del sistema compatibles con el macroestado donde se mantienen invariables el número de partículas N, la presión P y la temperatura T. En este colectivo, cada microestado se describe en base a las variables canónicas y el volumen, es decir, respecto al colectivo canónico se añade como variable fluctuante la variable conjugada de la nueva variable fija, la presión. Este colectivo es de gran interés ya que muchos fenómenos ocurren a presión constante, como los que tienen lugar a presión atmosférica. Es muy útil para estudiar sistemas cerrados en equilibrio térmico-isobárico. La función de partición del colectivo isotérmico-isobárico viene dada por:

$$Q_{NPT} = \frac{\beta P}{N!\Lambda^{3N}}\int dV\ V^N \exp(-\beta PV)\int d\mathbf{s}^N \exp\left[-\beta\mathcal{U}(\mathbf{s}^N;L)\right] \tag{2.15}$$

Utilizando la función de partición del colectivo canónico puede escribirse la función de partición del colectivo NPT de forma más compacta.

$$Q_{NPT} = \int dV \exp(-\beta PV) Q_{NVT} \tag{2.16}$$

Tal y como sucedía con el colectivo canónico, la función de estado natural correspondiente, que en este caso será la energía libre de Gibbs, G, la cual permite expresar las propiedades macroscópicas del sistema a partir de la descripción microscópica del sistema.

$$G = -k_B T \ln Q_{NPT} \tag{2.17}$$

Y, al igual que en el colectivo anterior, las propiedades termodinámicas de equilibrio pueden calcularse a partir de las correspondientes derivadas parciales de la energía libre de Gibbs.

$$\left(\frac{\partial G}{\partial T}\right)_{P,N} = -S,\ \left(\frac{\partial G}{\partial P}\right)_{T,N} = V,\ \left(\frac{\partial G}{\partial N}\right)_{T,P} = \mu \tag{2.18}$$

Así como se ha hecho para los colectivos canónico e isotérmico-isobárico, se puede utilizar una propiedad termodinámica para relacionar la descripción microscópica de un sistema con su comportamiento macroscópico. De este modo, basándonos en la función de densidad de probabilidades y de forma similar a la descrita anteriormente, es posible obtener equivalencias para el resto de colectivos. Pudiendo establecer así una conexión entre sistemas macroscópicos y sistemas microscópicos, además de poder estudiar el comportamiento termodinámico a partir de descripciones mecano-clásicas del comportamiento de las partículas que componen los sistemas.

Bibliography

[1] J. de la Rubia Pacheco and J. J. B. Abalo, *Introducción a la Mecánica Estadística*. Ediciones del Castillo, 1978.

[2] F. Reif, *Fundamentals of Statistical and Thermal Physics*. McGraw-Hill, 1965.

[3] D. McQuarrie, *Statistical Mechanics*. Harper & Row, 1976.

[4] P. Attard, *Thermodynamics and Statistical Mechanics: Equilibirium by Entropy Maximisation*. Academic Press, 2002.

[5] P. Ehrenfest and T. Ehrenfest, *The Conceptual Foundations of the Statistical Approach in Mechanics*. Dover Publications, 2002.

[6] G. D. Birkhoff *Proc. Natl. Acad. Sci.*, vol. 17, p. 656, 1931.

[7] D. Frenkel and B. Smit, *Understanding Molecular Simulations*. 2nd ed. Academic, San Diego, 2002.

Capítulo 3

Simulación Molecular

Anteriormente a la aparición de la simulación computacional, las propiedades de sustancias moleculares sólo podían ser predichas mediante descripciones aproximadas de dicha sustancia, ya que no son muchos los sistemas que podían estudiarse de forma exacta, solo los casos más simples como el gas ideal o el cristal armónico. Además, al comparar la estimación con los resultados experimentales, si los datos no concuerdan puede deberse a que la teoría es errónea, a una estimación incorrecta de las interacciones intermoleculares, o ambas cosas. La simulación molecular permite obtener resultados exactos para un sistema modelo sin utilizar teorías aproximadas. Esto hace posible comparar las propiedades del sistema modelo con los resultados experimentales, si no concuerdan será porque el modelo no es adecuado, y también podemos comparar los resultados del modelo con las predicciones de teóricas, si los resultados no concuerdan sabremos que la teoría es errónea. Así, se ha convertido en una herramienta de gran importancia que ha permitido la revisión de teorías y ha cambiado la forma de construir nuevas teorías y realizar experimentos. Además de ofrecer la posibilidad de estudiar situaciones inaccesibles experimentalmente, creando escenarios microscópicos hipotéticos. Los métodos de simulación molecular más extendidos son Monte Carlo y dinámica molecular. En este capítulo se describe de forma breve el método de dinámica molecular, el cual ha sido utilizado en este trabajo para el estudio de propiedaes y equilibrio de fases de los distintos sistemas.

3.1 Dinámica Molecular

La dinámica molecular, MD, (del inglés, *molecular dynamics*) es un método determinista utilizado en simulación molecular que resuelve las ecuaciones de movimiento de Newton de las moléculas para generar nuevos estados. Este método permite el estudio de la evolución temporal del sistema y evalúa las propiedades macroscópicas, permitiendo obtener propiedades termodinámicas en equilibrio y propiedades dinámicas dependientes del tiempo. Para ello, se calculan las trayectorias de los átomos o partículas que forman el sistema en distintos instantes de tiempo con objeto de obtener un conjunto de posiciones y velocidades. En esta técnica cada microestado es un punto en el espacio de fases, caracterizado por sus posiciones y momentos. Los estados generados resolviendo las ecuaciones de movimiento de las partículas del sistema se promedian, haciendo uso de la Mecánica Estadística, en el tiempo para calcular las propiedades del sistema. La integración de la propiedad macroscópica no se

extiende a un tiempo infinito, pero sí lo suficientemente largo para obtener promedios fiables de las variables.

Partiendo de una configuración inicial del sistema, es decir, las posiciones, $\mathbf{r}$ y velocidades, $\mathbf{v}$, para cada partícula que compone el sistema, se pueden utilizar las ecuaciones de movimiento de Newton para predecir las posiciones y velocidades en un instante futuro. Las ecuaciones de Newton para un sistema de N partículas corresponden a:

$$m_i \frac{d^2\mathbf{r}_i}{dt^2} = \mathbf{F}_i,\ i = 1...N. \tag{3.1}$$

$$\mathbf{v}_i = \frac{d\mathbf{r}_i}{dt} \tag{3.2}$$

siendo $\mathbf{F}_i$ la fuerza total que actúa sobre la partícula i. Cuando las fuerzas que actúan sobre la partícula i son conservativas pueden calcularse en base al gradiente de la energía potencial (U):

$$\mathbf{F}_i = \nabla U \tag{3.3}$$

La configuración inicial del sistema debe permitir la correcta solución de las ecuaciones de movimiento de Newton. Para las posiciones iniciales es habitual utilizar la red cristalina del fluido estudiado o partir de una configuración cuya energía haya sido minimizada previamente. Mientras que las velocidades iniciales se pueden generar a partir de una ejecución previa o de forma aleatoria, en base a una distribución uniforme o una distribución gaussiana.

3.1.1 Integradores numéricos

En lo que respecta a la simulación molecular, el cálculo de la fuerza es la operación más costosa. La resolución analítica de las ecuaciones de movimiento de Newton no es posible, por lo que se resuelven con métodos numéricos. Para su aplicación se requiere que la evolución temporal del sistema sea discretizada, caracterizándose por paso de tiempo Δt que corresponde al salto temporal entre un estado microscópico y el siguiente. Podría decirse que la evolución dinámica del sistema tiene lugar en saltos de tiempo pequeños y discretos, lo que permite resolver las ecuaciones de Newton mediante métodos numéricos. La resolución numérica puede realizarse con distintos algoritmos. La elección dependerá de la eficiencia, el rendimiento computacional y la exactitud de los resultados que genere. Para realizar este trabajo se ha utilizado el algoritmo de leap-frog o de salto de rana [1, 2].

El algoritmo de salto de rana, figura 3.1, almacena las posiciones $\mathbf{r}$ en un cierto instante de tiempo t junto con las velocidades $\mathbf{v}$ en un paso de tiempo intermedio y anterior, $t - 1/2\Delta t$, utilizando estas para obtener las posiciones en un instante $t + \Delta t$ y evaluar las velocidades en un instante futuro $t + 1/2\Delta t$. Estas relaciones se obtienen mediante las siguientes expresiones:

$$\mathbf{v}(t + \frac{1}{2}\Delta t) = \mathbf{v}(t - \frac{1}{2}\Delta t) + \frac{\Delta t}{m}\mathbf{F}(t) \tag{3.4}$$

$$\mathbf{r}(t + \Delta t) = \mathbf{r}(t) + \Delta t \mathbf{v}(t + \frac{1}{2}\Delta t) \tag{3.5}$$

donde $\mathbf{F}(t)$ son las fuerzas que actúan sobre el sistema en el instante de tiempo t.

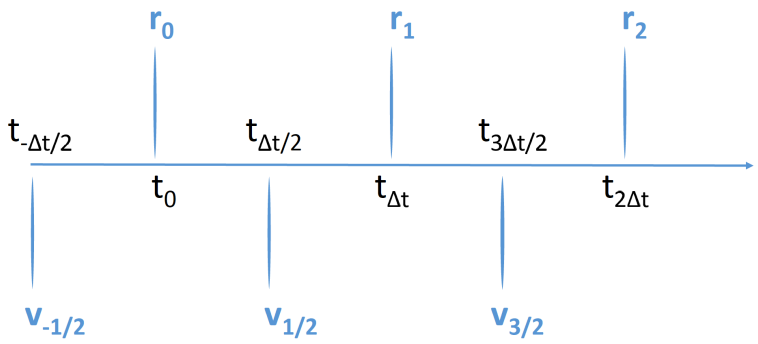

Figura 3.1: Representación visual de la obtención de las posiciones, **r**, y las velocidades, **v**, del sistema mediante el algoritmo del salto de rana.

En este método se considera que las fuerzas que actúan sobre cada partícula del sistema permanece constante durante el "salto" de tiempo. En base a esto, se pueden obtener las posiciones en un instante futuro $t + \Delta t$ a partir de las posiciones de las partículas en un instante dado t y las velocidades de un instante previo $t - 1/2\Delta t$. De forma muy similar, se obtendrá el valor de las velocidades para un instante futuro $t + 1/2\Delta t$. De tal forma que cada $1/2\Delta t$ se obtendrán las nuevas posiciones y velocidades. El paso de tiempo, Δt, tiene que ser suficientemente pequeño para muestrear correctamente la evolución del sistema, generalmente este paso de tiempo es del orden de los femtosegundos. Tras haber calculado las velocidades y posiciones del nuevo microestado, se vuelven a evaluar las fuerzas que actúan sobre cada partícula del sistema y comienza un nuevo ciclo de dinámica molecular. La evolución temporal del sistema se obtiene de la repetición de este proceso.

3.1.2 Termostato y Barostato

El colectivo natural utilizado en dinámica molecular es el colectivo microcanónico o NVE, ya que para sistemas cerrados y aislados por paredes rígidas la resolución de las ecuaciones de Newton genera una distribución de microestados que se corresponde con un macroestado de energía constante. Sin embargo, la mayoría de los experimentos no ocurre en estas condiciones por lo que es necesario utilizar otros colectivos, como NVT o NPT, para lo que se requiere el uso de termostatos y barostatos. El uso de los colectivos NVT y NPT implica la implementación de un termostato. Desde el punto de vista de la Mecánica Estadística, imponer una temperatura al sistema puede conseguirse poniendo el sistema en contacto con un baño de calor grande. En estas condiciones y para un sistema clásico, la probalilidad de encontrar el sistema en un determinado estado de energía viene dada por la distribución de velocidad de Maxwell-Boltzmann. Fijar la temperatura es más interesante y práctico que fijar la energía total del sistema. Entre los termostatos más usados se encuentran:

Termostato de Berendsen [3]. Este termostato escala la velocidad de las partículas según la temperatura de referencia de un baño externo T_0, que será la temperatura de interés. El reescalado va a depender del parámetro de acoplamiento, τ, y de la diferencia entre la temperatura del baño térmico (T_0) y la temperatura real del sistema (T).

$$\frac{dT(t)}{dt} = \frac{1}{\tau}(T_0 - T(t)) \tag{3.6}$$

Este termostato suprime las fluctuaciones de la energía cinética, es decir, genera un conjunto de microestados que, formalmente, no exploran de manera adecuada el colectivo de interés. El error de usar este termostato escala con 1/N. Este error supone que la mayoría de los promedios de las variables para sistemas muy grandes no se verán afectados de forma significativa, pero se verán afectadas propiedades de fluctuación como, por ejemplo, la capacidad calorífica.

Termostato de Reescalado de velocidades [4]. Este termostato se basa en el termostado de Berendsen, añadiéndole un término estocástico que asegura que la distribución de energía cinética será correcta al ser modificado según la ecuación:

$$dK = (K_0 - K)\frac{dt}{\tau_T} + 2\sqrt{\frac{KK_0}{N_f}}\frac{dW}{\sqrt{\tau_T}} \tag{3.7}$$

donde K y K_0 son las energías cinéticas del sistema real y del sistema a la temperatura de referencia, respectivamente, N_f se corresponde con el número de grados de libertad y dW es un proceso de Wiener. El proceso de Wiener es un tipo de proceso estocástico que asegura el correcto muestreo del colectivo canónico.

Termostato de Nosé-Hoover [5, 6]**.** Este termostato considera un sistema extendido, de manera que los termostatos sean parte del sistema. Dicho termostato fue introducido por Nosé y optimizado por Hoover. Nosé consideró el uso extendido del Hamiltoniano, es decir, las ecuaciones del movimiento de Newton son directamente modificadas por este termostato, modificando la velocidad de las partículas del sistema y, por tanto, su temperatura. El objetivo es introducir una variable dinámica ficticia de fricción, ξ, que aumente o disminuya la velocidad de las partículas en función de la temperatura:

$$\frac{d^2\mathbf{r}_i}{dt} = \frac{\mathbf{F}_i}{m_i} - \frac{p\xi}{Q}\frac{d\mathbf{r}_i}{dt} \tag{3.8}$$

donde Q es el llamado parámetro de masas, que dependede la temperatura de referencia (T_0) y del periodo de las fluctuaciones de temperatura en el equilibrio (τ_T):

$$Q = \frac{\tau_T^2 T_0}{4\pi^2} \tag{3.9}$$

siendo $p\xi$ el momento asociado al parámetro de fricción ξ, que depende de la diferencia entre la temperatura real del sistema para el instante t y la temperatura de referencia:

$$\frac{dp\xi}{dt} = (T(t) - T_0) \tag{3.10}$$

Este algoritmo genera distribuciones canónicas correctas para sistemas moleculares donde la cantidad se conserva o donde no hay fuerzas externas y el centro de masa permanece fijo. Esta última condición puede conseguirse, en la mayoría de los casos, inicializando el sistema con velocidad de centro de masa igual a cero.

Además de fijar la temperatura, también resulta interesante fijar la presión ya que la mayoría de los experimentos se realizan a presión constante. En cuanto a la simulación, el colectivo isotérmico-isobárico o NPT tiene como constantes el número de partículas, la temperatura y la presión. Para fijar esta

última variable en la simulación se implementa un barostato. Entre los barostatos más usados se pueden destacar:

Barostato de Berendsen. [7] Este barostato se basa en el reescalado de los lados de la caja de simulación, coordenadas y vectores, en cada paso de la simulación. Para ello utiliza una matriz de reescalado μ:

$$\mu_{ij} = \delta_{ij} - \frac{\Delta t}{3\tau_p}\beta_{ij}\left\{P_{0ij} - P_{ij}(t)\right\} \tag{3.11}$$

donde δ_{ij} toma el valor 0 si $i \neq j$ y 1 si $i = j$, P_0 es la presión de referencia, $P(t)$ es la presión del sistema en el instante dado t, β_{ij} es la compresibilidad isotérmica y τ_p es la constante de tiempo del acoplamiento del barostato. Durante el proceso las velocidades no se reescalan en función del cambio de tamaño de la caja, por lo que no asegura un correcto muestreo en el colectivo NPT.

Barostato de Parrinello-Rahman. [8, 9] El barostato de Parrinello-Rahman, al igual que el anterior, modifica la caja de simulación en cada paso de la simulación reescalando las coordenadas y vectores de la caja con una matriz de reescalado **b**:

$$\frac{d\mathbf{b}^2}{dt^2} = V\mathbf{W}^{-1}\mathbf{b}'^{-1}(P - P_0) \tag{3.12}$$

siendo V el volumen de la caja y **W** un parámetro que determina la fuerza del acoplamiento.

Este barostato, además, modifica las ecuaciones de movimiento de la siguiente forma

$$\frac{d^2\mathbf{r}_i}{dt^2} = \frac{\mathbf{F}_i}{m_i} - M\frac{d\mathbf{r}_i}{dt}, \tag{3.13}$$

$$M = \mathbf{b}^{-1}\left[\mathbf{b}\frac{d\mathbf{b}'}{dt} + \frac{d\mathbf{b}}{dt}\mathbf{b}'\right]\mathbf{b}'^{-1} \tag{3.14}$$

Así el barostato de Prrinello-Rahman asegura el correcto muestreo en el colectivo NPT. Sin embargo, puede ocasionar errores en sistemas muy alejados de la presión de equilibrio. Por ello se recomienda equilibrar previamente el sistema utilizando el barostato de Berendsen y, a continuación, usar el el barostato de Parrinello-Rahman.

3.2 Potencial de interacción

En sistemas condensados, las fuerzas de interacción entre las partículas que los forman deben ser consideradas para obtener una descripción realista del sistema. En el estudio de sistemas microscópicos condensados se considera que las fuerzas que afectan a las partículas del sistema son fuerzas conservativas, cada cual lleva asociada una energía llamada potencial de interacción (U), cuya relación se refleja en la Eq. (3.3). Por otro lado, los sistemas reales se componen de moléculas con una estructura interna, por lo que se suele distinguir entre fuerzas intermoleculares e intramoleculares según entre qué partículas se produzca la interacción. Las interacciones intermoleculares o no enalzadas son aquellas que se producen entre partículas o grupos químicos de diferentes moléculas. Mientras que las interacciones intramoleculares o enlazadas se dan entre átomos o grupos de la misma molécula. Ambos tipos de interacciones se describen más detalladamente a continuación.

3.2.1 Interacciones de no enlace

Las interacciones no enlazadas engloban a todas las interacciones aditivas por pares, que se producen entre grupos o partículas situados en moléculas diferentes o en la misma molécula pero separados por más de cuatro grupos. Este tipo de interacción incluye todos los potenciales de simetría esférica. Este tipo de interacciones se caracteriza por una contribución repulsiva de corto alcance, que cambia rápidamente en función de la distancia, y una contribución atractiva de largo alcance, que varía de forma mucho más suave según la distancia entre partículas. Debido a esto, cuando dos partículas eléctricamente neutras están suficientemente lejos entre ellas no existirá interacción entre ellas. Por una parte, la fuerza de atracción aparecerá al acercarse las partículas y, dicha fuerza, aumentará rápidamente al disminuir la distancia entre las partículas. El origen de la fuerza atractiva es la formación de dipolos, causada por el movimiento de los elctrones en torno al núcleo de las moléculas. Además, estos dipolos pueden inducir otros dipolos en átomos contiguos, generando así fuerzas de atracción electrostática entre los átomos. Las fuerzas atractivas contribuyen a la cohesión entre líquidos y sólidos. Además de estas fuerzas atractivas pueden generarse interacciones adicionales si en el sistema existen partículas cargadas eléctricamente. Por otro lado, no debemos olvidar la parte repulsiva, a distancias pequeñas los átomos experimentarán una fuerte repulsión debida a la proximidad entre sus capas electrónicas. El principal efecto de las fuerzas de repulsión es la greación de un orden de corte alcance que caracteriza las estructuras condensadas. El comportamiento de los sistemas en base a sus interacciones no enlazadas puede describirse mediante el uso de modelos matemáticos sencillos. Entre los más empleados podemos destacar:

Potencial de Lennard-Jones

El potencial de interacción de Lennard-Jones [10], LJ, es uno de los potenciales más conocidos y utilizados. Es un potencial de interacción continuo que continene una parte repulsiva, relevante a distancias intermoleculares pequeñas, y una parte atractiva, que tiende a cero a medida que aumenta la distancia intermolecular. Su expresión matemática se muestra a continuación:

$$U_{LJ}(r_{ij}) = 4\epsilon_{ij}\left[\left(\frac{\sigma_{ij}}{r_{ij}}\right)^{12} - \left(\frac{\sigma_{ij}}{r_{ij}}\right)^{6}\right] \tag{3.15}$$

donde r_{ij} es la distancia entre los sitios de interacción i y j y σ_{ij} es el diámetro del pozo de interacción y ϵ_{ij} es la profundidad del pozo de interacción (ver Fig. 3.2).

Como se observa en la ecuación (3.15), esta tiene dos contribuciones. La primera parte, $(\sigma_{ij}/r_{ij})^{12}$, describe la repulsión electrónica, que toma valores muy grandes a distancias cortas y luego decae rápidamente con el aumento de la distancia. La segunda parte, $(\sigma_{ij}/r_{ij})^{6}$, describe las fuerzas atractivas debidas a los dipolos que se generan. Al sumar ambas contribuciones se obtiene la distancia en que la interacción atractiva es máxima (ver figura 3.2).

Potencial de Mie

El potencial de Mie es similar al potencial de interacción de Lennard-Jones, siendo más útil y versátil que este último. Esto se debe a que no hay justificación teórica plena al considerar el término r-12 en la interacción repulsiva ni el término r-6 en la interacción atractiva. El potencial de Mie permite elegir los rangos de las distintas interacciones, atractivas y repulsivas, expresándose como:

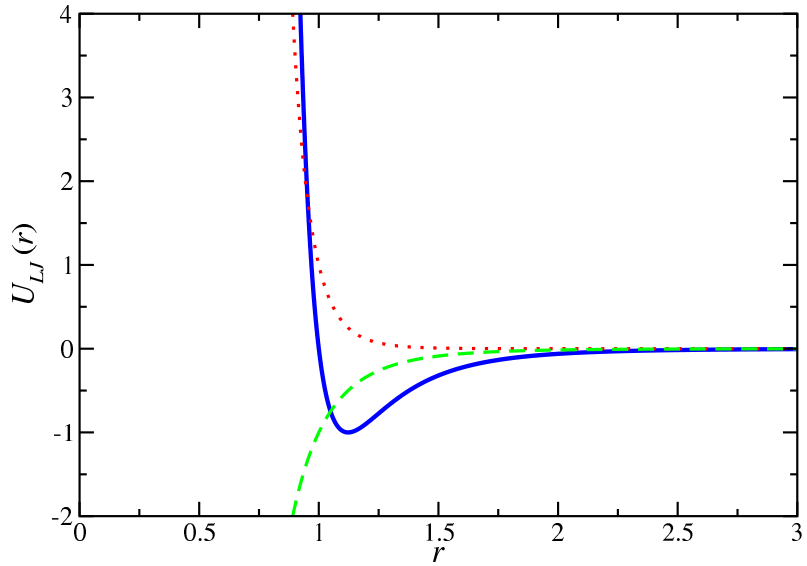

Figura 3.2: Representación de $U(\mathbf{r})$, frente a $\mathbf{r}$, para el potencial de Lennard-Jones (curva continua azul. Además del potencial completo se representa la contribución puramente repulsiva (curva punteada roja) y la contribución puramente atractiva (curva a trazos verde).

$$U_{Mie}(r) = C\epsilon\left[\left(\frac{\sigma}{r}\right)^{\lambda_r} - \left(\frac{\sigma}{r}\right)^{\lambda_a}\right] \tag{3.16}$$

En dicha expresión σ es un parámetro de tamaño que indica el diámetro de cada centro de interacción, ϵ es un parámetro de energía que representa la profundidad del pozo de potencial, λ_r es el exponente repulsivo, λ_a es el exponente atractivos y el parámetro $C(\lambda_r, \lambda_a)$ se define como

$$C = \frac{\lambda_r}{\lambda_r - \lambda_a}\left(\frac{\lambda_r}{\lambda_a}\right)^{\frac{\lambda_a}{\lambda_r - \lambda_a}} \tag{3.17}$$

En comparación con el potencial de Lennard-Jones, el potencial de Mie utiliza dos parámetros adicionales que pueden ser ajustados, λ_r y λ_a. Esta característica es de especial interés al estudiar propiedades derivadas segundas, que son muy sensibles a las interacciones repulsivas.

Potencial de Coulomb

El potencial de interacción entre dos partículas cargadas se describe medante la ley de Coulomb:

$$U_C(r_{ij}) = \frac{q_i q_j}{4\pi\epsilon_0 r_{ij}} \tag{3.18}$$

donde r_{ij} es la distancia entre los sitios de interacción i y j, q_i y q_j son las cargas parciales de los sitios de interacción i y j respectivamente y ϵ_0 es la permitividad del vacío. Esta interacción será repulsiva o atractiva en función de la interacción entre las partículas. La interacción será repulsiva si las partículas presentan el mismo tipo de carga, por otro lado, será atractiva si las cargas son contrarias.

3.2.2 Interacciones de enlace

Las interacciones de enlace hacen referencia a todas las interacciones entre átomos o grupos de la mismo molécula, considerando 2, 3 y 4 cuerpos adyacentes. Así, en función del número de enlaces químicos entre los cuerpos se pueden definir tres tipos de interacción y describirse mediante modelos matemáticos para simular el comportamiento de la molécula.

Potencial de enlace. Esta interacción se da entre átomos o grupos enlazados covalentemente. El potencial describe la variación del sistema cuando los cuerpos aumentan o disminuyen su longitud de enlace. La interacción se describe con un potencial armónico de vibración (U_b), que se caracteriza por la aparición de una fuerza recuperadora $\mathbf{F}$. La fuerza recuperadora se opone a que la distancia entre los cuerpos (r) se aleje de la posición de equilibrio fijada (b). Las expresiones del potencial armónico y la fuerza recuperadora serán:

$$U_b(r_{ij}) = \frac{1}{2}k_{ij}^b(r_{ij} - b_{ij})^2 \tag{3.19}$$

$$\mathbf{F}(r_{ij}) = k_{ij}^b(r_{ij} - b_{ij})\frac{\mathbf{r}_{ij}}{r_{ij}} \tag{3.20}$$

siendo k_{ij}^b la constante recuperadora del potencial.

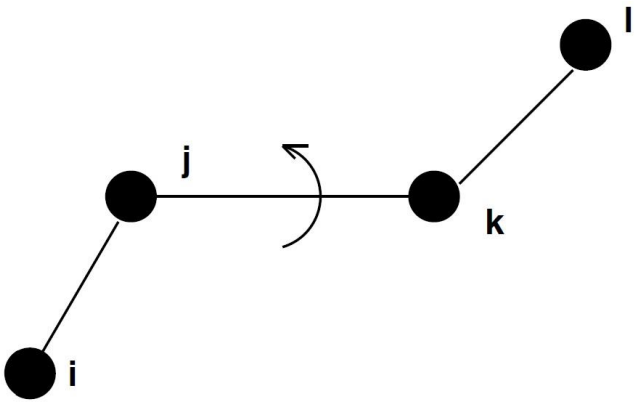

Figura 3.3: Representación gráfica de los sitios de interacción $i - j - k - l$ enlazados covalentemente formando una estructura lineal.

Potencial de flexión. La interacción de flexión o angular relaciona tres átomos o grupos separados por dos enlaces covalentes consecutivos. La interacción modula el ángulo formado por los cuerpos mediante un potencial armónico de flexión (U_α). Al igual que en el potencial de enlace, aparece una fuerza recuperadora que se opone a que el ángulo (θ) se aleje del ángulo de equilibrio (θ^0). La expresión de dicho potencial, para los átomos o grupos $i - j - k$ (ver figura 3.3), se define como:

$$U_\alpha(\theta_{ijk}) = \frac{1}{2}k_{ijk}^\theta(\theta_{ijk} - \theta_{ijk}^0)^2 \tag{3.21}$$

siendo k_{ijk}^θ la constante recuperadora del potencial. La fuerza que actúa sobre cada átomo se obtiene aplicando la regla de la cadena

$$\mathbf{F}_i = -\frac{d_\alpha(\theta_{ijk})}{d\mathbf{r}_i} \tag{3.22}$$

$$\mathbf{F}_k = -\frac{d_\alpha(\theta_{ijk})}{d\mathbf{r}_k} \tag{3.23}$$

$$\mathbf{F}_j = -\mathbf{F}_i - \mathbf{F}_k \tag{3.24}$$

siendo $\mathbf{r}_i$ y $\mathbf{r}_k$ los vectores de posición de los átomos i y k, respectivamente.

Potencial de torsión. Esta interacción se da entre cuatro átomos o grupos consecutivos y define el ángulo formado por los dos planos que se forman entre los tres primeros enlaces y los tres últimos (ver figura 3.3). Este potencial de torsión dihédrico se describe mediante una expansión en serie de cosenos (potencial de Ryckaert-Bellemans). En base a esto, el potencial de torsión dihédrico, U_{rb}, se corresponde con la expresión:

$$U_{rb}(\phi_{ijkl}) = \sum_{n=0}^{5} C_n(cos(\phi - \pi))^n \tag{3.25}$$

siendo ϕ el ángulo que se forma entre los planos ijk y jkl. Se considera la configuración cis (i y l en el mismo plano) como el ángulo cero. Los valores de C_n no son constantes, sino que dependen del modelo molecular utilizado.

El modelo molecular utilizado va a determinar si todos o alguno de los grados de libertad internos es prescindible, lo que mantendría una cierta estructura en la molécula al fijar distancias y ángulos. El modelo será flexible si no se fijan grados de libertad, semi-flexibles si se fija algún grado de libertad o rígido cuando se fijan todos los gradios de libertad internos. En este tarbajo se han empleado mayoritariamente modelos flexibles y semi-flexibles.

3.3 Condiciones de contorno periódicas

El objetivo de la simulación molecular es predecir el comportamiento macroscópico partiendo de un punto de vista microscópico. Para mantener el sistema en fase condesada es necesario establecer un potencial que actúe como un recipiente, es decir, que establezca unas condiciones de contorno para evitar que el sistema se expanda más allá dde dicho contorno. Por otro lado, simular un sistema macroscópico implicaría trabajar con un número de moléculas del orden del número de Avogadro (N_A), algo inviable computacionalmente, donde el número de moléculas utilizado está en torno a $100 \leq N \leq 10^5$. Por esta razón el uso de un potencial que simule un recipiente no es una solución adecuada, ya que se verían afectadas las propiedadees del sistema debido al contacto de las moléculas con la "pared de potencial" [11]. Este problema puede evitarse aplicando condiciones de contorno periódicas [12–14]. Esta técnica se basa en una red infinita que replica el sistema modelo, que se corresponde a la caja de simulación, en todas direcciones. Estas réplicas contienen el mismo número de moléculas que la caja original y reproducen los cambios que ocurren en la caja original (ver Fig. 3.4). Así se consigue que el sistema no esté confinado por paredes, sino por sistemas idénticos, asemejándose así al interior de una fase bulk. De esta forma, cuando alguna molécula abandona el sistema original

por una de sus caras, su imagen entrará al sistema, desde un sistema replicado, por la cara opuesta. Así se mantienen el número de partículas y la densidad del sistema, evitando el uso de paredes y los efectos de superficie que estas supondrían. Durante la simulación solo se almacenan las coordenadas de las moléculas del sistema original, no es necesario almacenar también las de los sistemas replicados.

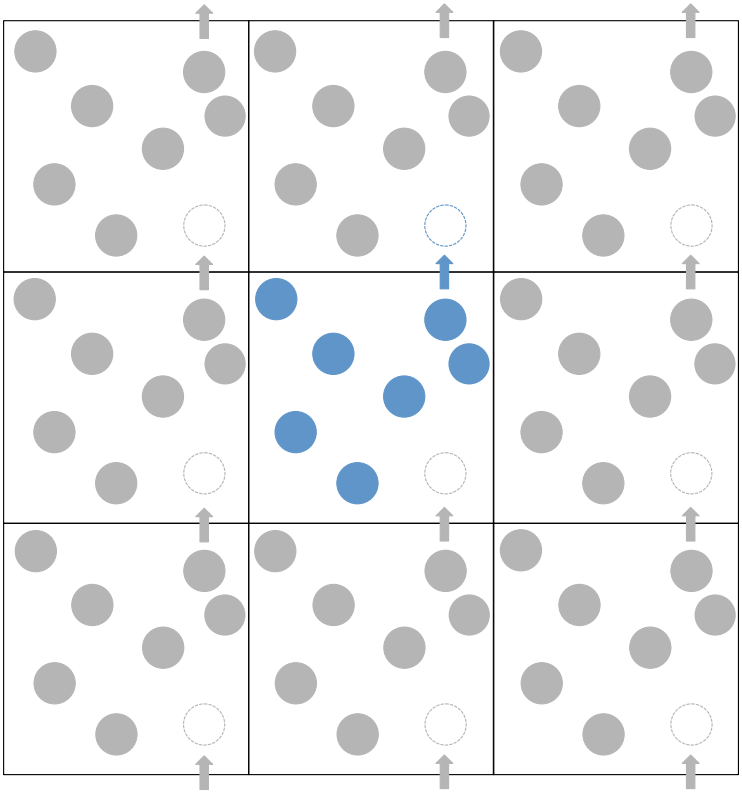

Figura 3.4: Representación gráfica en dos dimensiones de las condiciones de contorno periódicas mediante el replicado del sistema.

El uso de condiciones de contorno periódicas soluciona el problema causado por el uso de fronteras, sin embargo, aparecen otros problemas. Entre estos problemas destacan la aparición de una periodicidad artificial, que puede afectar a los resultados si el número de partículas en el sistema no es lo suficientemente grande, y la interacción de cada partícula del sistema con infinitas imágenes periódicas, problema que se evita utilizando métodos como la convención de mínima imagen y el truncamiento del potencial al usar un radio de corte.

3.4 Criterio de mínima imagen y truncamiento del potencial

En cuanto al cálculo de las fuerzas que actúan sobre cada partícula del sistema, la convención de mínima imagen [12–14], considera que cada partícula interacciona con el resto de partículas contenidas en una caja con mismas dimensiones que la caja de simulación primaria, pero centrada en la partícula cuyas interacciones se están considerando. Esto implica que solo se consideran las interacciones de la partícula con las $N-1$ partículas más cercanas.

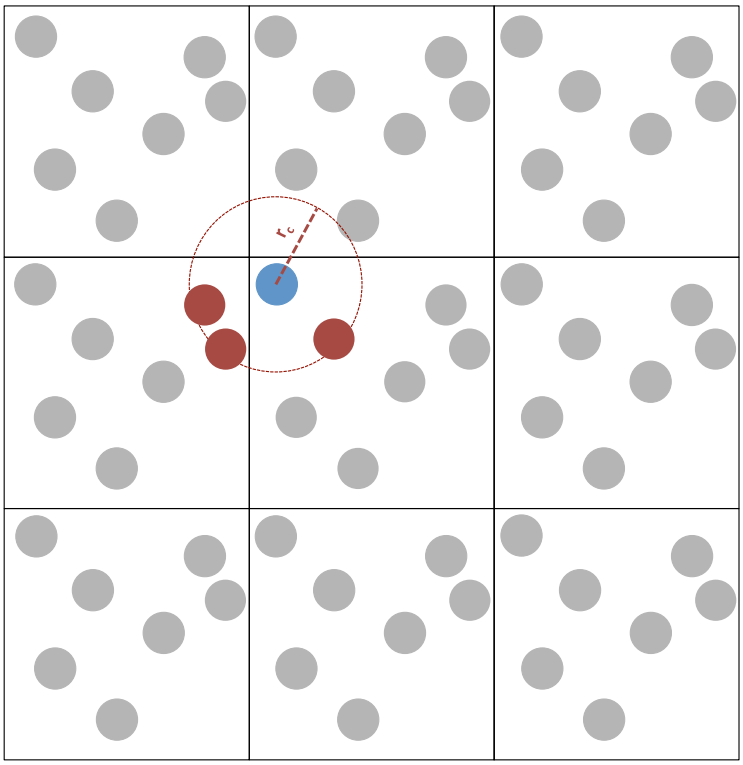

Figura 3.5: Representación gráfica en dos dimensiones del truncamiento del potencial de interacción.

Debido a que este sigue siendo un cálculo costoso, suele considerarse un cutoff esférico (ver Fig.3.5) que solo tiene en cuenta la interacción con los vecinos más cercanos, cuya interacción tiene mayor contribución. Dicho método se conoce como el método del radio de corte y es el método de truncamiento de potencial más habitual. Esta técnica considera que cada partícula interacciona con las partículas contenidas en una esfera centrada en ella. Para un sistema homogéneo en una caja de simulación cúbica con lado L, el radio o r_c suele ser igual o menor que la mitad del lado de la caja (ver Eq.3.28), con el objetivo de que sea consistente con la conveción de mínima imagen y se obtengan resultados fiables.

$$r_c \leq \frac{L}{2} \tag{3.26}$$

Si se consideran potenciales de corto alcance, como es el caso del potencial de Lennard-Jones, donde la energía potencial de la partícula se debe mayormente a la interacción con partículas vecinas, el error asociado a ignorar la interacción con partículas largas distancias es pequeño siempre que el radio de corte considerado sea suficientemente grande.

3.5 Método de Coexistencia Directa

Las fases inmiscibles producen interfases al entrar en contacto. Las moléculas cercanas a la interfase se comportan de forma distinta a las moléculas que se encuentran en el seno de cada una de las fases. Este comportamiento distinto se debe a la diferencia de fuerzas que sufre una molécula en el seno de la

fase respecto a las que sufre en las proximidades de la interfase. El estudio del comportamiento de las moléculas próximas a la interfase es objeto de interés en la actualidad, ya que el conocimiento de las propiedades en estos casos es escaso. Y estas propiedades, como por ejemplo las adsorción selectiva de moléculas en la interfase y la tensión interfacial, son propiedades de interés por sus aplicaciones industriales. El método empleado para simular varias inerfases en una caja de simulación es el método de coexistencia directa [15, 16]. Este método permite estudiar propiedades interfaciales, así como propiedades de equilibrio de fase en un sistema. El procedimmiento depende del sistema y las fases a estudiar. En concreto, los procedimientos usados en este trabajo han sido:

Líquido-vapor (Sistemas de n-alcanos + metano) : Para la construcción de los sistemas líquido-vapor correspondientes a las mezclas binarias de n-alcanos (n-decano, n-dodecano, n-tetradecano y n-hexadecano) con metano se partió de una configuración vapor-líquido-vapor, generada con Packmol, equilibrada en el colectivo NVT, que empleaba un potenical Lennard-Jonnes. Una vez obtenidos los sistemas iniciales, se dejaron evolucionar en el colecrtivo NVT, pero empleando un potencial de Mie tabulado en estos casos. Los disitintos sistemas se studiaron a distintas presiones para obtener las propiedades de interés.

Líquido-vapor (Sistemas de metil-ésteres puros): Para formar la interfase líquido-vapor de los sistemas puros de los ésteres seleccionados en la familia de metil-ésteres, desde metil-acetato hasta metil-heptanoato, primero se realizaron simulaciones de un líquido bulk en el colectivo NVT a las temperaturas deseadas. Partiendo de la fase equilibrada, se expandió la caja de simulación en el eje z triplicando su valor original. Así la fase líquida ocupó el centro de la caja de simulación y se formaron dos zonas vacías iguales a ambos lados. Este tipo de geometría hace que se cumplan las condiciones de contorno periódicas en todas las direcciones del espaciom, generando una caja vapor-líquido-vapor. Una vez obtenida la caja con las distintas fases se dejó evolucionar el sistema en el colectivo NVT, con lo que se consiguío que parte de las moléculas de la fase líquida formasen la fase vapor. Los sistemas evolucionaron hasta alcanzar las densidades y presiones de equilirbio correspondientes para cada metil-éster a las temperaturas deseadas.

Líquido-Líquido (Mezclas binarias metil-éster+ H_2O): Para construir las mezclas binarias de los distintos metil-ésteres con agua se utilizó un procedimiento similar al empleado para los sistemas puros. Primero se construyeron cajas de simulación para las distintas fases líquidas bulk de cada sistema. En concreto, se generó una fase rica en agua (acuosa) y otra fase rica en éster (orgánica). Estas fases fueron equilibradas en el colectivo NVT y se unieron para formar la caja final (acuosa-orgánica-acuosa). Las simulaciones con la caja final fueron realizadas en el colectivo $NP_z\mathcal{A}T$, fijando así el número de moléculas de los sistemas, la presión en el eje z y la temperatura. Estos sistemas se dejaron evolucionar hasta alocanzar las densidades de coexistencia para las condiciones de interés.

Bibliography

[1] R. Hockney, S. Goel, and J. Eastwood *J. Comput. Phys.*, vol. 14(2), pp. 148–158, 1974.

[2] H. J. Berendsen and W. F. Van Gunsteren *Molecular-Dynamics Simulation of Statistical-Mechanical Systems*, pp. 43–65, 1986.

[3] H. Berendsen, "Transport properties computed by linear response through weak coupling to a bath," in *Computer Simulation in Materials Science*, pp. 139–155, Springer, 1991.

[4] G. Bussi, D. Donadio, and M. Parrinello *J. Chem. Phys.*, vol. 126(1), p. 014101, 2007.

[5] S. Nosé *Mol. Phys.*, vol. 52(2), pp. 255–268, 1984.

[6] W. G. Hoover *Phys. Rev. A*, vol. 31(3), p. 1695, 1985.

[7] H. J. Berendsen, J. v. Postma, W. F. van Gunsteren, A. DiNola, and J. Haak *J. Chem. Phys.*, vol. 81(8), pp. 3684–3690, 1984.

[8] M. Parrinello and A. Rahman *J. Appl. Phys.*, vol. 52(12), pp. 7182–7190, 1981.

[9] S. Nosé and M. Klein *Mol. Phys.*, vol. 50(5), pp. 1055–1076, 1983.

[10] J. E. Lennard-Jones *Proceedings of the Physical Society*, vol. 43(5), p. 461, 1931.

[11] M. Born and T. von Kármán *Physikalische Zeitschrift*, vol. 13, pp. 297–309, 1912.

[12] D. Frenkel and B. Smit, *Understanding Molecular Simulations.* 2nd ed. Academic, San Diego, 2002.

[13] M. P. Allen and D. J. Tildesley, *Computer Simulation of Liquids.* Oxford University Press, 1987.

[14] N. Metropolis, A. W. Rosenbluth, M. N. Rosenbluth, A. H. Teller, and E. Teller *J. Chem. Phys.*, vol. 21, p. 1087, 1953.

[15] A. Ladd and L. Woodcock *Chem. Phys. Lett.*, vol. 51(1), pp. 155–159, 1977.

[16] A. Ladd and L. Woodcock *Mol. Phys.*, vol. 36(2), pp. 611–619, 1978.

Parte III

Resultados y Discusión

43

Capítulo 4

Phase equilibria and interfacial properties of selected methane + n-alkane binary mixtures

Abstract

Experimental determination, theoretical modeling, and molecular simulation have been combined to describe the bulk phase equilibria (*i.e.*, pressure, liquid, and vapor saturated mass densities) and interfacial properties (*i.e.*, interfacial concentration, adsorption, and interfacial tension) for methane + n-decane, n-dodecane, n-tetradecane and n-hexadecane binary mixtures at 344.15 K and in a pressure range between 0.1 and 30 MPa. Experimental determinations are carried out using a combined apparatus that includes a high-pressure vibrating tube densimeter and a high-pressure pendant drop tensiometer. The theoretical approach is based on the van der Waals gradient theory coupled to the Statistical Associating Fluid Theory of Variable Range employing a Mie potential (SAFT-VR-Mie) equation of state, where the fluids are described as Coarse Grained (CG) atoms. Molecular dynamics simulation for the same systems based on the CG Mie potential are reported. The three approaches are able to simultaneously predict phase equilibrium and interfacial properties, showing a very good agreement amongst themselves. For the systems and conditions studied here, the vapor mass density increases; the liquid mass density and interfacial tensions decrease as the pressure increases, and with a fixed temperature and pressure, the liquid mass density and interfacial tensions increase as the n-alkane molecular chain length increases. It is observed that methane is adsorbed along the interfacial region, whereas the n-alkanes (n-decane, n-dodecane, n-tetradecane, n-hexadecane) do not exhibit surface activity. The relative Gibbs adsorption of methane increases significantly with pressure until it reaches a maximum denoting adsorption saturation limit. It is also observed that the adsorption of methane only slightly increases with the chain length of the n-alkane.

4.1 Introduction

The phase and interfacial behavior of n-alkane mixtures have received continuous attention in applied thermodynamics. Their description and accurate prediction are key in the the petroleum and oil

refining industries, gas condensate recovery, liquefaction of natural gas, oil transportation, and recently have become relevant within the context of environmental control. [1] Particularly interesting are the asymmetric mixtures of methane with alkanes of high molecular weight that display a fascinating but complex behavior. They exhibit large departures from ideality, mainly caused by the differences in the molecular size of the components of the mixture, and also show several types of phase and interfacial behavior. Specifically, methane + n-alkane up to n-pentane mixtures are completely miscible in the liquid phase (with only vapor-liquid equilibria, VLE), and are described as Type I in the van Konynenburg and Scott classification. [2] From methane + n-hexane onwards, the phase behavior is complemented by the appearance of three-fluid phase line (*i.e.*, vapor-liquid-liquid equilibria, VLLE) near to the critical point of methane. This VLLE causes that the VLE critical line be separated into two branches: one of them initiates at the critical point of methane ascending up to the upper critical end point (UCEP) of the VLLE, and the second one from the lower critical end point (LCEP) of the VLLE with a maximum in the pressure up to the critical point of n-hexane. For the case of methane + n-heptane mixture, the VLLE is interrupted by another three-phase line: solid n-heptane+L+V (SLVE). This interception generates a quadruple point (solid n-heptane+L_1+L_2+V, SLLVE). For higher n-alkanes, the VLLE disappears, and the mixtures display two CEPs. At each CEP, the solid phase is in equilibrium with a critical VL phase. Therefore, methane + n-alkane mixtures (n-octane or higher) will exhibit several types of equilibria, namely solid-liquid (SLE), solid-vapor (SVE), SLVE, and vapor-liquid (VLE), the latter equilibrium also showing an interesting behavior where retrograde condensation is observed.

An initial and general discussion of these phase equilibria types was given by Davenport and Rowlinson, [3] who described the general trends of selected alkanes with liquid methane. This general description was complemented by Rijkers, [4] who described from an experimental and theoretical perspective the phase equilibrium of methane + n-decane, or n-dodecane, or n-hexadecane. In the case of interfacial behavior, the interfacial tension of the methane + n-alkane mixtures up to n-decane has been measured in a broad range of temperature and pressure under VLE conditions (see Pereira *et al.*, [5] and references therein). Other interfacial properties, such as concentration profile along the interfacial region and the Gibbs adsorption, have been calculated by using cubic equation of state (EoS) coupled to the van der Waals square gradient theory, [5–8] linear gradient theory, [5] and density functional theory (DFT) with Statistical Associating Fluid Theory (SAFT) EoS. [9] Recently, classical Molecular Dynamics (MD) simulations based on the united atoms description have also been applied to predict the interfacial behavior of these systems. [7, 8] Surprisingly, simultaneously description of available experimental data, theoretical predictions and molecular simulations only cover the methane + n-alkane mixtures up to n-decane, and to the best of our knowledge, only [8] have been recently explored some higher n-alkane (*i.e.*, n-dodecane and n-nonadecane).

The aim of this work is to describe simultaneously the bulk density phase equilibria and the interfacial properties for the case of methane + n-alkane mixtures [$CH_4(1)$ + $CH_nH_{2n+2}(2)$, with n = 10 (n-decane), 12 (n-dodecane), 14 (n-tetradecane), and 16 (n-hexadecane)] at 344.15 K and the thermodynamic conditions where the mixtures only display VLE. The selected temperature and pressure range have been selected as they represent commonly encountered conditions observed in gas-oil systems related to petroleum reservoirs.

The experimental phase equilibrium on PTx coordinates of these systems have been measured by several authors in a broad range of temperatures and pressures. [10] Of the particular relevance is the series of manuscripts from the Delft group, [4, 11–15] who provided not only new experimental data but also an EoS based modeling of the phase equilibrium. For the case of bulk fluid densities and

interfacial tensions, the spectrum of experimental information is reduced to the methane + n-decane binary mixture. [5, 16, 17] Adding to the experimental determinations of bulk fluid densities and interfacial tension, theoretical approaches, [5, 6, 9] and molecular simulations cover the methane + n-decane mixture, [7] and recently the methane + n-dodecane mixture. [8]

The research presented here combines experiments, theory, and molecular simulation. Specifically, the experiments are based on an experimental setup that includes a high pressure pendant drop tensiometer with a high pressure densimeter and covers the pressure range from 0.1 to 20 MPa. The theoretical approach is based on the van der Waals square gradient theory [18–20] coupled to the Statistical Associating Fluid Theory of Variable Range employing a Mie potential (SAFT-VR-Mie). [21] Computer simulations are carried out by using molecular dynamics (MD) employing the force field underlying the SAFT-VR-Mie approach. [22]. A distinctive aspect of this work is that in both the theoretical modeling (SAFT-VR-Mie coupled to SGT) and in the molecular dynamics simulations, the same set of CG Mie force field parameters are used. The advantage of this approach is that the results from the theory and the simulations can be directly compared. The same strategy has been previously used by some of us for describing CO_2 + hydrocarbon mixtures, [23, 24] N_2 + n-alkanes, [25] homonuclear ring fluid mixtures, [26] water + hexane mixture, [27] and Lennard-Jones mixtures, [28, 29] as well as by other authors, who have been recently employing the same strategy to relate the interfacial behavior to bulk phase behavior of Lennard-Jones mixtures, [30, 31] and to quantify the effect of the polar interactions on bulk and interfacial properties. [32]

4.2 Experimental Section

4.2.1 Pure fluids

Methane was purchased from AirLiquid with a certified purity greater than 99.9 %, whereas n-alkanes (*i.e.*, n-decane, n-dodecane, n-tetradecane and n-hexadecane) were purchased from Merck and used as received. Table 4.1 summarizes some purity indicators of the pure n-alkanes such as the purity reported by the manufactures and measured by gas chromatography (GC), the mass densities (ρ), and the interfacial tensions (γ) of the pure fluids at 344.15 K and 101.3 kPa. This table also includes the reference experimental values reported on the NIST-TDE database. [33]

Tabla 4.1: Gas chromatography (GC) purities (mass fraction, w), liquid mass densities (ρ) and interfacial tensions (γ) of pure n-alkanes at 344.15 K and 101.3 kPa* measured in this work (Exp.) and taken from the average of the data reported on the NIST-TDE database. [33] (Ref.).

Substance	source	w/ supplier	Purification	w / GC	ρ (kg/m^3)		γ (mN/m)	
					Exp.	Ref.	Exp.	Ref.
n-decane	Merck	> 0.99	none	0.999	691.21	690.50	19.01	19.14
n-dodecane	Merck	> 0.99	none	0.999	712.10	712.30	20.72	20.79
n-tetradecane	Merck	> 0.99	none	0.999	727.10	727.40	22.07	22.08
n-hexadecane	Merck	> 0.99	none	0.999	738.26	737.96	23.02	23.23

*The standard uncertainties (0.68 level of confidence) are: $u(T) = 0.1$ K. Instrument standard uncertainty are $\rho = 0.4$ kg/m^3 and $\gamma = 0.05$ mN/m. The combined expanded uncertainties (considering a 0.95 level of confidence, $k = 2$) are $U(\rho) = 1.1$ kg/m^3 and $U(\gamma) = 0.1$ mN/m.

4.2.2 Density measurements

The mass density of the pure fluids is measured at 344.15 K and 101.3 kPa using a DMA 5000 M densimeter (Anton Paar, Austria). For the case of mixtures (CH_4 + n-alkane) at 344.15 K and pressures over 101.3 kPa, the liquid and vapor densities are measured by using a DMA HP densimeter (Anton Paar, Austria), which is connected to the tensiometer chamber. In both cases (pure fluids and fluid mixtures), the mass density determination is based on measuring the period of oscillation of a vibrating U-shaped tube filled with the fluid sample. [34] These devices are calibrated by using two reference fluids. For the case of DMA 5000 M densimeter, ultrapure water and atmospheric air were used at 298.15 K and 101.3 kPa. For the case of DMA HP densimeter, N_2 and n-decane were used at 344.15 K and over the pressure range from 0.1 MPa to 30 MPa.

During the operation, the temperature of the apparatus is maintained constant to within ± 0.01 K. Pressure is measured by means a Swagelok type S pressure transducer connected to the densimeter and maintained constant to within ± 0.001 kPa by using a high-pressure syringe pump (Teledyne Isco Pump. Model 100DM, USA). The mass density is measured with an instrument standard uncertainty of 0.4 kg/m^3, and a combined expanded uncertainty (considering a 0.95 level of confidence, k = 2) of U(r) = 1.1 kg/m^3.

The experimental procedure to measure the fluid densities is as follows. The tensiometer cell is initially heated to 344.15 K and slightly pressurized with CH_4. The n-alkane (n-decane, n-dodecane, n-tetradecane, or n-hexadecane) is pumped through a stainless-steel tube to fill approximately 30% of its volume by visual observation, and then the pressure is increased to the desired experimental value. In the chamber, the gas will be saturated with the n-alkane, and some gas diffuses into the n-alkane. Once the equilibrium is reached, the saturated CH_4 is transported to the high-pressure densimeter through a heated stainless steel tube to measure the mass density of CH_4 saturated with n-alkane (ρ_V). The density measurements are repeated 10 times for each condition and averaged accordingly. The same procedure is carried out to measure the mass density of the n-alkane saturated with CH_4 (ρ_L) but in this case, the chamber is filled up to approximately 85% of its volume by visual observation.

4.2.3 Tensiometry measurements

The interfacial tension between a liquid mixture drop surrounded by a gas mixture at 344.15 K and over the pressure range from 0.1 to 20.0 MPa is measured using an IFT-10 high-pressure pendant drop tensiometer (Temco Inc., USA). This device is equipped with a cool light beam source and a video camera, which is connected to a personal computer through a frame grabber card. In order to avoid external vibrations, both the tensiometer and the camera are mounted on a vibration-free table. Specific technical details of this tensiometer device and its parts have been extensively described in previous works. [23, 35–40]

The experimental procedure is as follows. The tensiometer cell is initially heated to 344.15 K and slightly pressurized with CH_4. The n-alkane (n-decane, n-dodecane, n-tetradecane, and n-hexadecane) is pumped through a stainless-steel tube to fill one-third of the chamber in order to saturate the gas that fills the cell and allow some gas to diffuse into the n-alkane. The tensiometer cell is pressurized to the desired experimental pressure, and once the equilibrium is reached, a liquid drop of the n-alkane is generated at the tip of a stainless steel needle (1.4 mm i.d. and 2.45 mm o.d.) into the tensiometer chamber. Once the drop is formed, it is necessary to wait, approximately 10 - 15 min, to saturated

the liquid drop, and for the cell to reach a stable condition of pressure and temperature. After this equilibration step, the drop dimensions are recorded (for at least during 2 h) in order to check the stability of its geometry (*i.e.*, shape and volume of the drop). Once the shape and volume of the drop are deemed constant, the equatorial diameter of the drop, d_e (the largest one), and the horizontal diameter of the drop, d_s, which is located at a distance d_e from the apex of the drop, are recorded.

Based on the experimental measurements of ρ_L, ρ_V, d_e, d_s, the interfacial tension, γ, is calculated from the Laplace equation:

$$\gamma = (\rho_L - \rho_V)\, g\, d_e^2\, \Im\,(d_e, d_s) \tag{4.1}$$

where g is the local gravitational constant $\left(g = 9.81\,\mathrm{m/s^2}\right)$, and $\Im\,(d_e, d_s)$ represents a function related to the silhouette of the drop, whose values are determined from numerical tables. [41] In this device, the pressure and the temperature are maintained constant within ± 0.001 kPa, and ± 0.1 K, respectively. Additional details relating to the pendant drop technique can be found in references [42, 43] and

The numerical results of γ from Eq. (4.1) are affected by the value of pressure, density difference and the experimental reproducibility of γ. In order to quantify these effects on the reported value of γ, the uncertainties of γ are calculated from the expanded or combined relative uncertainty of γ, $u_c\,(\gamma)$: [44]

$$u_c^2\,(\gamma) = \left[\frac{1}{\gamma}\left(\frac{\partial\gamma}{\partial P}\right)_T \delta P\right]^2 + \left[\frac{\delta\Delta\rho}{\Delta\rho}\right]^2 + \left[\frac{\sigma\,(\gamma)}{\gamma}\right]^2 \tag{4.2}$$

In the latter expression, δP and $\delta\triangle\rho$ are the corresponding standard uncertainties in pressure and density, respectively. $\sigma\,(\gamma)$ is the standard deviation of γ, which together with the maximum experimental value of partial derivatives of γ in P permits to estimate the value of u_c. For the binary mixtures investigated here, the average of u_c was found to be 0.78%. Therefore, the expanded relative uncertainty of γ at 95% confidence was 1.5% or equivalently to 0.1 mN/m.

Finally, the measured data of density and interfacial tension can be also used to approximately estimate the magnitude of the Gibbs adsorption isotherm of CH_4 (1) relative to the n-alkane (2), Γ_{12}: [45]

$$\Gamma_{12} \approx -\frac{\rho_1}{M_{w_1}}\left(\frac{\partial\gamma}{\partial P}\right)_T \tag{4.3}$$

Here M_{w_1} and ρ_1 are the molecular weight and molar density of the pure CH_4, respectively. ρ_1 is evaluated at T and P, whereas the slope $(\partial\gamma/\partial P)_T$ is obtained from the experimental $\gamma - P$.

4.3 Theory

Theoretical predictions of bulk phase equilibria (*i.e.*, temperature, pressure, mole fraction and bulk liquid and vapor densities) and interfacial properties (*i.e.*, interfacial concentration profiles, surface activity, relative Gibbs adsorption and interfacial tension) are obtained by considering that the pure fluids and the binary fluid mixtures can be described as super united atoms, a coarse grained (CG) representation of molecules formed of segments interacting through the Mie potential, [46]

$$\phi^{Mie}(r_{ij}) = C\varepsilon\left[\left(\frac{\sigma}{r_{ij}}\right)^{\lambda} - \left(\frac{\sigma}{r_{ij}}\right)^{6}\right] \tag{4.4}$$

where λ is the repulsive parameter which dictates the range and softness of the intermolecular potential. r_{ij} is the center-to-center distance of the interacting segments, ε is the energy scale corresponding to the potential well depth, σ is the length scale, corresponding loosely with an effective segment diameter, and C is a constant defined as:

$$C = \frac{\lambda}{\lambda - 6}\left(\frac{\lambda}{6}\right)^{\frac{6}{\lambda-6}} \tag{4.5}$$

Within this CG approach, CH_4 is represented by one single sphere and n-alkanes are modeled as a chain of tangent spheres where bond distances are kept constant at a value of σ and no further intramolecular interactions are employed. Table 4.2 summarizes the numerical values of the Mie potential for the pure fluids used here. These values were obtained by invoking the corresponding state principle described in previous works. [47, 48]

Tabla 4.2: Molecular parameters of the Mie potential for the pure fluids

Substance	m_s	ε/k_B (K)	σ (Å)	λ
CH_4	1	170.754	3.752	16.391
$C_{10}H_{22}$	3	415.190	4.584	20.920
$C_{12}H_{26}$	4	378.560	4.351	18.410
$C_{14}H_{30}$	5	363.060	4.183	17.66
$C_{16}H_{34}$	5	418.130	4.432	21.20

In this work, the bulk phase or homogeneous region is described by the Statistical Associating Fluid Theory of Variable Range employing for molecules formed of segments interacting through the Mie potential (SAFT-VR-Mie). In this version of SAFT, the Helmholtz energy density for a non-associating chain fluid, a_0, is given by: [21]

$$a_0 = \left(a^{ig} + a^{mono} + a^{chain}\right)\rho\frac{N_{av}}{\beta} \tag{4.6}$$

where ρ is the molar density of the mixture, N_{av} is the Avogadro constant, $\beta = 1/k_BT$, T is the absolute temperature, and k_B is the Boltzmann constant. The contributions of the total Helmholtz energy are the ideal gas contribution, a^{ig}, the monomer (unbounded) contribution for a chain composed of m_s tangential segments, a^{mono}, and the formation of chain molecules, a^{chain}. For a complete overview of this model, the reader is referred to the original work [21]. Additionally, a summary of the main expressions can be found in Ref. [49]

Within the SAFT-VR-Mie EoS, pure non-associating fluids are characterized by the three Mie parameters $(\lambda, \varepsilon, \sigma)$ plus m_s. The numerical values of these parameters are summarized in Table 4.2.

According to the original work, [21] the SAFT-VR-Mie EoS is extended to mixtures by using the following combination rules for the unlike parameters for size, σ_{ij}, attractive interaction energy, ε_{ij}, and Mie exponents, λ_{ij}:

$$\sigma_{ij} = (\sigma_i + \sigma_j)/2 \; ; \; \varepsilon_{ij} = \sqrt{\varepsilon_i \varepsilon_j} \frac{\sqrt{\sigma_i^3 \sigma_j^3}}{\sigma_{ij}^3} (1 - k_{ij}) \; ; \; (\lambda_{ij} - 3) = \sqrt{(\lambda_{ii} - 3)(\lambda_{jj} - 3)} \tag{4.7}$$

where k_{ij} is a binary interaction parameter, which is obtained from experimental data of phase equilibria. In this work, this parameter has been obtained by minimizing the error between the predicted and experimental bubble point data [50] using available experimental PTx data. Table 4.3 collects the numerical values of k_{ij}, the cross parameters, the Absolute Average Deviation on pressure (AADP) and the reference data used for fitting. In the Supplementary Information, the PTx diagrams are included together with the experimental data used for this fitting.

Tabla 4.3: Molecular parameters for cross interactions

Mixture	k_{ij}	ε_{ij}/k_B (K)	σ_{ij} (Å)	λ_{ij}	%AADP*
CH_4+$C_{10}H_{22}$	−0.03263	270.854	4.168	18.491	0.76 [a]
CH_4+$C_{12}H_{26}$	−0.02199	257.711	4.052	17.365	1.21 [b]
CH_4+$C_{14}H_{30}$	−0.02874	255.011	3.968	17.012	4.00 [c]
CH_4+$C_{16}H_{34}$	−0.05264	278.363	4.092	18.611	7.31 [d]

* $\%\text{AADP} = 100(1/N_d)\sum_{i=1}^{N_d} \left| P_i^{exp} - P_i^{cal} \right| / P_i^{exp}$, where N_d is the number of experimental points used. Experimental data have been taken from: [a] [51], [16], and [12]; [b] [13, 52]; [c] [14, 53]; [d] [11, 15]

In order to predict the isothermal bulk phase equilibrium properties (*i.e.*, ρ^L, ρ^V and P^0) from the SAFT-VR-Mie EoS, the following phase equilibrium conditions are applied:

$$\Omega = -P^0 \tag{4.8}$$

$$\left(\frac{\partial \Omega}{\partial \rho_1}\right)^L_{T^0,V^0,\rho_2^0} = \left(\frac{\partial \Omega}{\partial \rho_1}\right)^V_{T^0,V^0,\rho_2^0} \tag{4.9}$$

$$\left(\frac{\partial \Omega}{\partial \rho_2}\right)^L_{T^0,V^0,\rho_1^0} = \left(\frac{\partial \Omega}{\partial \rho_2}\right)^V_{T^0,V^0,\rho_1^0} \tag{4.10}$$

In the latter equations, the superscript 0 represents equilibrium conditions and L and V refer to liquid and vapor, respectively. ρ_i is the molar density of component i, which is related to the molar fraction, x_i, and the molar density of the mixture, ρ, through $\rho_i = x_i\rho$, and Ω is the grand thermodynamical potential, which is defined as:

$$\Omega = a_0 - \rho_1 \left(\frac{\partial a_0}{\partial \rho_1}\right)^0 - \rho_2 \left(\frac{\partial a_0}{\partial \rho_2}\right)^0 = a_0 - \rho_1\mu_1^0 - \rho_2\mu_2^0 \tag{4.11}$$

where μ_i is the chemical potential of component i.

In summary, Eqs. (4.6)–(4.11) are used to predict the pressure and bulk phase equilibrium densities, which are the boundaries of the interfacial or inhomogeneous region. Specific details related to the numerical strategies to solve the phase equilibrium are described by some of us in a recent work. [49]

In this work, the interfacial properties are calculated from the van der Waals square gradient theory (SGT). [18–20] In SGT, the inhomogeneous Helmholtz energy density, a, is described by the sum of two contributions: the first part takes into account the Helmholtz energy density for the homogeneous fluid at a local density, a_0, while the second part represents the inhomogeneous contribution of Helmholtz energy by a product of square local-density gradients and a set of characteristic constants, called influence parameters, c_{ij}. For the case of a binary mixture in a planar interface along the z coordinate, and considering a geometric mixing rule for the cross-influence parameters (*i.e.*, $c_{12} = c_{21} = \sqrt{c_{11}c_{22}}$), a is given by the following expression:

$$a = a_0 + \frac{1}{2}\left[c_{11}\left(\frac{d\rho_1}{dz}\right)^2 + 2\sqrt{c_{11}c_{22}}\left(\frac{d\rho_1}{dz}\right)\left(\frac{d\rho_2}{dz}\right) + c_{22}\left(\frac{d\rho_2}{dz}\right)^2\right] \tag{4.12}$$

Within the theoretical framework of the SGT, the density distribution, $\rho_i(z)$, is obtained from Eq. (4.12) when a reaches a stationary minimum value. This condition leads to the following algebraic expression: [18–20]

$$\sqrt{c_{22}}\left(\mu_1(\rho_1,\rho_2) - \mu_1^0\left(\rho_1^0,\rho_2^0\right)\right) = \sqrt{c_{11}}\left(\mu_2(\rho_1,\rho_2) - \mu_2^0\left(\rho_1^0,\rho_2^0\right)\right) \tag{4.13}$$

In this work, μ_i are described by the SAFT-VR-Mie and the influence parameters for the pure components, c_{11} and c_{22} are calculated, independently of temperature and density, using the same molecular parameters used on SAFT-VR-Mie (see Table 4.2) and the expression: [54]

$$\sqrt{\frac{c_{ii}}{N_{av}^2\varepsilon_{ii}\sigma_{ii}^5}} = m_{s,i}\left(0.12008 + 2.21979\alpha_i\right) \tag{4.14}$$

where α_i is the van der Waals constant, in this case

$$\alpha_i = C_i\left[\left(\frac{1}{3}\right) - \left(\frac{1}{\lambda_i - 3}\right)\right] \tag{4.15}$$

By solving Eq. (4.13), ρ_1 (ρ_2) is obtained. Other interfacial properties, such interfacial concentration profiles along the spatial coordinate, the relative Gibbs adsorption, and interfacial tensions, can be calculated from the following expressions: [19, 20, 55]

$$\left(\frac{d\rho_2}{dz}\right)^2 = 2\left(\Omega + P^0\right)\left[1 + 2\left(\frac{d\rho_1}{d\rho_2}\right) + \left(\frac{d\rho_1}{d\rho_2}\right)^2\right]^{-1} \quad ; \quad \left(\frac{d\rho_1}{dz}\right) = \left(\frac{d\rho_1}{d\rho_2}\right)\left(\frac{d\rho_2}{dz}\right) \tag{4.16}$$

$$\Gamma_{12} = -\left(\rho_1^L - \rho_1^V\right)\int_{-\infty}^{+\infty}\left\{\frac{\rho_2(z) - \rho_2^L}{\rho_2^L - \rho_2^V} - \frac{\rho_1(z) - \rho_1^L}{\rho_1^L - \rho_1^V}\right\}dz \tag{4.17}$$

$$\gamma = \sqrt{2}\int_{\rho_2^{V,0}}^{\rho_2^{L,0}}\left(\left(\Omega + P^0\right)\left[c_2 + 2\sqrt{c_1c_2}\left(\frac{d\rho_1}{d\rho_2}\right) + c_1\left(\frac{d\rho_1}{d\rho_2}\right)^2\right]\right)^{1/2}d\rho_2 \tag{4.18}$$

The numerical details involved in the phase equilibrium, and interfacial properties calculations along with an open free software code to perform them have been recently described by some of us. [49]

4.4 Molecular Dynamics Simulations

MD simulations of bulk phase and interfacial properties of CH_4 + n-alkane (*i.e.*, $C_{10}H_{22}$, $C_{12}H_{26}$, $C_{14}H_{30}$ and $C_{16}H_{34}$) mixtures at 344.15 K are performed in the canonical ensemble (NVT). In this ensemble, N molecules at a fixed temperature T are placed in a parallelepiped simulation cell of a constant volume $V = L_x \times L_y \times L_z$. In this work, the N molecules that conform the mixture ($N = N_1 + N_2$) are described as freely-jointed tangent spheres that interact with each other according to an effective pairwise Mie potential. [46] The novelty of the MD simulations performed here is that force field Mie parameters are directly taken from the SAFT-VR-Mie EoS (see Tables 4.2 and 4.3), where CH_4 is represented by one single sphere, $C_{10}H_{22}$ as three tangent spheres, $C_{12}H_{26}$ is modeled as four tangent spheres, whereas $C_{14}H_{30}$ and $C_{16}H_{26}$ are is modeled as five tangent spheres. For a complete discussion of SAFT CG-Mie methodology and its top-down parameterization, the reader is directed to the review by [22].

In this work, we follow the procedure described by [56] to define the distribution of N_1 and N_2. This procedure is based on the phase equilibrium predictions using SAFT-VR-Mie EoS (see Sec. 4.3). All MD simulations are carried out using the same total number of Mie segments, $N_s = (m_1x_1 + m_2x_2)N$, for all the mixtures and at all thermodynamic conditions, $N_s = 8000$. Here m_1 and m_2 are the number of monomeric units and x_1 and x_2 are the mole fractions of components 1 and 2, respectively. This is done to ensure that all the systems are formed from the same number of monomers or interacting sites irrespective of the particular chain lengths in the different mixtures. We choose $L_x = L_y = 12\sigma = 55.02\,\text{Å}$, being σ the the largest monomeric diameter used in this work (n-decane). Note that we have chosen x- and y-axis as the directions containing the interface and the z-axis direction perpendicular to the VL interface. Since we are dealing with mixtures, not only ρ_L, the liquid density, and ρ_V, the vapor density, vary with pressure, but also the composition of the mixture in both phases, x_1 and y_1. Due to this, L_z is chosen appropriately to ensure phase separation at the corresponding thermodynamic conditions for all mixtures.

For a given mixture and pressure, we take ρ_L, ρ_V, x_1, and y_1 as obtained from the SAFT-VR-Mie predictions and use this information as starting values to prepare homogeneous liquid and vapor systems with the appropriate compositions in two parallelepiped simulation boxes. L_x and L_y are chosen as explained previously and L_z is fixed to reproduce the theoretical values of ρ_L and ρ_V. Depending on the mixture and pressure, L_z varies from $\sim 57\sigma \sim 261\,\text{Å}$, at low pressures, to $\sim 23\sigma \sim 105\,\text{Å}$, at high pressures. The two simulations boxes are then linked up forming a vapor-liquid-vapor system, which constitutes the initial simulation box used to study the coexisting and interfacial properties of the mixture at the desired pressure. The number of molecules of each species, the total length of the simulation box along the z-axis (L_z), and the equilibrium pressure obtained at the end of the NVT simulations of all the mixtures are summarized in the Supplementary Information. We use periodic boundary conditions in all three dimensions and a cutoff radius $r_c = 6\sigma = 27.504\,\text{Å}$, where $\sigma = 4.584\,\text{Å}$, the largest value of the size parameter of the Mie intermolecular potential used.

We use the GROMACS (version 4.6.1) [57] simulation suite to perform NVT MD simulations. We use the Verlet leapfrog algorithm with a time step of 0.001 ps, and the Nosé-Hoover thermostat, with a relaxation constant of $\tau = 1.0\,\text{ps}$. The vapor-liquid interfacial system is equilibrated for at least 10 ns. Additional 50 ns are also employed to calculate averages (production stage). Errors for equilibrium pressure and interfacial tension are estimated dividing the production period into M (independent) blocks. The statistical error is estimated from the standard deviation of the average $\overline{\sigma}/\sqrt{M}$. Here $\overline{\sigma}$ is

the variance of the block averages and $M = 10$ in this work.

In order to characterize the bulk phase equilibria and interfacial properties, the concentration profiles $\rho_i(z)$ are calculated by dividing the system in 200 slabs along the z direction. The molecular density profiles, $\rho_i(z)$, are obtained by assigning the position of each bead center, z_i, to the corresponding slab and constructing the molecular density from mass balance considerations. From the profiles, we have obtained the bulk liquid and vapor densities and the total density averaging $\rho_1(z)$, $\rho_2(z)$ and $\rho(z) = \rho_1(z) + \rho_2(z)$ over the appropriate regions sufficiently removed from the interfacial region. The statistical uncertainties of these values are estimated from the standard deviation of the mean values. From the $\rho_i(z)$ profiles, the surface activity (or absolute adsorption) of species along the interfacial region is also evaluated, and the relative Gibbs adsorption isotherm of a species i relative to a species j (Γ_{ij}) (see Eq. (4.17)) can be obtained from the MD approach. The equilibrium pressure, P, and interfacial tension, γ, are obtained using the Irving-Kirkwood method, where the pressure tensor diagonal elements are calculated employing the virial expression. The vapor pressure corresponds to the normal component of the pressure tensor, $P = P_{zz}$, while the interfacial tension is obtained using the pressure route:

$$\gamma = \frac{Lz}{2}\left[\langle P_{zz}\rangle - \frac{\langle P_{xx}\rangle + \langle P_{yy}\rangle}{2}\right] \tag{4.19}$$

In the equation above, $\langle\cdots\rangle$ represents ensemble average of the pressure tensor, and the leading factor (1/2) comes from having two interfaces present in the system. The details related to the technical implementation of the previous expressions and their evaluation have been discussed extensively in the literature (see [58] , [56] and references therein).

4.5 Results and discussion

In this work, experimental determinations, theoretical predictions, and molecular simulations are combined to explore and simultaneously describe the phase equilibria and the interfacial properties for four asymmetric binary mixtures, namely CH_4 + ($C_{10}H_{22}$, $C_{12}H_{26}$, $C_{14}H_{30}$ and $C_{16}H_{34}$) at the isothermal condition of 344.15 K and over a broad pressure range, where VLE is the only phase equilibrium type. The theoretical modeling and molecular simulation use the parameter described in Tables 4.2 and 4.3, which were obtained from corresponding state principia, [47, 48] and PTx experimental data from other data sources. In that sense, the results from the theoretical approach and MD simulations can be seen as an unbiased prediction and a test of the transferability of the thermodynamic models. The main results for this trilogy approach are described below, where some comparison to previous results are included.

4.5.1 Bulk Phase equilibrium

As described in Sec. 4.3, the bulk phase equilibrium is the boundary of the interfacial region. In this section, the equilibria bulk mass densities, as functions of pressure, are described for the four methane based binary mixtures using our three-pronged approach. The results are compared to the available experimental data, previous theoretical results and MD simulations. Table 4.4 summarizes the new experimental measurements, whereas Table 4.5 collects our MD results for the phase equilibria

bulk mass densities in the VLE region at the isothermal condition of 344.15 K for the CH_4 + n-alkanes ($C_{10}H_{22}$, $C_{12}H_{26}$, $C_{14}H_{30}$ and $C_{16}H_{34}$) mixtures.

Tabla 4.4: Phase equilibria bulk mass density measurements for $CH_4(1)$+$C_nH_{2n+2}(2)$ mixtures at 344.15 K* and different pressures.

$CH_4(1)$+$C_{10}H_{22}(2)$			$CH_4(1)$+$C_{12}H_{26}(2)$		
P (MPa)	ρ_L (kg/m^3)	ρ_V (kg/m^3)	P (MPa)	ρ_L (kg/m^3)	ρ_V (kg/m^3)
0.10	705.249	1.091	0.10	724.638	0.849
0.30	704.498	2.708	0.32	725.040	2.180
5.00	684.184	31.965	1.99	718.996	12.070
10.00	661.958	64.209	3.99	712.254	24.170
15.00	639.581	98.494	6.10	705.530	37.660
19.86	617.754	133.601	8.04	699.513	50.350
			10.05	693.255	63.640
			12.06	686.783	76.710
			14.07	679.906	90.350
			16.06	672.508	103.650
			18.03	664.424	116.860
			20.02	655.305	130.090
$CH_4(1)$+$C_{14}H_{30}(2)$			$CH_4(1)$+$C_{16}H_{34}(2)$		
P (MPa)	ρ_L (kg/m^3)	ρ_V (kg/m^3)	P (MPa)	ρ_L (kg/m^3)	ρ_V (kg/m^3)
0.10	740.324	1.876	0.10	752.266	0.565
0.34	740.905	2.316	0.36	752.073	2.883
1.98	737.221	11.724	2.02	750.434	12.039
4.09	733.282	24.714	4.04	747.617	24.598
6.08	729.692	37.209	6.09	744.027	37.410
8.05	725.749	50.035	8.01	740.176	49.697
10.04	721.079	63.096	10.02	735.829	62.851
12.06	715.544	76.439	12.03	731.349	76.129
14.16	709.079	90.450	14.07	726.865	89.557
16.02	703.059	102.570	16.04	722.786	102.358
18.06	696.687	115.764	18.04	719.086	115.110
20.12	691.300	140.713	20.01	716.061	127.385

*The standard uncertainties are $u(P) = 0.03$ kPa and $u(T) = 0.1$ K. Instrument standard uncertainty is $\rho = 0.4$ kg/m^3. The combined expanded uncertainty (considering a 0.95 level of confidence, $k = 2$) is $U(\rho) = 1.1$ kg/m^3.

In order to compare the reported experimental data, the theoretical predictions, and the MD results, Figure 4.1 shows the pressure−mass density ($P - \rho$) diagrams for each binary mixture. This figure includes the liquid and vapor mass saturated densities as a function of pressure measured in this work (*cf.* Table 4.4), the SAFT-VR-Mie EoS predictions, MD results (*cf.* Table 4.5) as well as the experimental data previously reported by [5] and [16] for methane + n-decane, and MD results for methane + n-decane from [7].

Figure 4.1 (a) (CH_4+$C_{10}H_{22}$) compares visually the experimental data with previous results from the literature. No apparent systematic error is seen, as our results fall between those of Ref. [5], [7] and [16]. Fig. 4.1 also present a direct comparison between the three methodologies (*i.e.*, experimental

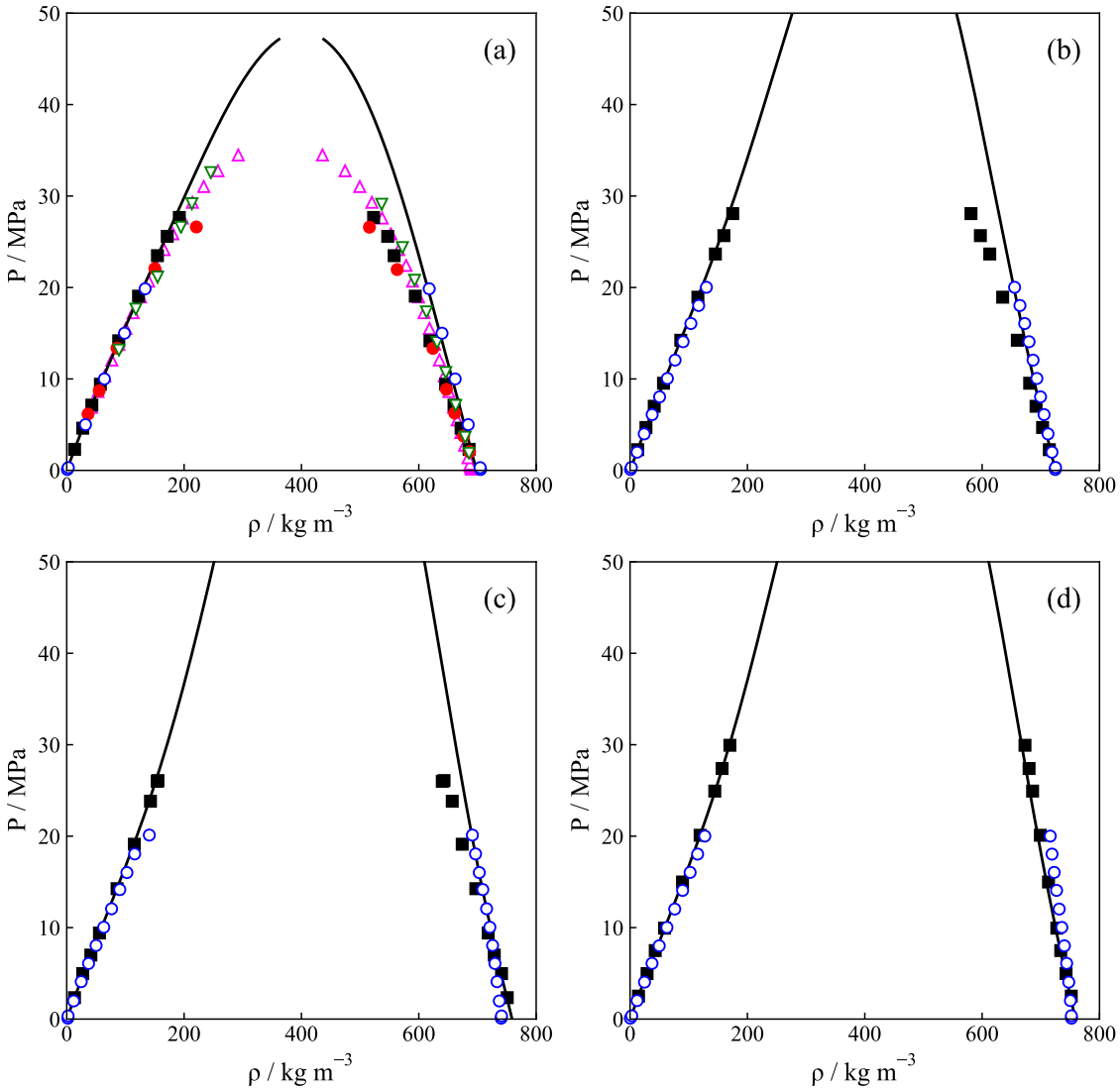

Figura 4.1: Pressure–mass density ($P - \rho$) diagram for $CH_4(1)$+$C_nH_{2n+2}(2)$ mixtures at 344.15 K. (a) CH_4+$C_{10}H_{22}$; (b) CH_4+$C_{12}H_{26}$; (c) CH_4+$C_{14}H_{30}$; (d) CH_4+$C_{16}H_{34}$. −, SAFT-VR-Mie EoS with binary interaction parameter, k_{12}, given in Table 4.3. Experimental data: ○ (blue), this work; △ (pink), [16]; ▽ (green), [5]; MD simulations: ■, this work; ● (red), [7].

Tabla 4.5: Phase equilibria results from molecular dynamics for $CH_4(1)+C_nH_{2n+2}(2)$ mixtures at 344.15 K and different pressures. The error estimation is explained in the text. 1.2(3) refers to 1.2 ± 0.3

$CH_4(1)+C_{10}H_{22}(2)$			$CH_4(1)+C_{12}H_{26}(2)$		
P (MPa)	ρ_L (kg/m^3)	ρ_V (kg/m^3)	P (MPa)	ρ_L (kg/m^3)	ρ_V (kg/m^3)
2.298(6)	685.7(6)	13.41(4)	2.266(8)	714.5(5)	13.02(7)
4.612(9)	672(1)	27.25(6)	4.69(1)	703(1)	27.09(9)
7.14(2)	660.0(8)	42.8(1)	7.01(1)	691.9(2)	41.2(1)
9.42(2)	645.7(9)	57.4(1)	9.53(2)	681(2)	57.0(2)
14.17(2)	619(2)	88.6(2)	14.23(4)	660(1)	86.42(9)
19.05(3)	594(2)	122.4(3)	18.94(4)	635(2)	115.6(2)
23.48(4)	558(2)	154.6(7)	23.66(5)	613(2)	145.4(5)
25.59(6)	547(3)	171.3(8)	25.67(5)	597(2)	159.9(4)
27.66(1)	523(2)	191.9(9)	28.08(5)	581(2)	175.0(9)
$CH_4(1)+C_{14}H_{30}(2)$			$CH_4(1)+C_{16}H_{34}(2)$		
P (MPa)	ρ_L (kg/m^3)	ρ_V (kg/m^3)	P (MPa)	ρ_L (kg/m^3)	ρ_V (kg/m^3)
2.341(6)	750.7(9)	13.25(4)	2.51(1)	751.9(7)	14.4(2)
4.97(1)	741(1)	27.27(5)	4.975(8)	743(1)	29.0(2)
7.00(2)	728.6(9)	41.12(5)	7.49(2)	734(8)	42.92(6)
9.41(2)	718.2(7)	55.78(7)	9.94(2)	727.3(8)	58.8(1)
14.26(2)	697.2(9)	85.8(1)	14.99(2)	713.1(6)	89.4(1)
19.12(3)	674(2)	115.2(2)	20.10(2)	699.2(8)	119.4(1)
23.82(3)	657(2)	142.7(3)	24.93(3)	686.0(8)	144.4(3)
26.00(5)	640(2)	154.3(3)	27.40(2)	680(1)	156.8(2)
26.08(4)	643(2)	155.4(4)	29.94(3)	673(2)	170.1(4)

determination, theoretical modeling and MD simulation). According to the results, the vapor mass density increases, whereas the liquid mass density decreases as the pressure increases or the molecular chain decreases. It is also observed that the density difference($\rho^L - \rho^V$) increases as the molecular chain length increases. This general behavior agrees with the expected results and is validated from the three used approaches.

Table 4.6 summarizes the Absolute Average Deviation (AAD) for theoretical predictions and MD simulations. From Fig. 4.1 and Table 4.6, an excellent agreement is observed between both methodologies. The results of MD and theoretical calculations are purposely not fitted to the experimental results but are based on the previously available information of the methane-alkane systems. The predictive and transferable nature of the models is an aspect we want to highlight in this contribution. However, it is noted that the SAFT-VR-Mie results considerably deviates near the mixture's critical point. This deviation is a known deficiency of molecular-based EoS whose parameters do not consider the critical point, but it can be solved by incorporating crossover treatments or by using an EoS parametrized at the critical point as it was demonstrated by [5] and [7, 8]using an optimized Peng-Robinson EoS. [59]

In order to compare the results reported here (*i.e.*, experimental determination, theoretical predictions and MD results), the values of the bulk density of vapor and liquid phases are compared to available information at the same conditions. Table 4.7 summarizes the corresponding AAD for the case of methane + n-decane mixture. The bulk densities have been previously measured by [16] at 344.26 K and more recently by [5] at 343.15 K, and reported from MD by [7]

Tabla 4.6: Absolute Average Deviation (%AAD) in liquid (ρ^L) and vapor (ρ^V) mass saturated densities for $CH_4(1)$+$C_nH_{2n+2}(2)$ mixtures at 344.15 K in the whole range of pressures considered.

	$CH_4(1)$+$C_{10}H_{22}(2)$		$CH_4(1)$+$C_{12}H_{26}(2)$	
Method	ρ^L	ρ^V	ρ^L	ρ^V
SAFT-VR-Mie + SGT	0.78	5.39	0.58	5.50
MD	2.95	5.82	2.02	5.02
	$CH_4(1)$+$C_{14}H_{30}(2)$		$CH_4(1)$+$C_{16}H_{34}(2)$	
Method	ρ^L	ρ^V	ρ^L	ρ^V
SAFT-VR-Mie + SGT	0.73	7.44	0.34	7.38
MD	1.97	11.30	1.26	6.01

Tabla 4.7: Absolute Average Deviation (%AAD) in liquid (ρ^L) and vapor (ρ^V) mass saturated densities for $CH_4(1)$+$C_{10}H_{22}(2)$ mixture at 344.15 K. References indicate the works in the literature used to compare our measurements, theoretical predictions and computer simulation values.

Method	ρ^L	ρ^V
Densimetry	2.06 [5]	2.72 [5]
	2.77 [16]	0.86 [16]
SAFT-VR-Mie + SGT	2.41 [5]	8.25 [5]
	1.43 [16]	2.76 [16]
MD	1.25 [7]	4.91 [7]

From the Table 4.7 is possible to observe that the reported experimental density of liquid and vapor bulk phases agree to previous densimetry values, the theoretical approach reproduces the experimental values within the expected deviations, and the reported MD agree with other MD simulations. However, we point out feat this work employs a CG force field that has an apparent lower fidelity than the UA force field employed in Ref. [7] which requires significantly over computational resources.

4.5.2 Interfacial Tensions

In this work, the three-pronged approach has been used to describe the variation of the interfacial tension with the pressure at the same isothermal condition as the bulk fluid densities. Tables 4.8 and 4.9 collect the tensiometry data and MD results, respectively.

Figure 4.2 displays the interfacial tension-pressure ($\gamma - P$) diagram for CH_4 + n-alkanes ($C_{10}H_{22}$, $C_{12}H_{26}$, $C_{14}H_{30}$ and $C_{16}H_{34}$) mixtures at 344.15 K. This figure includes interfacial tensions measured in this work (*cf.* Table 4.8), SAFT-VR-Mie EoS coupled to SGT calculations, MD results (*cf.* Table 4.9), as well as the available information (*i.e.*, tensiometry data for methane + n-decane, [5, 17] and MD results for methane + n-decane [7])

From Fig. 4.2, it is possible to observe that the interfacial tension, γ, decreases as the pressure increases and its value tends to zero as the pressure tends to its critical value. Additionally, at a fixed isobaric condition, the interfacial tension increases as the molecular chain increases, as it is expected. Comparing the reported results, a good agreement is observed between the three approaches presented herein from 0.1 to 10 MPa, but the agreement worsens at high pressures due to the inability of the models to describe the fluid behavior near the critical region. This fact has been noted for densities,

Tabla 4.8: Interfacial tension measurements for $CH_4(1)+C_nH_{2n+2}(2)$ mixtures at 344.15 K* and different pressures.

$CH_4(1)+C_{10}H_{22}(2)$		$CH_4(1)+C_{12}H_{26}(2)$		$CH_4(1)+C_{14}H_{30}(2)$		$CH_4(1)+C_{16}H_{34}(2)$	
P (MPa)	γ (mN/m)	P (MPa)	γ (mN/m)	P (MPa)	γ (mN/m)	P (MPa)	γ (mN/m)
0.10	18.96	0.10	20.70	0.10	22.03	0.10	23.02
0.30	18.40	0.32	19.63	0.34	21.71	0.36	22.66
5.00	13.03	1.99	18.03	1.98	19.20	2.02	20.78
10.00	9.29	3.99	15.95	4.09	16.70	4.04	18.51
15.00	5.51	6.10	13.87	6.08	13.80	6.09	16.24
19.86	3.69	8.04	12.31	8.05	11.36	8.01	14.18
		10.05	10.89	10.04	9.74	10.02	12.13
		12.06	9.48	12.06	8.51	12.03	10.21
		14.07	8.08	14.16	7.41	14.07	8.42
		16.06	6.81	16.02	6.53	16.04	6.89
		18.03	5.72	18.06	5.62	18.04	5.54
		20.02	4.78	20.12	4.76	20.01	4.46

* The standard uncertainties are $u(P) = 0.03\,\text{kPa}$ and $u(T) = 0.1\,\text{K}$. Instrument standard uncertainty is $\gamma = 0.05$ mN/m. The combined expanded uncertainty (considering a 0.95 level of confidence, $k = 2$) is $U(\gamma) = 0.03\,\text{mN/m}$.

which directly impact the interfacial tension results. Additionally, the reported results show that as the molecular chain length increases, the deviation with respect to experimental data increases. This is presumably a consequence of the fact that as molecular chain length increases, additional restrictions, such as intramolecular interactions (bond stretching and angle bending), which are not included, become incresingly relevant. In this work, we opted for a fully predictive and complete transferable approach between the theoretical modeling and molecular simulation, but further refinements can be incorporated by including these restrictions, as was demonstrated by one of us. [60] The corresponding statistical deviations are summarized in Table 4.10, where the deviations are reported from 0.1 to 10 MPa (%ADD-γ_{hr}) and over the full pressure range (%AAD-γ). The corresponding statistical deviations are summarized in Table 4.10, where the deviations are reported from 0.1 to 10 MPa (%ADD-γ_p) and over the full pressure range (%AAD-γ_T).

Tabla 4.10: Absolute Average Deviation (%AAD) in interfacial tension (γ) for $CH_4(1)+C_nH_{2n+2}(2)$ mixtures at 344.15 K and different range of pressure as indicated in the text.

	$CH_4(1)+C_{10}H_{22}(2)$		$CH_4(1)+C_{12}H_{26}(2)$	
Method	%AAD-γ_P	%AAD-γ_T	%AAD-γ_P	%AAD-γ_T
SAFT VR Mie + SGT	3.43	14.12	4.67	12.04
MD	3.99	13.17	8.56	15.98
	$CH_4(1)+C_{14}H_{30}(2)$		$CH_4(1)+C_{16}H_{34}(2)$	
Method	%AAD-γ_P	%AAD-γ_T	%AAD-γ_P	%AAD-γ_T
SAFT VR Mie + SGT	15.95	32.73	5.67	31.41
MD	26.44	41.63	15.97	32.29

The results reported in Tables 4.8 and 4.9, and statistics reported in Table 4.10 are in very good

Tabla 4.9: Interfacial tension from molecular dynamics for $CH_4(1)$+$C_nH_{2n+2}(2)$ mixtures at 344.15 K and different pressures. The error estimation is explained in the text. 1.2(3) refers to 1.2 ± 0.3

$CH_4(1)$+$C_{10}H_{22}(2)$		$CH_4(1)$+$C_{12}H_{26}(2)$		$CH_4(1)$+$C_{14}H_{30}(2)$		$CH_4(1)$+$C_{16}H_{34}(2)$	
P (MPa)	γ (mN/m)	P (MPa)	γ (mN/m)	P (MPa)	γ (mN/m)	P (MPa)	γ (mN/m)
2.298(6)	17.4(2)	2.266(8)	19.2(2)	2.341(6)	20.8(2)	2.51(1)	22.0(1)
4.612(9)	14.7(1)	4.69(1)	16.6(2)	4.97(1)	18.4(2)	4.975(8)	20.0(3)
7.14(2)	12.7(2)	7.01(1)	14.4(2)	7.00(2)	15.6(2)	7.49(2)	16.7(2)
9.42(2)	10.8(2)	9.53(2)	12.1(2)	9.41(2)	13.9(1)	9.94(2)	15.1(2)
14.17(2)	7.6(1)	14.23(4)	8.7(1)	14.26(2)	10.2(1)	14.99(2)	11.4(3)
19.05(3)	4.9(1)	18.94(4)	6.4(1)	19.12(3)	7.4(2)	20.10(2)	8.8(2)
23.48(4)	2.9(1)	23.66(5)	4.6(1)	23.82(3)	5.5(1)	24.93(3)	7.0(2)
25.59(6)	2.1(2)	25.67(5)	3.44(9)	26.00(5)	4.7(1)	27.40(2)	6.0(1)
27.66(1)	1.5(1)	28.08(5)	2.8(1)	26.08(4)	4.8(1)	29.94(3)	5.48(9)

agreement with the available tensiometry for the methane + n-decane mixture from experimental determinations, [4, 5, 12, 16, 51, 52, 61] theoretical predictions from SGT, [5–7] and from DFT combined with SAFT, [9] as well as from molecular simulations of [7, 8] A summary of this comparison is collected in Table 4.11, which compares the corresponding %AAD-γ_P and %AAD-γ_T.

Tabla 4.11: Absolute Average Deviation (%ADD) in the interfacial tension (γ) for $CH_4(1)$+$C_{10}H_{22}(2)$ mixture at 344.15 K and different range of pressure as indicated in the text.

Method	%AAD-γ_P	%AAD-γ_T
Tensiometry	———	3.77 [5]
	———	6.55 [17]
SAFT VR Mie + SGT	10.15 [5]	35.49 [5]
	0.89 [17]	48.33 [17]
	8.38 [7]	22.49 [7]

4.5.3 Interfacial profiles: the $z - \rho_i$ projections

In addition to the bulk phase densities and interfacial tensions, theoretical modeling, and MD simulation provide a route to explore interfacial properties such as the concentration profiles in the direction normal to the interface (the $z - \rho_i$ projections), from which surface activity or absolute adsorption of species in the interfacial region can be evaluated. Specifically, Figure 4.3 showcases the $z - \rho_i$ projections for three different pressures (or equivalently liquid molar fractions) as obtained from the SGT and the CG MD simulations.

In this latter figure, only one vapor-liquid interface is displayed, as the system is symmetric. In the density profiles, a positive surface activity (or absolute adsorption) is seen for CH_4 (*i.e.*, $d\rho_1/dz = 0$; $d^2\rho_1/dz^2 < 0$ in the interfacial region), whereas C_nH_{2n+2} does not exhibit surface activity (or absolute adsorption). From this figure, it is noted that the CH_4 surface activity increases as its liquid mole fraction or equilibrium pressure increases. Comparing the surface activity of CH_4, it is possible to observe that a fixed pressure, the maximum value increases as the molecular chain length increases. The SGT predictions are confirmed by the MD simulations, and agree with observations reported by [5–7, 9]. The MD results in Fig. 4.3 exhibit a slight sub-prediction of the profiles, which is caused,

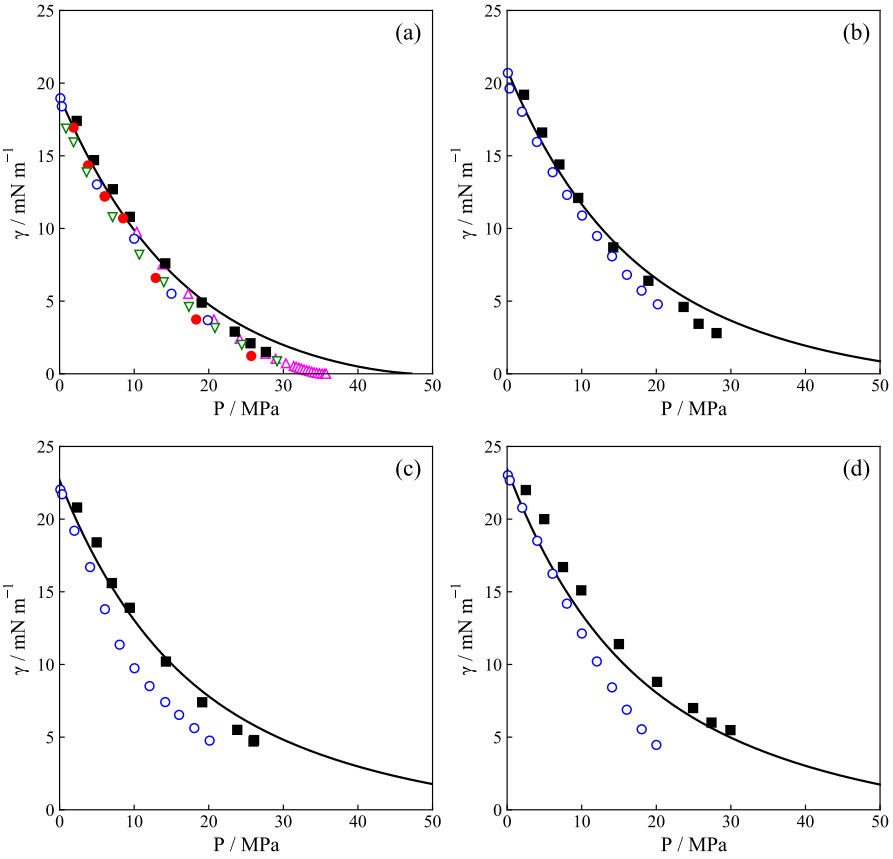

Figura 4.2: Interfacial–Pressure ($\gamma - P$) diagram for $CH_4(1)$+$C_nH_{2n+2}(2)$ mixtures at 344.15 K. (a) CH_4+$C_{10}H_{22}$; (b) CH_4+$C_{12}H_{26}$; (c) CH_4+$C_{14}H_{30}$; (d) CH_4+$C_{16}H_{34}$. 2501, SAFT-VR Mie EoS combined with SGT with binary interaction parameter, k_{12}, given in Table 4.3. Experimental data: ○ (blue), this work; △ (pink), [17]; ▽ (green), [5]; MD simulations: ■, this work; ● (red), [7].

in part, by the inaccuracies in the determination of the bulk phases, especially at the highest pressures considered.

Considering the definition of enrichment of component i at the interface, E_i, introduced by [62] (*i.e*, $E_i = \max(\rho_i(z))/\max\left(\rho_i^V, \rho_i^L\right)$), it is observed that E_{CH_4} decreases as the pressure increases but its approximately constant with the increment of the molecular chain of the larger hydrocarbon. Finally, comparing the surface activity (absolute adsorption) of CH_4 in CH_4+C_nH_{2n+2} mixtures to CO_2 in CO_2+C_nH_{2n+2} mixtures at same isothermal and isobaric conditions, [23, 37], it is possible to conclude that CO_2 displays higher surface activity than CH_4. In fact, it is observed that $E_{CO_2} \approx 2 \times E_{CH_4}$.

4.5.4 Relative Gibbs adsorption isotherm

The surface activity of CH_4 observed in $CH_4(1)$ + $C_nH_{2n+2}(2)$ mixtures can be quantified by means of the relative Gibbs adsorption isotherm, Γ_{12}, of $CH_4(1)$ with respect to $C_nH_{2n+2}(2)$ (see Eqs.(4.3)

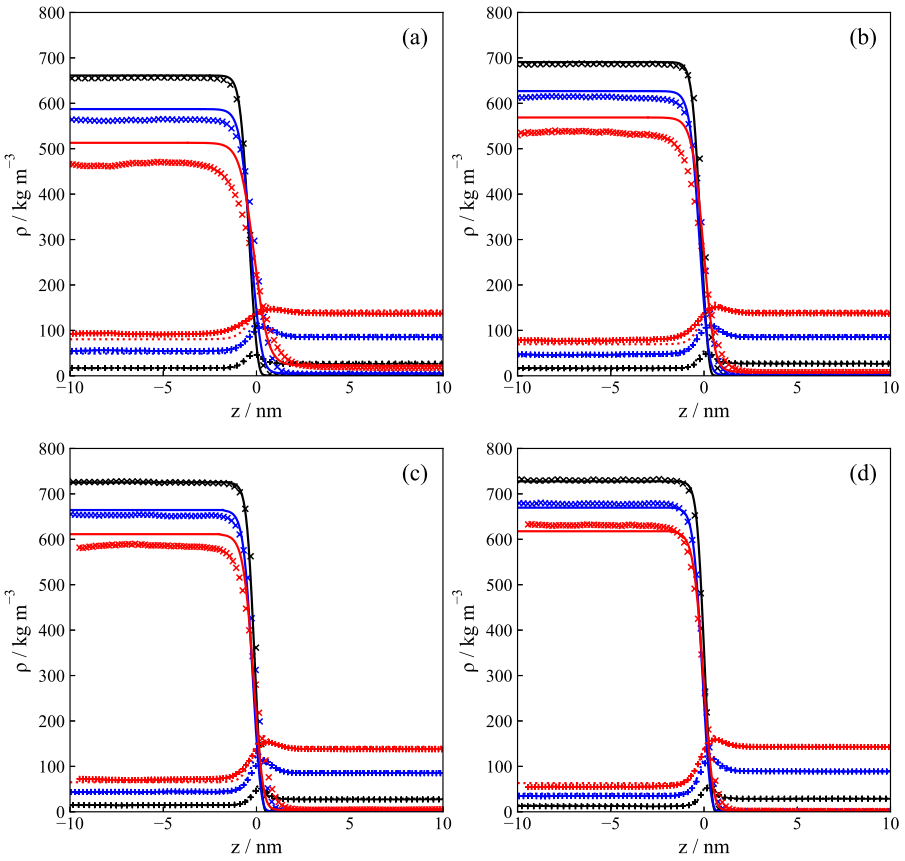

Figura 4.3: Density profiles of the (a) CH_4+$C_{10}H_{22}$, (b) CH_4+$C_{12}H_{26}$, (c) CH_4+$C_{14}H_{30}$ and (d) CH_4+$C_{16}H_{34}$ mixtures at 344.15 K and 5 (black), 15 (blue) and 25 MPa (red). Continous and dotted curves correspond to predictions as obtained from the SAFT-VR Mie combined with SGT with binary interaction parameter k_{12} given in Table 4.3 for components 2 and 1, respectively. MD computer simulation results are represented by + and n-alkane by x for CH_4 and n-alkanes, respectively.

and (4.17)). Figure 4.4 displays the variation of Γ_{12} as a function of pressure obtained in this work by using the three approaches. This figure also includes experimental results reported by [5] and MD results from Choudhary *et al.*, [7]

From these results, it is possible to observe that although Γ_{12} increases as the pressure increases, it reaches a maximum value. This maximum in Γ_{12} reflects an adsorption saturation limit. The Γ_{12} behavior predicted by SGT is confirmed by MD results as well as the approximate approach obtained from experimental data and the theoretical and MD results of [5, 7]. Γ_{12} is similar for all CH_4 + n-alkane mixtures, as is expected from the results reported in Sec. 4.5.3. However, it is noted that the Gibbs relative adsorption displays the same behavior for all mixtures until it reaches the maximum value. Past this point, the Gibbs relative adsorption decreases sharply as the molecular chain length decreases.

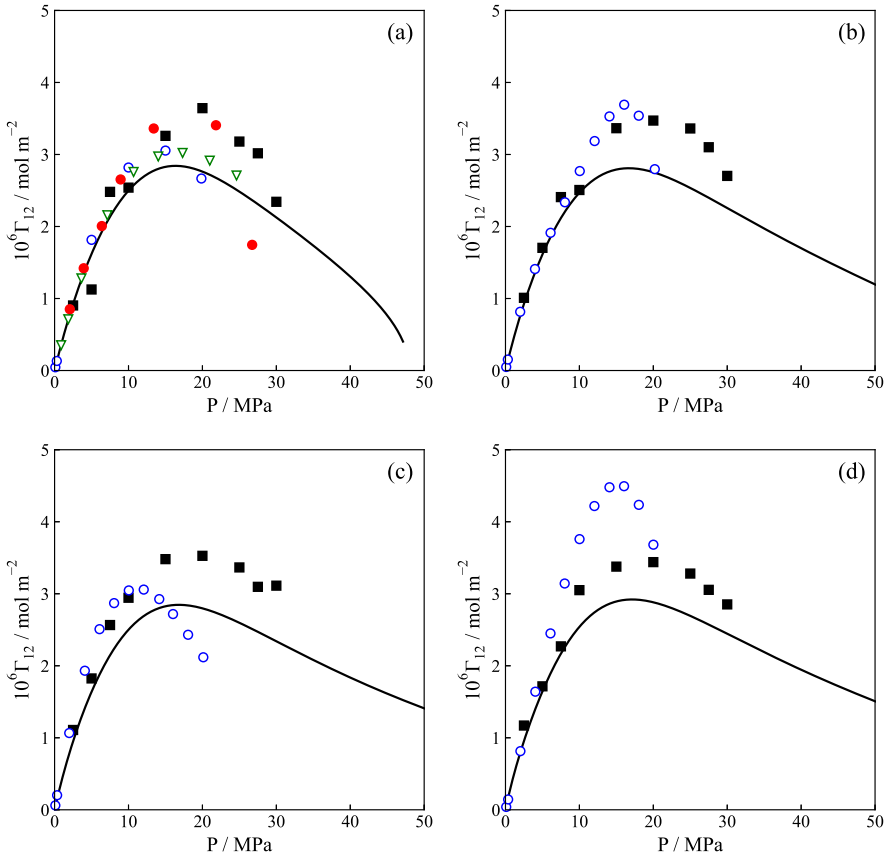

Figura 4.4: Relative Gibbs adsorption isotherm, Γ_{12}, for $CH_4(1) + C_nH_{2n+2}(2)$ mixtures at 344.15 K as a function of pressure, P.(a) CH_4+$C_{10}H_{22}$; (b) CH_4+$C_{12}H_{26}$; (c) CH_4+$C_{14}H_{30}$; (d) CH_4+$C_{16}H_{34}$. 2501, SAFT-VR Mie EoS combined with SGT with binary interaction parameter, k_{12}, given in Table 4.3 and Eq. 4.17; ○ (blue), Eq. 4.3 and the tensiometry data; ■, MD (Eq. 4.17); ▽ (green), [5]; ● (red), [7].

4.6 Conclusions

In this work, the bulk phase equilibria (*i.e.*, pressure, liquid and vapor mass densities) and interfacial properties (*i.e.*, interfacial concentration, adsorption and interfacial tension) for methane + n-alkane (*i.e.*, n-decane, n-dodecane, n-tetradecane, n-hexadecane) binary mixtures have been described by using experimental determinations, predictive theoretical modeling and MD simulation at the isothermal condition of 344.15 K and over a broad pressure range., observed a good agreement between the three approaches. The results show that the vapor mass density increases, whereas the liquid mass density and interfacial tension decrease as either the pressure increases or the length of molecular chain increases. This general behavior is expected and is exhibited across all three approaches. Interfacial profiles show a positive surface activity (or absolute adsorption) of methane on the interfacial region increasing as the pressure (or liquid mole fraction of methane) increases, whereas longer n-alkanes

do not exhibit surface activity. This behavior is reproduced by the theoretical results and molecular simulations and shows up in the relative Gibbs adsorption isotherm of methane on the n-alkane. These latter results show that the methane relative adsorption increases as the pressure increases and then reaches a maximum value. This maximum value reflects an adsorption saturation limit of methane. It is noted that the simulations and the equation of state should provide, by design, the same resulting volumetric properties over a wide range of parameters capable of representing both simple and very assymetric mixtures. However, the results shown here and other recentely reported in the literature (see for instances [63] and [64]) suggest that the critical region of mixtures is not accurately captured by the equation of state in a pressure - explicit representation. While this is a common feature of classical analytical equation of state, SAFT-VR-Mie includes a third order perturbation correction that allows the accurate depiction of the critical region for the monomer term. Notwithstanding, the treatment of mixtures might have to be revised.

4.7 Declaration of Competing Interest

The authors declare that they have no known competing financial interests or personal relationships that could have appeared to influence the work reported in this paper.

4.8 Acknowledgement

This work was financed by FONDECYT, Santiago, Chile (Project. 1190107). E.A.M. acknowledges the support from The U.K. EPSRC through research grants to the Molecular Systems Engineering group (grant nos. EP/E016340, EP/J014958). The authors also acknowledge the Centro de Supercomputación de Galicia (CESGA, Santiago de Compostela, Spain) for providing access to computing facilities, and Spanish Ministerio de Economía, Industria y Competitividad (Grant No. FIS2017–89361-C3-1-P), Junta de Andalucía (Grant No. P20-00363), both co-financed by EU FEDER funds, and Universidad de Huelva.

Bibliography

[1] J. G. Speight, *The Chemistry and Technology of Petroleum.* CRC Press, 2014.

[2] P. van Konynenburg and R. Scott, "Critical lines and phase equilibria in binary van der waals mixtures," *Philos. Trans. R. Soc. London, Ser. A*, vol. 298, p. 495, 1980.

[3] A. J. Davenport and J. S. Rowlinson, "The solubility of hydrocarbons in liquid methane," *Trans. Faraday Soc.*, vol. 59, p. 78, 1963.

[4] M. P. W. M. Rijkers, *Retrograde condensation of lean natural gas.* PhD thesis, Delft University of Technology, 1991.

[5] L. M. C. Pereira, A. Chapoy, R. Burgass, and B. Tohidi, "Measurement and modelling of high pressure density and interfacial tension of (gas + n-alkane) binary mixtures," *J. Chem. Thermodyn.*, vol. 97, p. 55, 2016.

[6] C. Miqueu, B. Mendiboure, C. Graciaa, and J. Lachaise, "Modelling of the surface tension of binary and ternary mixtures with the gradient theory of fluid interfaces.," *Fluid Phase Equilibria*, vol. 218, p. 189, 2004.

[7] N. Choudhary, A. K. N. Nair, M. F. A. C. Ruslan, and S. Sun, "Bulk and interfacial properties of decane in the presence of carbon dioxide, methane, and their mixture.," *Sci. Rep.*, vol. 9, p. 19784, 2019.

[8] N. Choudhary, M. F. A. C. Ruslan, A. K. N. Nair, and S. Sun, "Bulk and interfacial properties of alkanes in the presence of carbon dioxide, methane, and their mixture.," *Ind. Eng. Chem.*, vol. 60, p. 729, 2021.

[9] F. Llovell, A. Galindo, F. J. Blas, and G. Jackson, "Classical density functional theory for the prediction of the surface tension and interfacial properties of fluids mixtures of chain molecules based on the statistical associating fluid theory for potentials of variable range.," *J. Chem. Phys.*, vol. 133, p. 024704, 2010.

[10] G. DECHEMA Gesellschaft fur Chemische Technik und Biotechnologie e.V., Frankfurt am Main, "Dechema gesellschaft fur chemische technik und biotechnologie e.v., frankfurt am main, germany." http://i-systems.dechema.de/detherm/mixture.php/, 2021.

[11] M. Glaser, C. J. Peters, H. J. van der Kooi, and R. N. Lichtenthaler, "Phase equilibria of methane + n-hexadecane and (p, vm, t) of n-hexadecane," *J. Chem. Thermodyn.*, vol. 17, p. 803, 1985.

[12] M. P. W. M. Rijkers, M. Malais, C. J. Peters, and J. de Swaan Aron, "Measurements on the phase behavior of binary hydrocarbon mixtures for modelling the condensation behavior of natural gas. part i. the system methane + decane," *Fluid Phase Equilibria*, vol. 71, p. 143, 1992.

[13] M. P. W. M. Rijkers, V. B. Maduro, C. J. Peters, and J. de Swaan Aron, "Measurements on the phase behavior of binary mixtures for modeling the condensation behavior of natural gas. part ii. the system methane + dodecane," *Fluid Phase Equilibria*, vol. 72, p. 309, 1992.

[14] V. V. de Leeuw, T. W. de Loos, H. A. Kooijman, and J. de Swaan Arons, "The experimental determination and modelling of vle for binary subsystems of the quaternary system n2 + ch4 + c4h10 + c14h30 up to 1000 bar and 440 k," *Fluid Phase Equilibria*, vol. 73, p. 285, 1992.

[15] M. P. W. M. Rijkers, C. J. Peters, and J. de Swaan Arons, "Measurements on the phase behavior of binary mixtures for modeling the condensation behavior of natural gas: Part iii. the system methane + hexadecane," *Fluid Phase Equilibria*, vol. 85, p. 335, 1993.

[16] H. H. Reamer, R. H. Olds, B. H. Sage, and W. N. Lacey, "Phase equilibria in hydrocarbon systems: Methane-decane system.," *Ind. Eng. Chem.*, vol. 34, p. 1526, 1942.

[17] G. L. Stegemeier, B. F. Pennington, E. B. Brauer, and E. W. Hough, "Interfacial tension of the methane-normal decane system," *SPE J.*, vol. 000, p. 257, 1962.

[18] J. D. van der Waals, "Thermodynamische theorie der kapillarita? unter voraussetzung stetiger dichtea?derung," *Zeit.Phys.Chem.*, vol. 13, p. 657, 1893.

[19] H. T. Davis and L. E. Scriven, "Stress and structure in fluid interfaces," *Adv. Chem. Phys.*, vol. 49, p. 357, 1982.

[20] J. S. Rowlinson and B. Widom, *Molecular Theory of Capillarity*. Oxford University Press, 1998.

[21] T. Lafitte, A. Apostolakou, C. Avendaño, A. Galindo, C. S. Adjiman, E. A. Müller, and G. Jackson, "Accurate statistical associating fluid theory for chain molecules formed from mie segments," *J. Chem. Phys.*, vol. 139, p. 154504, 2013.

[22] E. A. Müller and G. Jackson, "Force-field parameters from the saft-? equation of state for use in coarse-grained molecular simulations," *Annu. Rev. Chem. Biomol. Eng.*, vol. 5, p. 405, 2014.

[23] A. Mejía, M. Cartes, H. Segura, and E. A. Müller, "Use of equations of state and coarse grained simulations to complement experiments: describing the interfacial properties of carbon dioxide + decane and carbon dioxide + eicosane mixtures," *J. Chem. Eng. Data*, vol. 59, p. 2928, 2014.

[24] H. Cárdenas and A. Mejía, "Phase behavior and interfacial properties of ternary system co2 + n-butane + n- decane: Coarse-grained theoretical modeling and molecular simulations.," *Mol. Phys.*, vol. 114, p. 2627, 2016.

[25] J. M. Garrido, M. Cartes, H. Segura, and A. Mejía, "Coarse-grained theoretical modeling and molecular simulations of nitrogen + n-alkanes: (n-pentane, n-hexane, n-heptane, n-octane)," *Journal of Supercritical Fluids*, vol. 129, p. 83, 2017.

[26] E. A. Müller and A. Mejía, "Extension of the saft-vr mie eos to model homonuclear rings and its parameterization based on the principle of corresponding states.," *Langmuir*, vol. 33, p. 11518, 2017.

[27] G. Alonso, G. Chaparro, M. Cartes, E. A. Müller, and A. Mejía, "Probing the interfacial behavior of type iiia binary mixtures along the three-phase line employing molecular thermodynamics.," *Molecules*, vol. 25, p. 1499, 2020.

[28] A. Mejía, J. Pàmies, D. Duque, H. Segura, and L. F. Vega, "Phase and interface behavior in type i and type v lennard-jones mixtures: Theory and simulations.," *J. Chem. Phys.*, vol. 123, p. 034505, 2005.

[29] A. Mejía and L. F. Vega, "Perfect wetting along a three-phase line: Theory and molecular dynamics simulations.," *J. Chem. Phys.*, vol. 124, p. 2445051, 2006.

[30] S. Stephan, K. Langenbach, and H. Hasse, "Interfacial properties of binary lennard- jones mixtures by molecular simulation and density gradient theory.," *J. Chem. Phys.*, vol. 150, p. 174704, 2019.

[31] S. Stephan and H. Hasse, "Interfacial properties of binary mixtures of simple fluids and their relation to the phase diagram.," *Phys. Chem. Chem. Phys*, vol. 22, p. 12544, 2020.

[32] S. Stephan, K. Langenbach, and H. Hasse, "Quantifying the effect of polar interactions on the behavior of binary mixtures: Phase, interfacial, and excess properties.," *J. Chem. Phys.*, vol. 154, p. 164503, 2021.

[33] V. Diky, R. D. Chirico, M. Frenkel, A. Bazyleva, J. W. Magee, E. Paulechka, A. Kazakov, E. W. Lemmon, C. D. Muzny, A. Y. Smolyanitsky, S. Townsend, and K. Kroenlein, *Thermo Data Engine (TDE) version 10.1 (Pure compounds, Binary mixtures, Ternary mixtures and Chemical reactions). NIST Standard Reference Database 103b. Thermodynamics Research Center (TRC).* Applied Chemicals and Material Division. Standard Reference Data Program, National Institute of Standards and Technology (NIST), 2016.

[34] A. Goodwin, K. N. Marsh, and W. A. Wakeham, *Measurement of the Thermodynamic Properties of Single Phases.* Elsevier, 2003.

[35] M. Cartes, G. Chaparro, and A. Mejía, "A novel experimental procedure to measure the bulk mass densities and interfacial tensions for mixtures at vapor-liquid-liquid equilibria.," *J. Chem. Eng. Data*, vol. 65, p. 3344, 2020.

[36] J. M. Garrido, L. Cifuentes, M. Cartes, H. Segura, and A. Mejía, "High-pressure interfacial tensions for nitrogen + ethanol, or hexane or 2-methoxy-2-methylbutane. a comparison between experimental tensiometry and monte carlo simulations," *Journal of Supercritical Fluids*, vol. 89, p. 78, 2014.

[37] C. Cumicheo, M. Cartes, H. Segura, E. A. Müller, and A. Mejía, "High-pressure densities and interfacial tensions of binary systems containing carbon dioxide + n-alkanes: (n-dodecane, n-tridecane, n-tetradecane)," *Fluid Phase Equilibria*, vol. 380, p. 82, 2014.

[38] C. Cumicheo, M. Cartes, E. A. Müller, and A. Mejía, "Experimental measurements and theoretical modeling of high-pressure mass densities and interfacial tensions of carbon dioxide + n-heptane + toluene and its carbon dioxide binary systems," *Fuel*, vol. 228, p. 92, 2018.

[39] J. Algaba, J. M. Garrido, J. M. Míguez, A. Mejía, I. Moreno-Ventas Bravo, and F. J. Blas, "Interfacial properties of tetrahydrofuran and carbon dioxide mixture from computer simulation," *J. Phys. Chem. C*, vol. 122, p. 16142, 2018.

[40] J. M. Garrido, M. Cartes, A. Mejía, J. Algaba, J. M. Míguez, I. Moreno-Ventas Bravo, M. M. Piñeiro, and F. J. Blas, "Measurement and modeling of high pressure density and interfacial tension of carbon dioxide + tetrahydrofuran mixture," *Journal of Supercritical Fluids*, vol. 128, p. 359, 2017.

[41] J. M. Andreas, E. A. Hauser, and W. B. Tucker, "Boundary tension by pendant drops," *J. Chem. Phys.*, vol. 42, p. 1001, 1938.

[42] A. I. Rusanov and V. A. Prokhorov, *Interfacial Tensiometry*. Elsevier, 1996.

[43] M. J. B. Evans, "Measurement of surface and interfacial tension," in *Measurement of the Thermodynamic Properties of Multiple Phases* (R. D. Weir and T. W. de Loos, eds.), Elsevier, 2006.

[44] B. Taylor and C. E. Kuyatt, "Guidelines for evaluating and expressing the uncertainty of nist measurement results," *NIST*, 1994.

[45] W. L. Masterton, J. Blanchi, and J. Slowinski, E. J., "Surface tension and adsorption in gas-liquid systems at moderate pressure," *J. Chem. Phys.*, vol. 67, p. 615, 1962.

[46] G. Mie, "Zur kinetischen theorie der einatomigen körper," *Ann. Phys.*, vol. 316, p. 657, 1903.

[47] A. Mejía, C. Herdes, and E. A. Müller, "Force felds for coarse-grained molecular simulations from a corresponding states correlation," *Ind. Eng. Chem. Res.*, vol. 53, p. 4131, 2014.

[48] Ervik, A. Mejía, and E. A. Müller, "Bottled saft: A web app providing saft-gamma mie force field parameters for thousands of molecular fluids," *J. Chem. Inf. Model*, vol. 56, p. 1609, 2016.

[49] A. Mejía, E. A. Müller, and G. Chaparro, "Sgtpy: A python open-source code for calculating the interfacial properties of fluids based on the square gradient theory using the saft-vr mie equation of state," *J. Chem. Inf. Model*, vol. 61, p. 1244, 2021.

[50] M. L. Michelsen and J. M. Mollerup, *Thermodynamic Models: Fundamentals and Computational Aspects*. Tie-Line Publications, 2007.

[51] J. M. Beaudoin and J. P. Kohn, "Multiphase and volumetric equilibria of the methane-n-decane binary system at temperatures between -36 deg and 150 deg. c.," *J. Chem. Eng. Data*, vol. 12, p. 189, 1967.

[52] S. Srivastan, N. A. Darwish, K. A. M. Gasem, and R. L. Robinson Jr., "Solubility of methane in hexane, decane, and dodecane at temperatures from 311 to 423 k and pressures to 10.4 mpa.," *J. Chem. Eng. Data*, vol. 37, p. 516, 1992.

[53] H. Nourozieh, M. Kariznovi, and J. Abedi, "Vapor-liquid equilibrium measurement and thermodynamic modeling of binary systems methane + n-tetradecane," *Fluid Phase Equilibria*, vol. 318, p. 96, 2012.

[54] J. M. Garrido, M. M. Piñeiro, F. J. Blas, E. A. Müller, and A. Mejía, "Interfacial tensions of industrial fluids from a molecular-based square gradient theory," *AIChE Journal*, vol. 62, p. 1781, 2016.

[55] M. M. Telo da Gama and R. Evans, "The structure and surface tension of the liquid-vapour interface near the upper critical end point of a binary mixture of lennard-jones fluids: I. the two phase region," *Molecular Physics*, vol. 48, p. 229, 1983.

[56] E. A. Müller, Ervik, and A. Mejía, "A guide to computing interfacial properties from molecular simulations.," *Living J. Comp. Mol. Sci.*, vol. 2, p. 21385, 2021.

[57] D. van der Spoel, E. Lindahl, B. Hess, G. Groenhof, A. E. Mark, and H. J. Berendsen, "Gromacs: Fast, flexible, and free.," *J. Comput. Chem.*, vol. 26, p. 1701, 2005.

[58] M. P. Allen and D. J. Tildesley, *Computer Simulation of Liquids*. Oxford University Press, second ed., 2017.

[59] J. N. Jaubert and F. Mutelet, "Vle predictions with the peng-robinson equation of state and temperature dependent kij calculated through a group contribution method," *Fluid Phase Equilibria*, vol. 224, p. 285, 2004.

[60] S. Rahman, O. Lobanova, G. Jiménez-Serratos, C. Braga, V. Raptis, E. A. Müller, G. Jackson, C. Avendaño, and A. Galindo, "Saft?? force field for the simulation of molecular fluids. 5. hetero-group coarse-grained models of linear alkanes and the importance of intramolecular interactions.," *J. Phys. Chem. B*, vol. 122, p. 9161, 2018.

[61] B. H. Sage, H. M. Lavender, and W. N. Lacey, "Phase equilibria in hydrocarbon systems methane-decane system," *Ind. Eng. Chem.*, vol. 32, p. 743, 1940.

[62] S. Becker, S. Werth, M. Horsch, K. Langenbach, and H. Hasse, "Interfacial tension and adsorption in the binary system ethanol and carbon dioxide: Experiments, molecular simulation and density gradient theory.," *Fluid Phase Equilibria*, vol. 427, p. 476, 2016.

[63] A. Aasen, M. Hammer, E. A. Müller, and Wilhelmsen, "Equation of state and force fields for feynman?hibbs-corrected mie fluids. ii. application to mixtures of helium, neon, hydrogen, and deuterium," *J. Chem. Phys.*, vol. 152, p. 074507, 2020.

[64] L. Zheng, F. Bresme, J. P. Martin Trusler, and E. A. Müller, "Employing saft coarse-grained force fields for the molecular simulation of thermodynamic and transport properties of co2?n-alkane mixtures," *J. Chem. Eng. Data*, vol. 65, p. 1159, 2020.

Capítulo 5

Vapour-liquid phase equilibria and interfacial properties of fatty acid methyl esters from molecular dynamics simulations

Abstract

We have determined the phase equilibria and interfacial properties of a methyl ester homologous series (from methyl acetate to methyl heptanoate) using direct simulation of the vapour-liquid interface. The methyl esters are modelled using the united atom approach in combination with transferable parameters for phase equilibria (TraPPE) force fields for alkanes, alkenes, carbon dioxide, ethers, and carboxylic acids in a transferable way. This allows us to take into account explicitly both dispersive and coulombic interactions, as well as the repulsive Pauli-exclusion interactions. Simulations are performed in the NVT or canonical ensemble using molecular dynamics. Vapour-liquid surface tension is determined using the virial route, i.e., evaluating the normal and tangential components of the pressure tensor along the simulation box. We have also calculated density profiles, coexistence densities, vapour pressures, surface entropies and enthalpies, and interfacial thickness as functions of temperature, as well as the normal boiling temperatures and the critical temperatures, densities, and pressures for each member of the series. Special attention is paid to the comparison between experimental data taken from the literature and our results obtained using molecular dynamic simulations. We also analyze the effect of increasing the molecular weight of the methyl esters (at fixed temperature) on all the properties considered, with special emphasis on phase equilibria envelopes and surface tension. The TraPPE force fields transferred from other molecules and chemical families are able to predict very accurately the experimental vapour-liquid phase envelopes of methyl esters. We also compare the results obtained from simulations of the surface tension, with experimental data taken from the literature. To our knowledge, this is the first time that vapour-liquid phase equilibria and interfacial properties, and particularly surface tension, of the methyl esters homologous series are obtained using computer simulation.

5.1 Introduction

Current environmental regulations and energy directives recommend and promote an increase, of at least 10%, the use of renewable fuels for transport by 2020, and also to dramatically reduce the transportation emission levels by 2030 [1]. These initiatives have been motivated to reduce greenhouse gas emissions, where transportation contributes 34% of the total emissions. One of the most groundbreaking alternatives to accomplish these targets is to replace (partially or totally) fossil-fuels with biofuels (fuels produced from natural renewable sources), where one of the most recently emerging biofuels is biodiesel. Biodiesels are considered to be the third (or fourth) generation of biofuels [2] as they are renewable, biodegradable, non-toxic, produce less carbon dioxide than fossil fuels, and also they can replace petroleum diesel and be used either in their neat form or blended with fossil diesel inside of the compression ignition engines without any extensive engine modification. In general terms, biodiesel can be obtained from a group of mono-alkyl esters [3] that, depending on the alcohol (methanol or ethanol) used for the transesterification process, become fatty acid methyl esters (FAMEs) or fatty acid ethyl esters (FAEEs), respectively. From a technical viewpoint, the use of FAMEs as a fuel is more developed than FAEEs [4, 5] for efficient use.

Despite the novel use of FAMEs as diesel fuel, systematic research concerning the characterization of interfacial properties (*e.g.*, the interfacial concentration of species, the interfacial thickness, the superficial enthalpy and entropy, and surface or interfacial tension) of pure FAMEs and mixtures containing FAMEs is very limited. For the case of pure short chain FAMEs (*i.e.*, from methyl acetate to methyl heptanoate), the available experimental data for interfacial tensions reported in DECHEMA [6] and Landolt-Börnstein [7–9] databases and also the DIRPP [10] and NIST data [11], only cover a narrow temperature range (273 K to 360 K). Theoretical models, such as the square gradient theory [12], need the experimental data of interfacial tensions to fit their parameters and use them as a model to predict the other interfacial properties. In the case of mixtures, the scenario is even worse, especially for the case of mixtures of hydrocarbons or aromatics with FAMEs, where interfacial properties are unexplored and only very few sparse data can be found. The only exception is the case of water and FAMEs mixtures, where both experimental determinations and theoretical modeling have been carried out. [13] Therefore, considering the environmental regulations and energy directives, it is necessary to carry out systematic exploration of the interfacial behavior of the compounds involved in biodiesel production. These properties are the key requirement for their future use as a fuel, as well as for environmental issues, such as the removal of contaminants from water and for groundwater remediation [14, 15]. Consequently, this work has focused on the determination of some selected interfacial properties for the case of pure short-chain FAMEs from methyl acetate to methyl heptanoate.

Due to the lack of predictive theories, molecular dynamics (MD) simulations can be used as a predictive tools to explore both bulk properties (*i.e.*, coexistence density curve, $T-\rho$, vapour pressure or Clapeyron curve, $P-T$) and interfacial properties (*e.g.*, interfacial concentration of species, the interfacial thickness, the superficial enthalpy and entropy, and surface or interfacial tension) from low temperature to near the critical point.

In the last few decades, computer simulation has become an essential tool for modelling and predicting thermodynamic properties, including phase equilibria and interfacial properties, of complex systems of fundamental and applied interest. In particular, during the last twenty years, remarkable progress has been made in the development of new force fields for describing complex molecules from a molecular perspective. Perhaps, the most relevant example of this kind of force fields is the

transferable parameters for phase equilibria (TraPPE) approach of Siepmann and coworkers, that allows to determination, with high accuracy, thermodynamic and structural properties of complex molecules. The key idea behind the TraPPE models is transferability, i.e., to predict the behaviour of a given molecule or set of molecules only from the knowledge of molecular parameters for particular chemical groups taken unchanged from other systems and unchanged, regardless of the atomic makeup of the rest of the molecule. This strategy allows us to truly predict the thermodynamic and other structural and dynamical properties, without the need of adjustments to experimental data of the system under study.

In this work, we use the united-atoms (UA) version of the TraPPE approach (TraPPE-UA) to predict the phase behaviour and interfacial properties of FAMEs. As mentioned in the previous paragraph, it should be possible to obtain new molecular parameter values according to the TraPPE-UA force fields by fitting them to experimental vapour-liquid phase equilibria. However, following Kamath *et al.* [16], it is also possible to use the parameter values from the TraPPE-UA database for chemical groups that describe different molecules, including alkane and alkenes, carbon dioxide, ethers, and carboxylic acids, and transfer them to predict the phase equilibria and interfacial properties of the first members of the methyl esters chemical family. The main goal of this work is to use the transferable molecular parameters of the TraPPE-UA force field to predict the phase equilibria and interfacial properties of the first members of linear methyl esters using MD simulation. In particular, we use the direct coexistence technique in the NVT or canonical ensemble. The results obtained from MD simulations are compared with experimental data taken from the literature [11] to critically assess the models' ability. To our knowledge, this is the first time that the vapour-liquid interfacial properties, and particularly the surface tension, of the first members of the methyl esters chemical family are determined using computer simulations.

The organization of this paper starts with the description of the molecular models in Section 4.2. In the next section, Section 4.3, simulation details are provided and explained briefly. In Section 4.4, the main interfacial property results are presented and discussed. Finally, the main conclusions are summarized in the last section.

5.2 Molecular Models and Theory

As we have mentioned, methyl esters have been modelled following the united-atom approach. In all cases, the force fields use the Lennard-Jones (LJ) and Coulomb potentials to describe the non-bonded interactions,

$$U(r_{ij}) = 4\epsilon_{ij}\left[\left(\frac{\sigma_{ij}}{r_{ij}}\right)^{12} - \left(\frac{\sigma_{ij}}{r_{ij}}\right)^{6}\right] + \frac{q_i q_j}{4\pi\epsilon_0 r_{ij}} \tag{5.1}$$

where r_{ij} is the distance between interacting sites i and j, σ_{ij} and ϵ_{ij} are the diameter and well depth associated with the LJ intermolecular potential, q_i and q_j are the partial charges on interacting sites i and j, and ϵ_0 the permittivity of vacuum. All the LJ parameters for unlike interactions are obtained using the Lorentz-Berthelot combining rules.

According to the TraPPE-UA philosophy, molecular parameters are taken from existing parametrizations and combined to form the molecules of interest, as has been explained in the previous section.

Tabla 5.1: Well depth, ϵ, size, σ, and partial charges, q, parameters for the TraPPE-UA force field corresponding to non-bonded interactions of methyl-esters (from methyl acetate to methyl heptanoate). The letters in parentheses indicate the atom a particular site is bonded to. All values are taken from the works of Siepmann and co-workers [17–20]. See also the TraPPE webpage [21].

Atom	ϵ/k_B(K)	σ(Å)	q(e)
$\mathbf{CH_3}-$(O)	98.0	3.75	0.25
$-\mathbf{O}-$	55.0	2.80	-0.40
$\mathbf{C}=$(O)	41.0	3.90	0.55
$\mathbf{O}=$(C)	79.0	3.05	-0.45
$\mathbf{CH_3}-$(C)	98.0	3.75	0.05
$\mathbf{CH_2}-$(C)	46.0	3.95	0.05
$\mathbf{CH_3}-(CH_x)$	98.0	3.75	0.00
$\mathbf{CH_2}-(CH_x)$	46.0	3.95	0.00

Molecular parameters for non-bonded interactions for the carbonyl chemical group (C=O) are taken from molecular parameters of two different molecules: the parameters of the carbonyl oxygen are taken from the oxygen parameters of the carbon dioxide model proposed by Potoff and Siepmann [17], and the parameters of the carbonyl carbon are taken from the carbon parameters of the carboxylic acids models proposed by Kamath *et al.* [18]. The molecular parameters involved in the methoxy chemical group (or terminal methyl group bonded to the ether oxygen, –O–CH_3), i.e., the ether oxygen and the methyl group CH_3 (sp^2), are taken from the work of Stubbs *et al.* [19] The molecular parameters of methyl (CH_3– not bonded to the oxygen ether) and methylene (–CH_2– not bonded to the carbon –C– atom) groups are taken from the TraPPE-UA parameter values of alkanes proposed by Martin and Siepmann [20]. It is interesting to mention that Maerzke *et al.* [22] considered TraPPE force fields for acrylates and metacrylates that share some of the same UA as the FAMEs studied in this work. However, these substances contain conjugated double bonds. In our work, we consider methyl esters that do not contain this kind of bonds, and therefore use the TraPPE molecular parameters of Kamath *et al.* [18] and Stubbs *et al.* [19]. All the molecular parameters used in this work to describe the non-bonded interactions, including the partial charge values for electrostatic interactions of all the chemical groups, are summarized in Table 5.1. As in the case of the LJ parameters and partial charges, bond lengths, bending, and torsional force field parameters characterizing the bonded interactions are obtained from the TraPPE-UA values of different chemical groups. Tables 5.2-5.4 show all the parameter values used in this work. Note that according to the usual TraPPE-UA force field approach, the bond lengths between different chemical groups are fixed.

5.3 Simulation details

All MD simulations are carried out in conditions at which the vapour-liquid interface is present, following the standard methodology [23, 24] for all models studied. In particular, simulations are performed in the NVT canonical ensemble using GROMACS (version 4.6.1) [25] at a fixed temperature T, in a parallelepipedic simulation cell of constant volume $V = L_x \times L_y \times L_z$, where L_x, L_y, and L_z are the dimensions of the simulation box. We use periodic boundary conditions in all three directions.

A homogeneous liquid system is first equilibrated in a parallelepiped simulation box. The dimensions of the box are $L_x = L_y = 3.9\,\text{nm}$ for the case of methyl acetate and $L_x = L_y = 3.95\,\text{nm}$ for the rest of methyl esters. For the lengths of the simulation boxes along the z-axis we have used the following

Tabla 5.2: Bond length values for the TraPPE-UA force field corresponding to methyl-esters (from methyl acetate to methyl heptanoate). All values are taken from the TraPPE approach [21].

Bond	Bond length (Å)
C = O	1.200
C – O	1.344
CH_3 – O	1.410
CH_x – C	1.520
CH_2 – CH_x	1.540

Tabla 5.3: Bending potential parameters for the TraPPE-UA force field corresponding to methyl-esters (from methyl acetate to methyl heptanoate). All values are taken from the TraPPE approach [21].

Bending	θ (deg)	k_θ/k_B (K/rad^2)
CH_3–O–C	115	62500
O–C=O	125	62500
O–C–CH_3	110	70596
O=C–CH_3	125	62500
O=C–CH_2	125	62500
C–CH_2–CH_2	114	62500
CH_2–CH_2–CH_2	114	62500
CH_2–CH_2–CH_3	114	62500

sizes: $L_z = 11$ nm (methyl acetate), $L_z = 13$ nm (methyl propionate), $L_z = 16$ nm (methyl butyrate), $L_z = 19$ nm (methyl valerate), $L_z = 20$ nm (methyl hexanoate), and $L_z = 23$ nm (methyl heptanoate). We consider $N = 1100$ molecules for all the methyl esters studied in this work. After equilibration of these bulk-liquid systems, the box is expanded along the z direction leaving the liquid phase slab at the center. The final overall dimensions of the vapour-liquid-vapour configuration box are therefore $L_x = L_y = 3.9$ nm and $L_z = 33$ nm for the case of methyl acetate, and $L_x = L_y = 3.95$ nm and $L_z = 39$, 48, 57, 60, and 69 nm for the methyl propionate, methyl butyrate, methyl valerate, methyl hexanoate, and methyl heptanoate, respectively.

In order to reduce the truncation and system size effects involved in the phase equilibrium and interfacial properties calculations, the cut-off radius (r_c) has been taken to be equal to a value of 5σ

Tabla 5.4: Torsional potential parameters for the TraPPE-UA force field corresponding to methyl-esters (from methyl acetate to methyl heptanoate). All values are taken from the TraPPE approach [21].

Torsion	c_0/k_B (K)	c_1/k_B (K)	c_2/k_B (K)	c_3/k_B (K)
CH_3–O–C=O	11594.6	3374.2	-4118	-613.6
CH_3–O–C–CH_3	6551.3	1566.1	-4196	789.2
CH_3–O–C–CH_2	6551.3	1566.1	-4196	789.2
O–C–CH_2–CH_2	839.87	-2133.17	106.68	3097.72
O–C–CH_2–CH_3	839.87	-2133.17	106.68	3097.72
O=C–CH_2–CH_2	1121.13	142.79	-115.68	-1172.92
O=C–CH_2–CH_3	1121.13	142.79	-115.68	-1172.92
C–CH_2–CH_2–CH_2	1009.97	-2018.93	136.38	3165.28
C–CH_2–CH_2–CH_3	1009.97	-2018.93	136.38	3165.28
CH_2–CH_2–CH_2–CH_2	1009.97	-2018.93	136.38	3165.28
CH_2–CH_2–CH_2–CH_3	1009.97	-2018.93	136.38	3165.28

($r_c = 1.95\,\text{nm}$ for methyl acetate and 1.975 nm for the rest of methyl esters). It has been shown by several authors [26–28] that such a value provides a reasonable description for the interfacial properties. Long-range interactions are determined using three-dimensional Ewald technique with a convergence parameter of 0.1 Å^{-1} and a maximum value for the reciprocal lattice equal to 31.

We have used the Verlet leapfrog [29] algorithm with a time step of 0.001 ps. It is important to note in this case that the time step value chosen has been necessary to sample correctly the torsional potentials of the ester models. A Nosé-Hoover thermostat [30] with large time constant equal to 1.0 ps has been used. Simulations of the homogeneous liquid systems are equilibrated during 5 ns. After this, the vapour-liquid-vapour systems are also equilibrated during 5 ns. After the systems reach equilibrium, the properties of the coexisting vapour and liquid phases are obtained as appropriate averages during 20 ns. In order to estimate errors on the variables computed, the sub-blocks average method was applied. [31] In such approach, the production period is divided into M independent blocks. The statistical error is then deduced from the standard deviation of the average $\bar{\sigma}/\sqrt{M}$, where $\bar{\sigma}$ is the variance of the block averages and M has been fixed in this work to $M = 10$.

The equilibrium vapour pressure, P, and interfacial tension, γ, are obtained from the diagonal components of the pressure tensor. The vapour pressure corresponds to the normal component, $P \equiv P_{zz}$, of the pressure tensor, while the interfacial tension is obtained using the mechanical route [32–35] as:

$$\gamma = \frac{L_z}{2}\left[P_{zz}(z) - \frac{P_{xx}(z) + P_{yy}(z)}{2}\right] \tag{5.2}$$

In Eq. (5.2), the additional factor 1/2 comes from having two interfaces in the system, and L_z is the size of the simulation box in the z direction, defined along the longitudinal dimension across the interface.

The experimental determination of the critical state of FAMEs is extremely difficult due to their thermal instability. One alternative route to obtain the critical coordinates, i.e., critical pressure, P_c, temperature, T_c, and density, ρ_c, is to use the vapour-liquid equilibrium MD results together the scaling law [36, 37] given by:

$$\rho_L - \rho_V = A\,(T - T_c)^{\beta} \tag{5.3}$$

and the corresponding law of rectilinear diameters

$$\frac{\rho_L + \rho_V}{2} = \rho_c + B\,(T - T_c) \tag{5.4}$$

β is the corresponding critical exponent [33], with a universal value of $\beta = 0.325$, and A, B, T_c and ρ_c are four unknown constants obtained by fitting to the simulation results. ρ_L and ρ_V are the liquid and vapour coexistence densities at the corresponding temperature T, respectively. Critical temperature, T_c, and density, ρ_c, can be easily obtained from Eqs. (5.3) and (5.4).

An independent way to calculate T_c is to apply an alternative scaling law using interfacial information from the system. [38, 39] Following this route, γ is related to T_c by the following expression:

$$\gamma = \gamma_0\,(1 - T/T_c)^{\mu} \tag{5.5}$$

where γ_0 is the so-called "zero-temperature" surface tension and μ is the corresponding critical exponent. Here, we fix μ to the universal value $\mu = 1.258$ as obtained from renormalization-group theory. [33] Once again, the unknown constants, γ_0 and T_c are found by fitting the interfacial tension data with temperature.

The critical pressure can be estimated from an extrapolation of the Clausius-Clapeyron relation to the critical temperature obtained from Eq. (5.3) or Eq. (5.5):

$$\ln P = C_1 + \frac{C_2}{T} \tag{5.6}$$

where C_1, and C_2 are correlation parameters. The value of P_c is obtained using Eq. (5.6) at $T = T_c$. The critical temperature value, T_c, used in the previous equation is obtained from Eq. (5.3).

The surface entropy (Δs^γ) and surface enthalpy (Δh^γ) change of surface formation can be also determined using the temperature dependence of the surface tension from the following derivative expressions [33, 40]:

$$\Delta s^\gamma = -\left(\frac{\partial \gamma}{\partial T}\right)_P \tag{5.7}$$

$$\Delta h^\gamma = \gamma + T\Delta s^\gamma \tag{5.8}$$

Finally, an interesting property that can be obtained from the calculation of density profiles is the interfacial width along the vapour-liquid equilibrium. Implicitly this property is defined by fitting the curves from the original mean field van der Waals theory, [33] described by

$$\rho(z) = \frac{\rho_L + \rho_V}{2} - \frac{\rho_L - \rho_V}{2} \tanh\left[\frac{\alpha(z - z_0)}{d}\right] \tag{5.9}$$

where the constant $\alpha = 2\tanh^{-1}(0.8)$ is chosen so that d is the 10-90 interfacial thickness and z_0 the position of the Gibbs dividing surface. If coexistence densities are calculated first (see the next section for further details), d and z_0 could be treated as adjustable parameters in Eq. (5.9). Since two interfaces are simulated simultaneously during each simulation, it is possible to compare the interfacial thickness values obtained from both interfaces. In this work, the values determined are always found to be the same within statistical uncertainty, indicating that the inhomogeneous systems are properly equilibrated at all temperatures.

5.4 Results and discussion

In this section we present the main results from the simulations of the six methyl esters using the TraPPE-UA molecular models described in the previous sections. We focus on the interfacial properties, such as density profiles, interfacial thickness, surface entropy and enthalpy, and surface tension. We also examine the temperature dependence of these properties, and compare our results for the different models with experimental data taken from the literature [11]. We analyze the thermodynamic and interfacial behavior of all the FAMEs at different temperatures using the same methodology as in our previous work. [41–47] Density profiles are calculated by dividing the system in 200 slabs along the z

direction. The molecular density profiles, $\rho_i(z)$, are obtained by assigning the position of each united atom center, z_i, to the corresponding slab and constructing the molecular density from mass balance considerations. The bulk vapour and liquid densities in each system are calculated by averaging $\rho_i(z)$ over appropriate regions sufficiently removed from the interfacial region. In addition to that, the final bulk vapour density value, at each temperature and chain length, is obtained after averaging the density profiles on both sides of the liquid film. We show in Fig. 5.1 the density profiles $\rho(z)$ for the six methyl esters considered in this work, from methyl acetate up to methyl heptanoate, at different temperatures as modelled using the TraPPE-UA models. For the sake of clarity, we only present one half of the profiles corresponding to one of the interfaces. Also for convenience, all density profiles have been shifted to place z_0 at the origin.

As can be seen, liquid density decreases and vapour density increases as the temperature is increased in all cases as expected. The slope of each density profile, in absolute values, along the interfacial region becomes smaller as the temperature approaches the critical point for each system. According to the near-critical scaling laws [33], the interfacial thickness must diverge as the temperature approaches the critical temperature. The results presented in Fig. 5.1 corroborate this behaviour.

From the density profiles depicted in Fig. 5.1, it is possible to obtain the vapour-liquid phase envelopes of the different FAMEs studied in this work. Results corresponding to the vapour and liquid coexistence densities, at different temperatures, are presented in Table 5.5.

Fig. 5.2 shows the phase diagrams of all the systems considered as obtained from MD computer simulations. Experimental data taken from the literature [11] is also included for comparison. In general, computer simulation is able to predict very accurately the vapour and liquid densities in the whole range of temperatures considered, from near the triple-point to the critical temperature. Very small differences between simulation and experimental data for the liquid branch of the phase envelope can be seen at low temperatures in the case of methyl acetate, methyl propionate, and methyl butyrate.

In addition to the vapour and liquid coexistence densities, we have also determined the coordinates of the critical points of all the FAMEs for the MD simulation results using the scaling laws given by Eqs. (5.3) and (5.4). In particular, we follow the methodology explained in the previous section. As in the case of the vapour and liquid coexistence densities, we compare our results obtained from the analysis described above with experimental data taken from the literature [11]. The critical temperatures and densities of all the FAMEs obtained from MD simulations are presented in Table 5.6. Comparison between simulation and experimental critical coordinates can also be observed in Fig. 5.2. Agreement between simulation and experiments is excellent in all cases. Computer simulation results overestimate the experimental values less than a 3% (2.7% is the case of methyl hexanoate and 0.7% in the case of methyl butyrate). Differences between experiments and simulations could be due to finite-size scaling effects that occur during simulations when the system is close to the critical state. These effects can be taken into account explicitly using advanced simulation techniques, such as the Finite-Size Scaling procedure of Binder [48]. However, this kind of analysis is out of the scope of this work. Critical densities of the homologous chemical family is also accurately predicted by the TraPPE-UA models of FAMEs. Deviation between simulation and experiment for ρ_c is always below 2%, except in the case of methyl valerate (5.9%). In all cases, critical densities are slightly overestimated as expected.

We have also determined the normal boiling temperature of each methyl ester. This has been done using Eq. (5.6) with an evaluating the pressure set at $P = 101325\,\mathrm{Pa}$. The predictions from simulations are shown in Table 5.6. Comparison between values taken from the literature and the predictions

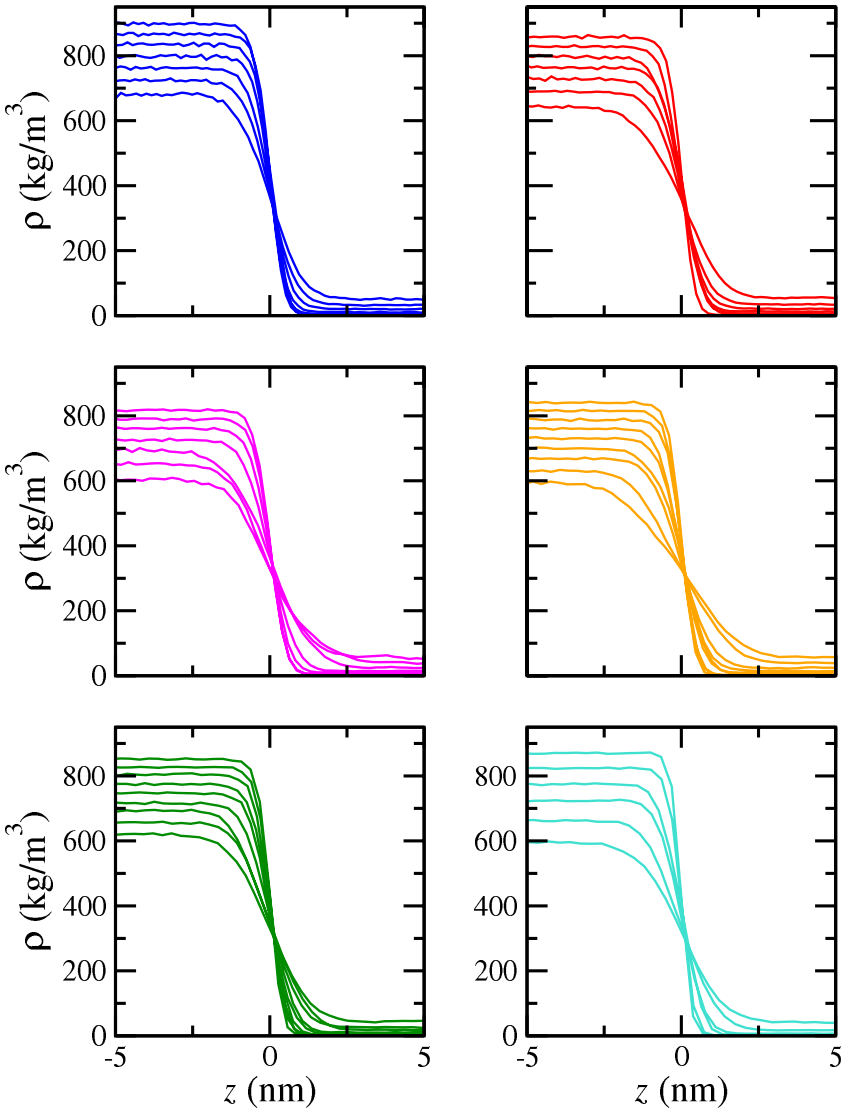

Figura 5.1: Simulated equilibrium density profiles across the vapour-liquid interface of methyl esters as obtained from MD NVT simulations using the TraPPE -UA models for (a) methyl acetate (blue curves), (b) methyl propionate (red curves), (c) methyl butyrate (magenta curves), (d) methyl pentanoate (orange curves), (e) methyl hexanoate (green curves), and (f) methyl heptanoate (turquoise curves) at different temperatures. From bottom to top (in the liquid region): 300, 325, 350, 375, 400, 425, 450, 475, 500, 525, and 550 K

Tabla 5.5: Liquid density ρ_L, vapour density ρ_V, vapour pressure P, compressibility factor Z, and surface tension γ at different temperatures, as obtained from MD NVT simulations for methyl esters (from methyl acetate to methyl heptanoate). The errors are estimated as explained in the text.

T(K)	ρ_L(kg/m^3)	ρ_V(kg/m^3)	P(MPa)	Z	γ(mN/m)
		Methyl acetate			
300	897(3)	1.2(1)	0.041(3)	1.06 (1)	-
325	867(3)	3.3(2)	0.114(7)	0.946(2)	22.3(3)
350	835(3)	6.5(3)	0.231(8)	0.90(1)	18.4(2)
375	800(4)	10.7(5)	0.42(1)	0.93(2)	15.4(3)
400	763(3)	20.0(6)	0.78(1)	0.86(1)	12.0(4)
425	722(8)	32.0(7)	1.26(2)	0.821(7)	9.0(5)
450	679(4)	51(1)	1.92(1)	0.75(1)	6.4(2)
		Methyl propionate			
325	858(2)	1.8(2)	0.06(3)	1.07(4)	21.7(3)
350	828(2)	3.6(2)	0.111(4)	0.94(2)	19.2(2)
375	797(3)	7.2(0.4)	0.233(9)	0.91(2)	15.7(6)
400	765(3)	12.8(5)	0.45(1)	0.93(2)	12.2(3)
425	729(3)	21.1(6)	0.726(9)	0.86(1)	9.9(3)
450	687(4)	34.7(7)	1.16(1)	0.788(8)	8.1(3)
475	643(3)	54(1)	1.78(3)	0.733(3)	5.1(3)
		Methyl butyrate			
350	818(4)	2.0(3)	0.063(5)	1.10(8)	19.0(3)
375	790(2)	4.8(3)	0.140(6)	0.95(2)	16.1(4)
400	759(3)	8.9(5)	0.267(5)	0.92(3)	13.4(4)
425	726(3)	15.3(5)	0.472(8)	0.89(1)	10.6(3)
450	694(4)	26(1)	0.77(1)	0.81(1)	8.0(2)
475	653(3)	39.3(1)	1.14(2)	0.751(8)	6.2(2)
500	608(5)	54(2)	1.64(2)	0.75(8)	4.1(4)
		Methyl valerate			
375	789(3)	2.5(3)	0.066(5)	0.98(4)	16.7(4)
400	761(3)	5.1(4)	0.134(6)	0.92(3)	14.3(4)
425	731(2)	9.4(3)	0.27(1)	0.928(9)	12.1(3)
450	701(2)	15.1(6)	0.42(1)	0.858(9)	10.0(3)
475	670(2)	24.0(5)	0.70(1)	0.860(6)	8.1(5)
500	630(3)	37.8(1)	1.06(2)	0.782(8)	5.8(5)
525	589(4)	56.9(2)	1.52(3)	0.710(5)	4.0(4)
		Methyl hexanoate			
375	802(3)	1.7(2)	0.037(4)	0.92(3)	17.7(5)
400	775(2)	2.9(2)	0.073(5)	0.984(4)	15.4(5)
425	748(2)	5.9(3)	0.152(6)	0.95(1)	13.5(4)
450	719(4)	9.7(5)	0.26(1)	0.935(9)	11.3(3)
475	690(4)	17.6(5)	0.47(1)	0.873(2)	9.8(3)
500	657(3)	26.5(8)	0.68(1)	0.80(1)	7.3(3)
525	621(2)	43(1)	1.07(2)	0.742(7)	5.1(4)
		Methyl heptanoate			
300	870(2)	0.02(1)	-	-	25.1(8)
350	824(2)	0.36(4)	-	-	21.1(8)
400	775(2)	2.2(2)	0.046(5)	0.993(4)	16.1(6)
450	722(2)	6.1(4)	0.15(1)	1.06(1)	11.8(4)
500	663(2)	17.4(6)	0.43(1)	0.944(9)	9.0(3)
550	597(3)	41(1)	1.03(2)	0.869(8)	4.0(5)

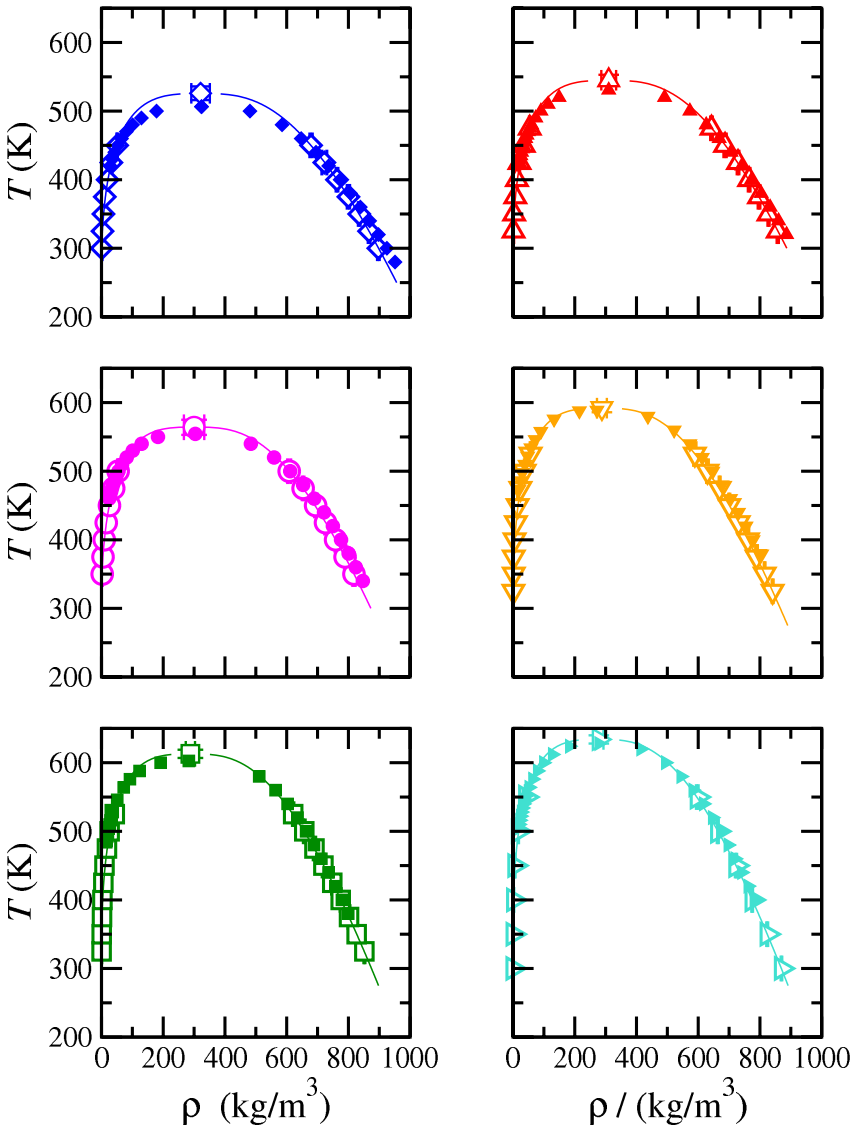

Figura 5.2: Vapour-liquid coexistence densities of methyl esters. The open symbols correspond to the coexistence densities obtained from MD NVT simulations and the filled symbols to the experimental data taken from the literature [11] for methyl acetate (blue diamonds), methyl propionate (red triangles up), methyl butyrate (magenta circles), methyl pentanoate (orange triangles down), methyl hexanoate (green squares), and methyl heptanoate (turquoise triangles right). The continuous curves correspond to the fits of the simulation data presented in this work to Eqs. (5.3) and (5.4). Symbols at the highest temperatures for each coexistence curve represent the critical points estimated from Eqs. (5.3) and (5.4) (filled symbols) and the experimental critical points taken from the literature [11] (open symbols).

obtained from the simulations show good agreement between both results. As can be seen, in most cases the deviation is $\approx 2.2 - 3.8\%$, except in the case of methyl hexanoate, in which deviation is 4.69%, approximately. Vapour pressure of FAMEs is also calculated from MD simulation. Since we are simulating planar vapour-liquid interfaces, the system is inhomogeneous. Consequently, the pressure is no longer a scalar magnitude but a tensorial quantity. In this case, the normal component of the pressure tensor (acting perpendicularly to the planar interface) is equal to the vapour pressure of the system. The results obtained from computer simulations are shown in Table 5.5. We have also presented the vapour pressure, as functions of temperature, of all the FAMEs studied in this work in Figure 5.3. The predictions obtained from computer simulations provide, in general, a good description of the vapour pressure curves, particularly for methyl acetate, methyl propionate, and methyl heptanoate. As can be seen in Figure 5.3, in the case of methyl butyrate, methyl valerate, and methyl hexanoate, MD simulation results overestimate the vapour pressure at mid and high temperatures.

We have also represented the vapour pressure data in a Clausius-Clapeyron plot (Figure 5.4). TraPPE-UA models are able to predict very accurately the vapour pressure of all the FAMEs, from methyl acetate up to methyl heptanoate, at low temperatures.

One of the main goals of this work is to predict the interfacial properties of FAMEs. Figure 5.5 displays the variation of the interfacial thickness, d, as a function of temperature obtained using Eq. (5.9) for each FAME. From this Figure it is possible to observe that d increases with increasing temperature. This means that the interfacial region becomes wider as the temperature is increased. At low temperatures, the density profiles show sharp interfaces, which can be identified with low values of interfacial thickness. An increase of the temperature results in a wider interfacial region as the system approaches the critical point, and consequently, the interfacial thickness increases. As $T \to T_c$, the interfacial thickness diverges as the liquid and vapour phases become identical.

The surface entropy, Δs^{γ}, that can obtained from the temperature derivative of the surface tension according to Eq. (5.7), is an useful magnitude in studies involving surfaces in which temperature, and also surface tension, is non-uniform, leading to the well-known Bénard-Marangoni convection phenomena [49]. Fig. 5.6 shows the surface entropy change of surface formation for FAMEs as a function of temperature. Δs^{γ} is obtained from MD computer simulations of the interfacial tension in combination with Eq. (5.7). Δs^{γ} varies linearly with T for all the methyl esters considered here, and slightly decreases with increasing temperature. This behaviour is related to the slight curvature of the surface tension as a function of temperature (see below). In addition to this, for a fixed temperature, Δs^{γ} exhibits its largest values for short methyl esters and gets smaller as the molecular weight of the FAME increases. This indicates that curvature of surface tension, as a function of temperature, is larger for short methyl esters than for long FAMEs. Interestingly, as the temperature increases, differences between Δs^{γ} for FAMEs becomes smaller, showing that curvature of surface tension, at high temperature, is similar for all methyl esters. This is a clear indication of the universal behaviour of $\gamma = \gamma(T)$ for different members of the homologous series as the system approaches the critical region. It is possible to obtain the surface enthalpy, Δh^{γ}, as a function of temperature, for the FAMEs studied in this work. Similar to the case of the surface entropy, Δh^{γ} can be determined from MD simulation data of the interfacial tension using Eq. (5.8). According to this, surface enthalpy is computed directly from surface tension values and the numerical derivative of $\gamma(T)$ with respect to the temperature. Fig. 5.7 shows Δh^{γ}, as a function of temperature, of the methyl esters. As can be seen, this property decreases with temperature, as expected. A nearly linear behaviour is observed for the shortest FAMEs. However, the $\Delta h^{\gamma} - T$ plots show a certain curvature as the molecular weight is increased. At fixed temperature, the surface enthalpy decreases as the lengths of the methyl esters are increased. Although

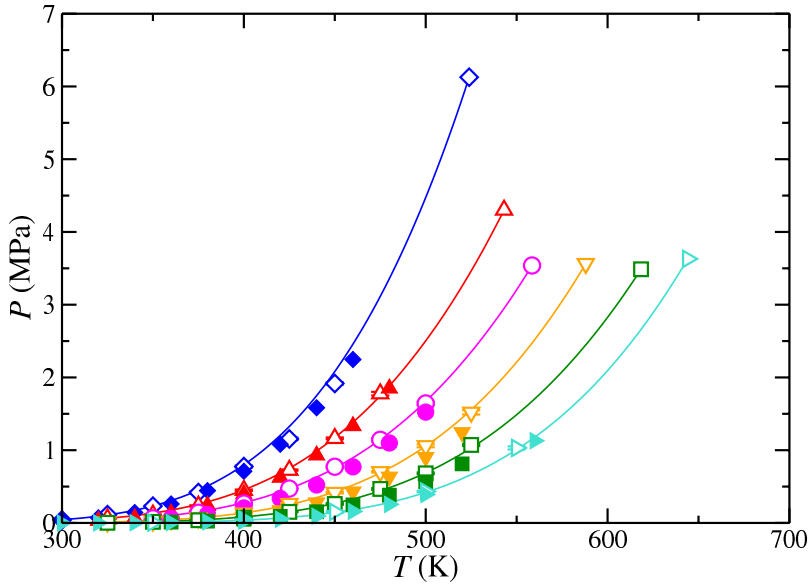

Figura 5.3: Vapour pressure of methyl esters (from methyl acetate to methyl heptanoate). The meaning of the symbols is the same as in Fig. 5.2. The continuous curves correspond to the fits of the simulation data presented in this work to Eq. (5.6). Filled symbols at the highest temperature for each vapour pressure curve represent the critical points obtained from Eq. (5.6) using the critical temperature values obtained from Eq. (5.3).

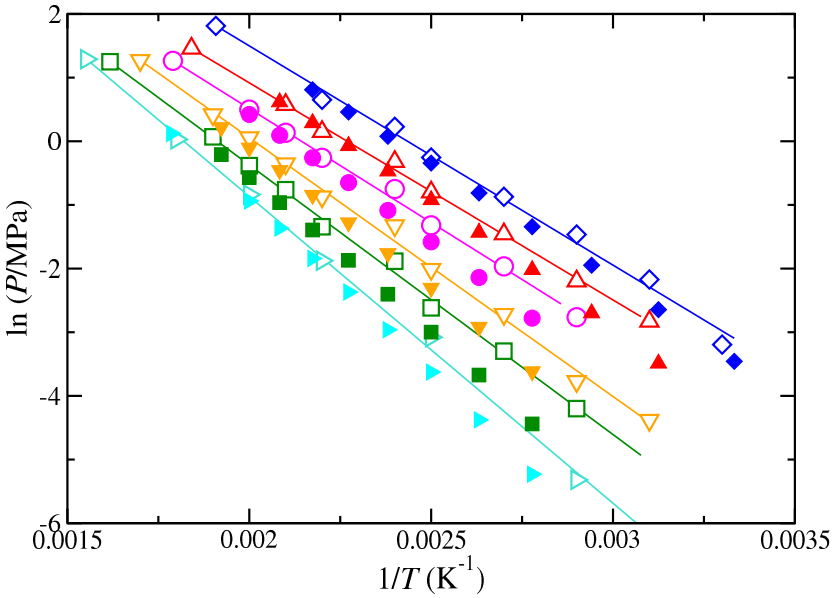

Figura 5.4: Clausius-Clapeyron representation of the vapour pressure of methyl esters (from methyl acetate to methyl heptanoate). The meaning of the symbols is the same as in Fig. 5.2.

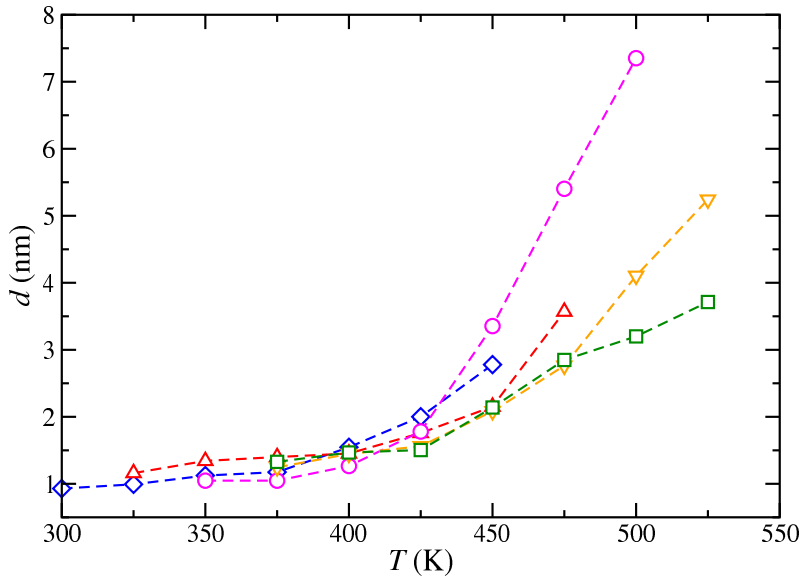

Figura 5.5: 10-90 interfacial thickness d as a function of the temperature for methyl esters (from methyl acetate to methyl heptanoate). The symbols correspond to the values obtained from density profiles obtained from MD NVT simulations and the dashed curves are included as a guide to the eye. The meaning of the symbols is the same as in Fig. 5.2.

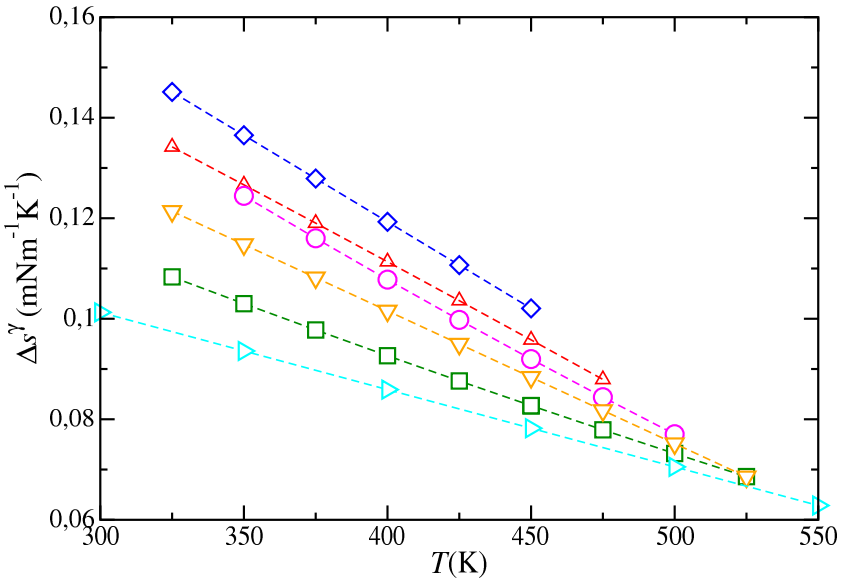

Figura 5.6: Surface entropy of methyl esters (from methyl acetate to methyl heptanoate) as obtained from the combination of the MD NVT simulation results and Eq. (5.7). The meaning of the symbols is the same as in Fig. 5.2.

this is true at low and mid temperatures, this trend seems to change as T is high.

Finally, we consider the vapour-liquid interfacial tension of methyl esters, from methyl acetate up to methyl heptanoate. Fig. 5.8 shows the surface tension, as a function of temperature, as obtained from MD simulations using the virial or mechanical route. According to this, the surface tension is calculated using Eq. (5.2), i.e., as the difference between the normal and tangential macroscopic components of the pressure tensor. We have also included experimental data taken from the literature [11] in order to compare the predictions from the TraPPE-UA molecular models. The simulation results obtained in this work show an excellent agreement with experimental data in the temperature range at which experimental data is available ($T \lesssim 360\,\mathrm{K}$). Simulation results obtained from the use of TraPPE-UA models for methyl esters seem to slightly overestimate the surface tension at low temperatures for methyl acetate, methyl propionate, and methyl butyrate. For longer molecules, agreement between simulation and experimental data is excellent.

As in the case of the vapour-liquid phase envelopes, we have also fit the simulation data using the well-known Guggenheim's scaling law for the surface tension as a function of temperature according to Eq. (5.5) [38, 39]. This allows us to obtain the critical temperature of each methyl ester and compare these values with the experimental critical values. Table 5.6 includes the values found in this work. It is interesting to compare the critical values obtained from Eqs. (5.3)-(5.4) and (5.5). As can be seen, critical temperatures determined using surface tension values and vapor and liquid coexistence densities are different. A priori, one expects that both values should be the same. However, one should take into account the following points: (1) Strictly speaking, the scaling laws given by Eqs. (3) and (5) are only valid in the asymptotic limit $T \to T_c$; in this work, as it is usual in the literature [41, 42, 44, 50, 51],

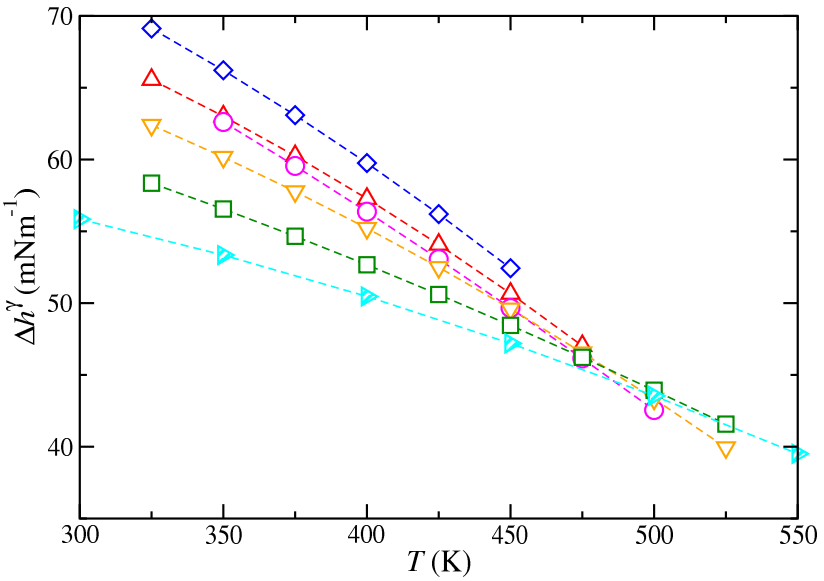

Figura 5.7: Surface enthalpy of methyl esters (from methyl acetate to methyl heptanoate) as obtained from the combination of the MD NVT simulation results and Eq. (5.8). The meaning of the symbols is the same as in Fig. 5.2.

Tabla 5.6: Experimental (T_c^{exp}, ρ_c^{exp}, P_c^{exp}, and T_b^{exp}) and predicted ($T_c^{\dagger}$, $T_c^{\S}$, $\rho_c^{\dagger}$, $P_c^{\dagger}$, and T_b) critical temperatures, densities, and pressures and normal boiling temperatures of methyl esters (from methyl acetate to methyl heptanoate). Critical temperatures, $T_c^{\dagger}$ and $T_c^{\S}$, are obtained from the analysis of the MD NVT coexistence densities using Eqs. (5.3) and (5.4), and the analysis of the MD NVT tension data using Eq. (5.5), respectively. Critical densities, $\rho_c^{\dagger}$, are also obtained from the analysis of the MD NVT coexistence densities using Eq. (5.4). Critical pressures, $P_c^{\dagger}$, are obtained using Eq. (5.6) evaluating the temperature $T_c^{\dagger}$ as obtained from Eq. (5.3). Normal boiling temperatures are obtained using Eq. (5.6) evaluating the pressure at $P = 101325\,\mathrm{Pa}$.

Substance	T_c^{exp}(K)	$T_c^{\dagger}$(K)	$T_c^{\S}$(K)	ρ_c^{exp}(kg/m^3)	$\rho_c^{\dagger}$(kg/m^3)	P_c^{exp}(MPa)	$P_c^{\dagger}$(MPa)	P_b^{exp}(MPa)	P_b(MPa)
Methyl acetate	510.0	523.9	525.14	324.0	321.0	4.692	6.127	322.63	330.09
Methyl propionate	531.5	543.1	550.38	310.0	310.0	3.986	4.302	340.10	352.44
Methyl butyrate	554.5	558.8	571.65	304.0	300.0	3.464	3.538	359.35	373.60
Methyl valerate	566.9	558.0	589.80	272.0	288.0	3.090	3.564	388.09	400.65
Methyl hexanoate	602.6	618.4	597.46	283.0	288.0	2.797	3.487	407.72	427.81
Methyl heptanoate	628.0	644.1	635.28	278.0	278.0	2.543	3.630	435.71	446.15

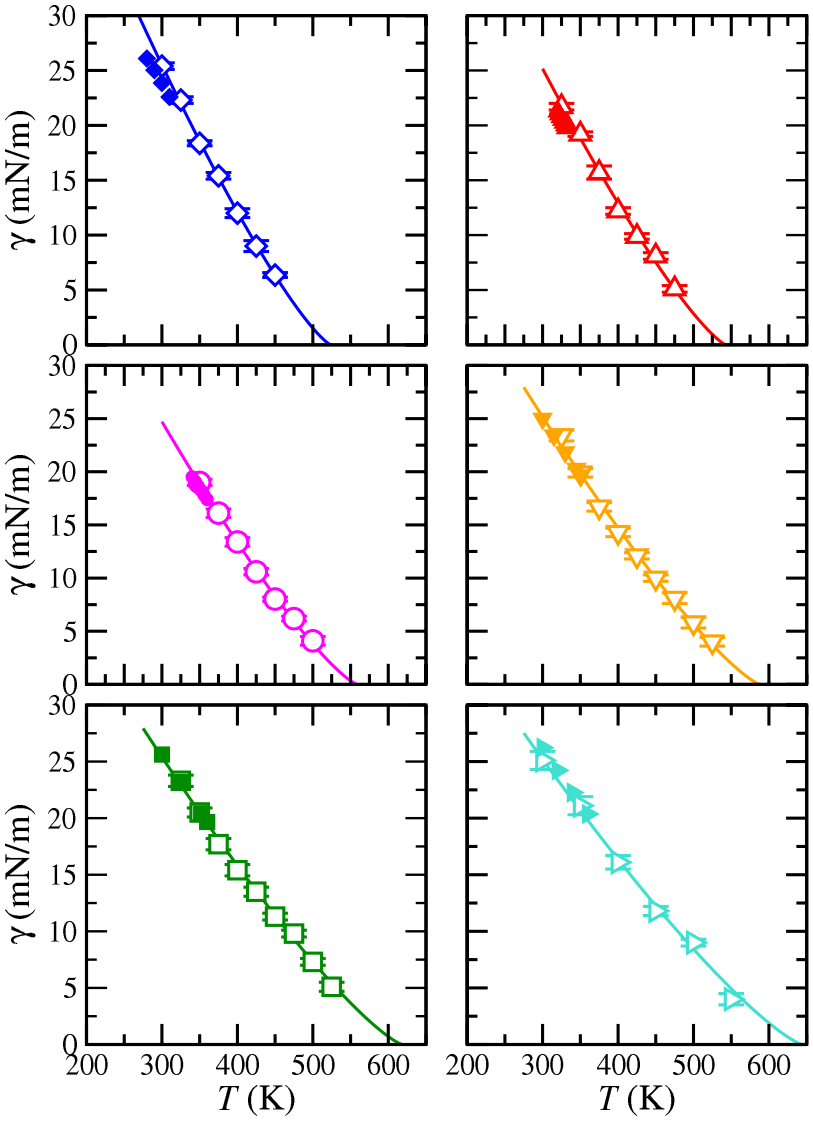

Figura 5.8: Vapour-liquid surface tension as function of temperature for methyl esters (from methyl acetate to methyl heptanoate). The meaning of the symbols is the same as in Fig. 5.2. The continuous curves correspond to the fits of the simulation data presented in this work to Eq. (5.5).

we have used data corresponding to states located at T far away from T_c (data corresponding to temperatures from around a $30-40\%$ below the critical temperature up to near the critical point); (2) the estimation of the critical coordinates depends critically on the size of the system; here we use only 1100 molecules, which in our opinion, is not enough to avoid the finite-size effects of the systems under study [52]; (3) the location of the critical coordinates depends also critically on the cutoff distance used during the simulation, and if tail corrections are applied or not. This is especially important if we are using two different kind of properties (density and surface tension values) to obtain the critical temperature since they are affected by the truncation of the intermolecular potential in a different way, as probably happens in this work. (4) Finally, the goal of the this work is not to obtain accurate values of critical temperatures and densities of methyl esters but to check if TraPPE force field is able to predict, in a transferable manner, the phase equilibria and interfacial properties of methyl esters. We think a procedure similar to that followed by Dinpajooh *et al.* [52], finite-size scaling [53] or mixed-field theory using the Binder cumulant parameter [54] methodologies, is the correct approach to be followed if accurate estimations of critical points are needed. Unfortunately, this is out of the scope of this work. It is interesting to mention that experimental data taken from the literature [11] is only available at low temperatures, from 300 up to 360 K, approximately. The reason for which there is no experimental data at higher temperatures is that methyl esters become unstable at high temperatures, generating micro bubbles in the tensiometer and densimeter, making it impossible to measure this property accurately. Fortunately, this is not the case for computer simulations. Our study allows us to obtain the surface tension of all the methyl esters analyzed in this work up to $450-550$ K, depending on the critical temperature of each substance. It is important to recall that the simulated surface tension values in this work are, to the best of our knowledge, reported for the first time. This is particularly important in this case since there is no experimental data at temperatures above 360 K for any of the FAMEs studied, as just commented. The excellent agreement found, not only for surface tension at low temperatures, but also for vapour-liquid coexistence densities and vapour pressures in wide ranges of temperatures, makes the TraPPE-UA models proposed and used in this work excellent candidates for predicting the phase equilibria and interfacial properties of FAMEs. The simulation data presented in this work could be used, not only for theoretical modelling of these compounds, but also for the design and use of new chemical processes involving FAMEs as future and alternative diesel fuels, as well as for environmental issues, including the removal of contaminants from water and for groundwater remediation.

5.5 Conclusions

We have studied the phase equilibria and interfacial properties of a methyl esters homologous series (from methyl acetate to methyl heptanoate) using the TraPPE force fields for different molecules and chemical families in a transferable way. In particular, we use the direct coexistence technique, in combination with MD NVT simulations, to study inhomogeneous systems of pure esters containing two vapour-liquid interfaces.

We examine the vapour-liquid surface tension using the virial route, i.e., calculating the normal and tangential components of the pressure tensor. We have also determined density profiles, coexistence densities, vapour pressures, surface entropies and enthalpies, interfacial thickness, and critical temperature, density, and pressure as functions of temperature for all the methyl esters considered. Predictions from the MD simulation for vapour-liquid coexistence densities and vapour pressures are compared with experimental data taken from the literature. These three properties are predicted remarkably well

by the TraPPE models. This is particularly important since the molecular parameters of the TraPPE force fields are taken in a transferable way from other molecules and chemical families without need adjustment.

We also predict the behaviour of interfacial thickness, surface entropy, and surface enthalpy, as functions of temperatures, and consider the effect of increasing the molecular weight of the homologous family. Particularly interesting are the results for the surface tension of methyl esters. The TraPPE models and the molecular parameters transferred from other molecules and chemical families are able to predict very accurately the surface tension of all the methyl esters studied in this work at low temperatures. Although experimental data is only available at temperatures below 360 K, computer simulations allows us to provide surface tension up to the pure critical points of each substance. This is an important result since this is the first time the vapour-liquid surface tension of methyl esters is determined in the literature at these conditions. In fact, this is the first computer simulation work devoted to the prediction of the vapour-liquid equilibria and interfacial properties of the homologous series.

5.6 Acknowledgement

The authors acknowledge Centro de Supercomputación de Galicia (CESGA, Santiago de Compostela, Spain) for providing access to computing facilities, and Ministerio de Economía, Industria y Competitividad through Grant with reference FIS2017-89361-C3-1-P co-financed by EU FEDER funds. A.M. acknowledges funding from Fondecyt (Chile) through Grant 1190107. Further financial support from Junta de Andalucía and Universidad de Huelva is also acknowledged. J.A.F. acknowledges Contrato Predoctoral de Investigación from XIX Plan Propio de Investigación de la Universidad de Huelva and a FPU Grant (Ref. FPU15/03754) from Ministerio de Educación, Cultura y Deporte. J.A., J.M.M., P.G.-A., and F.J.B. thankfully acknowledge the computer resources at Magerit and the technical support provided by the Spanish Supercomputing Network (RES) (Project QCM-2018-2-0042).

Bibliography

[1] "https://ec.europa.eu/energy/en/topics/renewable-energy/renewable-energy-directive, (retrieved november, 2019)."

[2] M. Faith Demirbar, "Biorefineries for biofuel upgrading: A critical review," *Applied Energy*, vol. 86, pp. S151–S161, 2009.

[3] L. C. B. A. Bessa, M. C. Ferreira, C. R. A. Abreu, E. A. C. Batista, and A. J. A. Meirelles, "A new unifac parameterization for the prediction of liquid-liquid equilibrium of biodiesel systems," *Fluid Phase Equil.*, vol. 425, pp. 98–107, 2016.

[4] N. D. D. Carareto, M. C. Costa, A. J. A. Meirelles, and J. Pauly, "High pressure solid–liquid equilibrium of fatty acid ethyl esters binary systems," *Fluid Phase Equil.*, vol. 382, pp. 158–163, 2014.

[5] N. D. D. Carareto, C. Y. C. S. Kimura, E. C. Oliveira, M. C. Costa, and A. J. A. Meirelles, "Flash points of mixtures containing ethyl esters or ethylic biodiesel and etanol," *Fuel*, vol. 96, pp. 319–326, 2012.

[6] "Dechema gesellschaft für chemische technik und biotechnologie e.v., frankfurt am main, germany, https://i-systems.dechema.de/detherm/, (retrieved november, 2019)."

[7] C. Wohlfarth and B. Wohlfarth, "Numerical data and functional relationships in science and technology, surface tension of pure liquids and binary liquid mixtures," in *New Series Group IV Physical Chemistry* (M. Lechner, ed.), vol. 16, Springer Verlag, Berlin, Heidelberg, 1997.

[8] C. Wohlfarth and B. Wohlfarth, "Numerical data and functional relationships in science and technology, surface tension of pure liquids and binary liquid mixtures," in *New Series Group IV Physical Chemistry* (M. Lechner, ed.), vol. 24, Springer Verlag, Berlin, Heidelberg, 2008.

[9] C. Wohlfarth and B. Wohlfarth, "Numerical data and functional relationships in science and technology, surface tension of pure liquids and binary liquid mixtures," in *New Series Group IV Physical Chemistry* (M. Lechner, ed.), vol. 28, Springer Verlag, Berlin, Heidelberg, 2016.

[10] T. E. Daubert and R. P. Danner, *Physical and Thermodynamic Properties of Pure Chemicals. Data Compilation.* Taylor and Francis, Bristol, 1989.

[11] E. W. Lemmon, M. O. McLinden, D. G. Friend, C. Wohlfarth, and B. Wohlfarth, "Thermophysical properties of fluid systems," in *NIST Chemistry WebBook, NIST Standard Reference Database Number 69* (P. J. Linstrom and W. G. Mallard, eds.), National Institute of Standards and Technology: Gaithersburg MD, 2019.

[12] H. T. Davies and L. E. Scriven, "Stress and structure in fluid interfaces," *Adv. Chem. Phys.*, vol. 49, p. 357, 1982.

[13] I. del Pozo, M. Cartes, F. Llovell, and A. Mejía, "Densities and interfacial tensions for fatty acid methyl esters (from methyl formate to methyl heptanoate) + water demixed mixtures at atmospheric pressure conditions," *J. Chem. Thermodynamics*, vol. 121, pp. 121–128, 2018.

[14] T. J. Bruno, T. M. Loestead, J. R. Riggs, E. L. Jorgenson, and M. L. Huber, "Comparison of diesel fuel oxygenate additives to the composition-explicit distillation curve method. part 1: Linear compounds with one to three oxygens," *Energy Fuels*, vol. 25, pp. 2493–2507, 2011.

[15] J. E. Landmeyer, P. M. Bradley, D. A. Trego, K. G. Hale, and J. E. Haas, "Mtbe, tba, and tame attenuation in diverse hyporheic zones," *Ground Water*, vol. 48, pp. 30–41, 2010.

[16] G. Kamath, J. Robinson, and J. J. Potoff, "Application of trappe-ua force field for determination of vapor–liquid equilibria of carboxylate esters," *Fluid Phase Equil.*, vol. 240, pp. 46–55, 2006.

[17] J. J. Potoff and J. I. Siepmann, "Vapor-liquid equilibria of mixtures containing alkanes, carbon dioxide, and nitrogen," *AIChE Journal.*, vol. 47, pp. 1676–1682, 2001.

[18] G. Kamath, F. Cao, and J. J. Potoff, "An improved force field for the prediction of the vapor-liquid equilibria for carboxylic acids," *J. Phys. Chem. B*, vol. 108, pp. 14130–14136, 2004.

[19] J. Stubbs, J. J. Potoff, and J. I. Siepmann, "Transferable potentials for phase equilibria. 6. united-atom description for ethers, glycols, ketones, and aldehydes," *J. Phys. Chem. B*, vol. 108, pp. 17596–17605, 2004.

[20] G. M. Martin and J. I. Siepmann, "Transferable potentials for phase equilibria. 1. united-atom description of n-alkanes," *J. Phys. Chem. B*, vol. 102, pp. 2569–2577, 2001.

[21] "http://chem-siepmann.oit.umn.edu/siepmann/trappe/index.html, (retrieved november, 2019)."

[22] K. A. Maerzke, N. E. Schultz, R. B. Ross, and J. I. Siepmann, "Trappe-ua force field for acrylates and monte carlo simulations for their mixtures with alkanes and alcohols," *J. Phys. Chem. B*, vol. 113, pp. 6415–6425, 2009.

[23] D. Frenkel and B. Smit, *Understanding Molecular Simulations.* 2nd Ed. Academic, San Diego, 2002.

[24] M. P. Allen and D. J. Tildesley, *Computer Simulation of Liquids, 2 Ed.* Oxford University PressClaredon, Oxford, 2017.

[25] D. van der Spoel, E. Lindahl, B. Hess, G. Groenhof, A. E. Mark, and H. J. Berendsen, "Gromacs: Fast, flexible, and free," *J. Comput. Chem.*, vol. 26, no. 16, pp. 1701–1718, 2005.

[26] G. Galliero, M. M. Piñeiro, B. Mendiboure, C. Miqueu, T. Lafitte, and D. Bessieres, "Interfacial properties of the mie n-6 fluid: Molecular simulations and gradient theory results," *J. Chem. Phys.*, vol. 130, pp. 104704/1–10, 2009.

[27] G. Galliero, "Surface tension of short flexible lennard-jones chains: Corresponding states behavior," *J. Chem. Phys.*, vol. 133, pp. 074705/1–7, 2010.

[28] J. M. Míguez, M. M. Piñeiro, and F. J. Blas, "Influence of the long-range corrections on the interfacial properties of molecular models using monte carlo simulation," *J. Chem. Phys.*, vol. 138, pp. 034707/1–11, 2013.

[29] M. A. Cuendet and W. F. V. Gunsteren, "On the calculation of velocity-dependent properties in molecular dynamics simulations using the leapfrog integration algorithm," *J. Chem. Phys.*, vol. 127, pp. 184102/1–9, 2007.

[30] S. Nosé, "A molecular dynamics method for simulations in the canonical ensemble," *Mol. Phys.*, vol. 52, pp. 255–268, 1984.

[31] H. J. C. Berendsen, J. P. M. Postma, W. F. V. Gunsteren, A. D. Nola, and J. R. Haak, "Molecular dynamics with coupling to an external bath," *J. Chem. Phys.*, vol. 81, pp. 3684/1–8, 1984.

[32] H. Hulshof, "Ueber die oberflachenspannung," *Ann. Phys. (Berlin)*, vol. 4, pp. 165–186, 1901.

[33] J. S. Rowlinson and B. Widom, *Molecular Theory of Capillarity.* Claredon Press, 1982.

[34] E. D. Miguel, F. J. Blas, and E. M. D. Río, "Molecular simulation of model liquid crystals in a strong aligning field," *Mol. Phys.*, vol. 104, pp. 2919–2927, 2006.

[35] E. D. Miguel and G. Jackson, "The nature of the calculation of the pressure in molecular simulations of continuous models from volume perturbations," *J. Chem. Phys.*, vol. 125, pp. 164109/1–12, 2006.

[36] J. S. Rowlinson and F. L. Swinton, *Liquids and Liquid Mixtures.* Butterworth, London, 1982.

[37] H. W. Xiang, *The Corresponding-States Principle and Its Practice Thermodynamic. Transport and Surface Properties of Fluids.* Elsevier, Amsterdam, 2005.

[38] E. A. Guggenheim, "," *J. Chem. Phys.*, vol. 13, pp. 253–261, 1945.

[39] B. Widom, "Surface tension and molecular correlations near the critical point," *J. Chem. Phys.*, vol. 43, p. 3892, 1965.

[40] M. Modell and J. D. Tester, *Thermodynamics and its applications, thrid edition.* iPrentice-Hall, New York, 1998.

[41] F. J. Blas, L. G. MacDowell, E. D. Miguel, and G. Jackson *J. Chem. Phys.*, vol. 129, p. 144703, 2008.

[42] L. G. MacDowell and F. J. Blas *J. Chem. Phys.*, vol. 131, pp. 074705/1–10, 2009.

[43] J. G. Sampayo, F. J. Blas, E. D. Miguel, E. A. Müller, and G. Jackson *J. Chem. Eng. Data*, vol. 55, p. 4306, 2010.

[44] F. J. Blas, A. I. Moreno-Ventas Bravo, J. M. Míguez, M. M. Piñeiro, and L. G. MacDowell *J. Chem. Phys.*, vol. 137, p. 084706, 2012.

[45] J. M. Garrido, M. Cartes, A. Mejía, J. Algaba, J. M. Míguez, F. J. Blas, A. I. Moreno-Ventas Bravo, and M. M. Piñeiro, "Measurement and modeling of high pressure density and interfacial tension of carbon dioxide + tetrahydrofuran mixture," *J. Supercrit. Fluids*, vol. 128, pp. 359–369, 2017.

[46] J. Algaba, J. M. Garrido, J. M. Míguez, A. Mejía, A. I. M.-V. Bravo, and F. J. Blas, "Interfacial properties of tetrahydrofurane and carbon dioxide mixture from computer simulation," *J. Phys. Chem. C*, vol. 122, pp. 16142–16153, 2018.

[47] J. Algaba, M. Cartes, A. Mejía, J. M. Míguez, and F. J. Blas, "Phase equilibria and interfacial properties of the tetrahydrofuran + methane binary mixture from experiment and computer simulation," *J. Phys. Chem. C*, vol. 123, pp. 20960–20970, 2019.

[48] K. Binder *Z. Phys. B Condensed Matter*, vol. 43, p. 119, 1981.

[49] E. Salomon and M. Mareschal, "," *J. Phys.: Condens. Matter*, vol. 3, p. 3645, 1991.

[50] F. J. Blas, A. I. Moreno-Ventas Bravo, J. A. Fernández, F. J. Martínez-Ruiz, and L. G. MacDowell *J. Chem. Phys.*, vol. 140, pp. 114705/1–114705/11, 2014.

[51] F. J. Martínez-Ruiz, F. J. Blas, B. Mendiboure, and A. I. Moreno-Ventas Bravo *J. Chem. Phys.*, vol. 141, p. 184701, 2014.

[52] M. Dinpajooh, P. Bai, D. A. Allan, and J. I. Siepmann, "Accurate and precise determination of critical properties from gibbs ensemble monte carlo simulations," *J. Chem. Phys.*, vol. 143, pp. 114113–1–114113–13, 2015.

[53] J. J. Potoff and T. Z. Panagiotopoulos, "Critical point and phase behavior of the pure fluid and a lennard-jones mixture," *J. Chem. Phys.*, vol. 109, pp. 10914–10920, 1998.

[54] J. Pérez-Pellitero, P. Ungerer, G. Orkoulas, and A. D. Mackie, "Critical point estimation of the lennard-jones pure fluid and binary mixtures," *J. Chem. Phys.*, vol. 125, pp. 054515–1–054515–9, 2006.

Capítulo 6

Molecular dynamics of liquid-liquid equilibrium and interfacial properties of aqueous solutions of methyl esters

6.1 Abstract

In this work, liquid-liquid phase equilibria and interfacial properties of methyl ester + water binary mixtures are determined at atmospheric pressure and from 278 to 358 K combining the direct coexistence technique and molecular dynamics simulations. Methyl esters are modelled using new parametrizations based on the united atom TraPPE model force field proposed recently by us [*Phys. Chem. Chem. Phys.* **22**, 4974-4983 (2019)] that are able to predict the vapour-liquid interfacial properties of pure methyl esters with high accuracy. In the case of water, we consider the well-known TIP4P/2005 model, the most popular rigid and non-polarizable model to describe the interfacial properties of pure water. The simulations are performed using the direct coexistence technique in the isothermal-isobaric or $NP_z\mathcal{A}T$ ensemble in combination with molecular dynamics. We obtain density profiles, temperature-densities and temperature-composition projections of the phase diagrams, and interfacial tensions. The liquid-liquid interfacial tension is calculated from the normal and tangential components of the pressure tensor according to the mechanical virial route. We pay attention particularly to the ability of the molecular models in predicting the experimental behavior of the systems. Simulation results are able to account for the liquid-liquid phase equilibria of these binary mixtures, in good agreement with experimental data taken from the literature. Unfortunately, experimental values for interfacial tensions are substantially overestimated by predictions from computer simulations in all cases. To our knowledge, this is the first time liquid-liquid phase equilibrium and interfacial properties of methyl ester + water mixtures are predicted from computer simulations.

6.2 Introduction

Biodiesel is considered a clean, renewable, and eco-friendly alternative to reduce the use and production of diesel from fossil fuel sources. The main advantages are that biodiesel can be used as a liquid fuel in diesel engines without any extensive modification, and it can be used as pure or

blended with petroleum diesel in any percentage, where the most common blend is 20% biodiesel and 80% petroleum diesel. Biodiesel can be produced by reacting an alcohol (or bioalcohol) with a group of mono-alkyl esters, which are obtained from vegetable oil, animal fat, or recycled cooking grease. Depending on the alcohol (methanol or ethanol) used in the transesterification reaction route, it is possible to obtain Fatty Acid Methyl Esters (FAMEs) or Fatty Acid Ethyl Esters (FAEEs), respectively. [1–3] Both FAMEs and FAEEs are good substitutes for petroleum-based diesel, moreover, FAEEs is more ecosystemic and renewable than FAMEs due to ethanol can be also obtained from a renewable source (e.g. food crops, waste vegetables, algae, fruits, root vegetables, wood waste, cellulose, forest waste, etc.). [1, 2, 4]

Unfortunately, the production of biodiesel based on FAEEs is not yet sufficiently developed for efficient use. [5] On the other side, the production and technical use of FAMEs are mature but the evaluation of its environmental impact is limited due to the thermophysical properties needed to describe the phase and interfacial behavior of FAME in contact with water is scared, especially for the case of interfacial properties. Interfacial properties, such as interfacial tension, surface activity, and wettability of these aqueous mixtures at liquid-liquid (LL) equilibrium are key properties not only to evaluate the environmental impact of FAME on water but also to design technical strategies to remove it from water and for groundwater remediation. [6]

Focused on measurable properties related to interfacial properties, the only available contributions are the works of Gros and Feuge [7] and del Pozo *et al.* [8] In the first case, the authors reported the interfacial tension for binary mixtures of methyl valerate and methyl heptanoate with water. However, these reported data have been measured only at 348.15 K and the used device (Noüy tensiometer) is not the most appropriated and accurate tensiometer for LL system. In the second case, a systematic determination of both liquid densities and interfacial tensions as a function of temperature are reported for aqueous binary mixtures from methyl formate to methyl heptanoate, where the more adequate and precise tensiometer was used (i.e., a spinning drop tensiometer). From the tensiometry results, it is interesting to observe the parabolic behavior of the interfacial tension with the temperature and the dependence of the interfacial tension with the molecular chain length. In order to explain the interfacial behavior in terms to these latter variables (i.e., temperature, and molecular chain length), del Pozo et al. [8] used a simplified version of the van der Waals square gradient theory [9] couple to the Non-Random-Two Liquid model (NRTL) activity coefficient model proposed by Renon and Prausnitz. [10] The used model provides a route to correlate the experimental information but not bring a molecular description of the interfacial concentration of species at the interfacial region, which is the fundamental piece to explain the parabolic behavior of the interfacial tension.

Unfortunately, little information on what type of phase behaviour is exhibited by these mixtures and on the existence of critical points is available from the experimental data. To the best of our knowledge, the only mixture for which experimental information about the existence of critical point exist is the methyl acetate + water binary system. According to the review of Mączyński and collaborators [11], this mixture exhibits an upper critical solution temperature (UCST) at ambient pressure and 381.2 K, for a molar fraction of methyl acetate $x_1 = 0.212$. However, there is not information about which particular type of phase behaviour exhibits nor experimental information for the rest of the members of the homologous series. Preliminary calculations have been performed using the well-known SAFT-VR Mie formalism and determined that these mixtures exhibit vapour-liquid, liquid-liquid, and vapour-liquid-liquid phase equilibria [12]. In addition to that, the methyl acetate + water binary mixture exhibits type II phase behaviour according to the classification Scott and Konynenburg [13, 14].

In order to fill the gap between experimental results and a molecular level explanation of the thermal and molecular chain length impact on the behavior of the interfacial tension, this work is focused on the molecular dynamics simulation of the selected binary mixtures of FAMEs (i.e., from methyl acetate to methyl heptanoate) with water in LL equilibrium. The main advantage of this approach is to obtain a molecular picture of FAMEs and water at the interfacial region and to relate this behavior to the surface activity of the interfacial concentration of species and the corresponding interfacial tension.

The main goal of this work is to predict the LL phase equilibria and the anomalous interfacial tension in aqueous solutions of the first members of methyl esters chemical family (from methyl acetate to methyl heptanoate) described by using the new transferable molecular parameters [15] of the TraPPE-UA force field, proposed in the last year. To our knowledge, this is the first time that the LL interfacial properties, and particularly the interfacial tension, of the methyl ester + water systems are studied from computer simulations.

Note that the use of a group contribution approach allows the direct generalization of the models to other compounds and mixtures of the same chemical family. This transferable approach provides an important predictive character of the models, which is very useful when experimental data is not available. However, a different approach it is also possible, especially in cases in which predictions from a group contribution fails for certain chemical groups in small molecules of a given homologous series, such as alkanes and alcohols [16, 17]. For theses cases, it is possible to use specific shape and/or interaction parameter values for some groups. However, one of the goals of the current work is to check if the use of transferable parameters taken directly from the TraPPE database is able to provide an appropriate description of the vapor-liquid phase equilibria and interfacial properties of aqueous solutions of methyl esters.

The organization of this paper starts with the description in Sections 2 and 3 of the force fields used to described FAMEs and water and the simulations details. In the next section, the main results of interfacial properties are presented and discussed. Finally, the main conclusions are summarized in the last section.

6.3 Molecular models

Methyl esters have been recently modeled as linear flexible molecules using the TraPPE-UA approach by Feria *et al.* [15] to predict their liquid-vapor phase behavior and interfacial properties, from methyl acetate to methyl heptanoate. According to this, molecular parameters are taken from existing parametrizations for other molecules, including alkanes and alkenes, carbon dioxide, ethers, and carboxylic acids, to predict the behaviour of the methyl ester homologous series. [18] Particularly, the parameters of the carbonyl oxygen (=O) are those used for the oxygen in the carbon dioxide model proposed by Potoff and Siepmann [19], and the carbonyl carbon (C=) is modeled using the carboxylic acids models proposed by Kamath *et al.* [20] The molecular parameters involved in the methoxy group (–O–CH_3, CH_3–C and CH_2-C) are taken from the work of Stubbs *et al.* [21] Finally, the parameters of methyl (CH_3–CH_x) and methylene (–CH_2–CH_x) chemical groups are those of linear alkanes proposed by Martin and Siepmann. [16] Table 6.1 includes the well depth, size, and partial charge parameters for the TraPPE-UA force fields used in this work corresponding to non-bonded interactions of all the chemical groups.

Tabla 6.1: Lennard-Jones well depth, ε, size, σ, and partial charge q, parameters for the TIP4P/2005 and TraPPE-UA force fields corresponding to non-bonded interactions of water and methyl esters. The letters in parenthesis indicate the atom a particular site is bonded to. Parameter values for water are taken from the work of Abascal *et al.* [22] and those for methyl esters from the work of Siepmann and co-workers. [16, 19–21] See also the the TraPPE webpage [23] and our previous work. [15]

Atom	ε/k_B(K)	σ(Å)	$q(e)$
H_2O (TIP4P/2005)			
O	93.20	3.1589	0.0
H	0.0	0.0	0.5564
M	0.0	0.0	−1.1128
Methyl Esters(TraPPE-UA)			
$\mathbf{CH_3}-$(O)	98.0	3.75	0.25
$-\mathbf{O}-$	55.0	2.80	-0.40
$\mathbf{C}=$(O)	41.0	3.90	0.55
$\mathbf{O}=$(C)	79.0	3.05	-0.45
$\mathbf{CH_3}-$(C)	98.0	3.75	0.05
$\mathbf{CH_2}-$(C)	46.0	3.95	0.05
$\mathbf{CH_3}-(CH_x)$	98.0	3.75	0.00
$\mathbf{CH_2}-(CH_x)$	46.0	3.95	0.00

There exists a considerably large number of molecular models for water, including the well-known SPC/E [24], TIP4P [25], and TIP5P [26] families. The TIP4P models (TIP4P [25], TIP4P/EW [27] and TIP4P/2005 [22]) consist of four interacting sites placed on the oxygen atom (O), on each of the hydrogen atoms (H), and along the H–O–H bisector (the so-called M site). In this case, we have selected the well-known rigid and non-polarizable TIP4P/2005 version [22]. This model is able to provide accurate estimates of thermodynamic properties, phase equilibria, and interfacial properties of pure water compared with similar models. [28, 29] In addition to that, the model is remarkably proficient in the estimation of LL phase equilibria and interfacial properties of binary and ternary mixtures containing water, including CH_4 + H_2O [30], CO_2 + H_2O [31] and CH_4 + CO_2 + H_2O [32] systems. Molecular parameters for the TIP4P/2005 model for water are also included in Table 6.1.

The nonbonded intermolecular and intramolecular interactions between chemical groups separated by more than three bonds are accounted for the Lennard-Jones (LJ) and Coulomb potentials,

$$U\left(r_{ij}\right)=4\varepsilon_{ij}\left[\left(\frac{\sigma_{ij}}{r_{ij}}\right)^{12}-\left(\frac{\sigma_{ij}}{r_{ij}}\right)^{6}\right]+\frac{q_iq_j}{4\pi\varepsilon_0 r_{ij}} \tag{6.1}$$

where r_{ij} is the distance between interacting sites i and j, σ_{ij} and ϵ_{ij} are the diameter and well depth associated with the LJ intermolecular potential, respectively, q_i and q_j are the partial charges on these sites, and ε_0 is the permittivity of vacuum. The molecular parameters used in this work to describe the nonbonded interactions of water and methyl esters, including partial charges values for electrostatic interactions, are listed in Table 6.1. All the LJ parameters for unlike interactions are obtained using the well-known Lorentz-Berthelot combining rules.

The values of the fixed bond lengths for water and methyl esters, presented in Table 6.2, are taken from the original works of Abascal and Vega [22] and from the TraPPE webpage [23], respectively. The bending and torsional force field parameters corresponding to the bonded interactions for the methyl

esters are obtained from the TraPPE-UA force fields [23]. The bond bending potential is controlled through a harmonic function,

$$U_{bend}(\theta) = \frac{1}{2}\kappa_\theta \left(\theta - \theta_0\right)^2 \tag{6.2}$$

where θ, θ_0 and κ_θ are the measured bending angle, the equilibrium bending angle, and the force constant, respectively. Table 6.3 contains a list of the θ_0 and κ_θ values used in this work. According to the philosophy of the TraPPE-UA force field approach, the dihedral rotations around bonds connecting four chemical groups account for the standard cosine series of the dihedral angle,

$$U_{tor}(\phi) = c_0 + c_1\left[1 + \cos(\phi)\right] + c_2\left[1 + \cos(2\phi)\right] + c_3\left[1 + \cos(3\phi)\right] \tag{6.3}$$

where the Fourier coefficients c_i, for i = 0,..., 3 are listed in Table 6.4.

6.4 Simulation details

We combine molecular dynamics (MD) computer simulations and the direct coexistence methodology to obtain the phase equilibria and interfacial properties of aqueous solutions of several methyl esters. Computer simulations are performed at atmospheric pressure and temperatures varying from 278 to 358 K for each aqueous mixture. In particular, we simulate the LL interfaces using the isothermal-isobaric or $NP_z\mathcal{A}T$ ensemble to ensure that temperature and pressure are constants. According to this, the interfacial area $\mathcal{A} = L_x \times L_y$ is kept constant and only L_z is varied along the simulation. Here, L_x, L_y, and L_z are the dimensions of the simulation box along the x-, y-, and z-axis, respectively. For convenience, the z-axis is chosen perpendicular to the planar LL interface, i.e., parallel to the direction along which the system exhibits the inhomogeneity. We use periodic boundary conditions in all three directions.

The simulation boxes used to study the LL interfaces considered in this work have been prepared as follows. For each mixture and temperature, we first equilibrate two independent simulation boxes using the isothermal-isobaric ($NP_z\mathcal{A}T$) ensemble at atmospheric pressure and the corresponding temperature. Particularly, we equilibrate independently two bulk pure liquid phases, one containing $N_o = 1000$

Tabla 6.2: Bond length values of the TIP4P/2005 and the TraPPE-UA force fields corresponding to water and methyl esters. All values are taken from the work of Abascal *et al.* [22] and the TraPPE webpage, [23] respectively.

Bond	Bond length (Å)
H_2O (TIP4P/2005)	
O-H	0.9572
O-M	0.1546
Methyl Esters(TraPPE-UA))	
C = O	1.200
C – O	1.344
CH_3 – O	1.410
CH_x – C	1.520
CH_2 – CH_x	1.540

Tabla 6.3: Bending potential parameters for the TraPPE-UA force field corresponding to methyl esters. All values are taken from the TraPPE webpage. [23]

Bending	θ (deg)	k_θ/k_B (K rad^{-2})
CH_3–O–C	115	62500
O–C=O	125	62500
O–C–CH_3	110	70596
O=C–CH_3	125	62500
O=C–CH_2	125	62500
C–CH_2–CH_2	114	62500
CH_2–CH_2–CH_2	114	62500
CH_2–CH_2–CH_3	114	62500

Tabla 6.4: Torsional potential parameters for the TraPPE-UA force field corresponding to methyl esters. All values are taken from the TraPPE webpage. [23]

Torsion	c_0/k_B (K)	c_1/k_B (K)	c_2/k_B (K)	c_3/k_B (K)
CH_3–O–C=O	11594.6	3374.2	-4118	-613.6
CH_3–O–C–CH_3	6551.3	1566.1	-4196	789.2
CH_3–O–C–CH_2	6551.3	1566.1	-4196	789.2
O–C–CH_2–CH_2	839.87	-2133.17	106.68	3097.72
O–C–CH_2–CH_3	839.87	-2133.17	106.68	3097.72
O=C–CH_2–CH_2	1121.13	142.79	-115.68	-1172.92
O=C–CH_2–CH_3	1121.13	142.79	-115.68	-1172.92
C–CH_2–CH_2–CH_2	1009.97	-2018.93	136.38	3165.28
C–CH_2–CH_2–CH_3	1009.97	-2018.93	136.38	3165.28
CH_2–CH_2–CH_2–CH_2	1009.97	-2018.93	136.38	3165.28
CH_2–CH_2–CH_2–CH_3	1009.97	-2018.93	136.38	3165.28

Tabla 6.5: Liquid density of the organic-rich phase, $\rho^{(O)}$, liquid density of the water-rich phase, $\rho^{(W)}$, molar fraction of methyl ester in the organic-rich phase, $x_1^{(O)}$, molar fraction of methyl ester in the water-rich phase, $x_1^{(W)}$, and LL interfacial tension, γ, at 1 bar and different temperatures as obtained from MD $NP_z\mathcal{A}T$ simulations.

T (K)	$\rho^{(O)}$ (kg/m^3)	$\rho^{(W)}$ (kg/m^3)	$x_1^{(O)}$	$x_1^{(W)}$	γ (mN/m)
Methyl acetate (1) + water (2)					
278	922 (2)	989(2)	0.99771 (8)	0.001494 (2)	24.2 (2)
298	898 (2)	996(2)	0.998 (3)	0.001913 (2)	24.3 (2)
308	886 (2)	993(2)	0.997 (4)	0.00404 (4)	24.2 (2)
318	874 (2)	989(2)	0.997 (4)	0.00626 (4)	24.0 (2)
328	861 (2)	984(2)	0.998 (3)	0.00661 (3)	24.0 (1)
Methyl propionate (1) + water (2)					
278	909 (2)	1000 (3)	0.99872 (7)	0.00172 (2)	27.9 (2)
298	887 (2)	996 (1)	1.000 (4)	0.00324 (3)	28.1 (1)
308	876 (2)	993 (2)	1.000 (3)	0.003050 (2)	28.3 (2)
318	864 (2)	989 (2)	1.000 (4)	0.002719 (3)	28.7 (2)
338	841 (2)	979 (2)	0.999 (1)	0.00603 (3)	27.9 (1)
Methyl butyrate (1) + water (2)					
278	895 (2)	999 (1)	0.9998 (2)	0.00051 (1)	30.5 (2)
298	875 (2)	996 (1)	0.9999 (2)	0.00301 (3)	31.0 (2)
308	864 (2)	993 (1)	1.0000 (9)	0.00279 (3)	30.8 (2)
318	853 (2)	989 (2)	1.0000 (7)	0.00183 (1)	31.3 (3)
338	831 (2)	979 (2)	1.000 (1)	0.00508 (2)	30.7 (3)
Methyl valerate (1) + water (2)					
278	891(3)	999 (3)	1.000 (6)	0.000323 (8)	32.3 (2)
298	871(3)	997 (2)	1.000 (8)	0.00155 (1)	32.9 (4)
308	861(3)	994 (2)	1.000 (1)	0.000778 (8)	32.1 (2)
318	852(2)	989 (2)	1.000 (1)	0.00143 (1)	32.6 (2)
338	830(2)	980 (1)	1.000 (1)	0.00313 (1)	32.6 (3)
358	807(6)	972 (1)	1.000 (2)	0.006009 (2)	31.8 (2)
Methyl hexanoate (1) + water (2)					
278	889(6)	999 (2)	0.999985 (2)	0.000066 (2)	33.2 (4)
298	868(8)	999 (2)	1.000 (2)	0.000044 (2)	34 (3)
308	859(8)	997 (2)	1.000 (2)	0.000053 (2)	34 (4)
318	850(1)	995 (1)	1.000 (3)	0.000037 (1)	34 (3)
338	830(1)	989 (1)	1.0000 (4)	0.0000147(6)	34.2 (3)
358	808(1)	981 (1)	1.000 (2)	0.00370 (2)	33.9 (2)
Methyl heptanoate (1) + water (2)					
278	889 (2)	999 (1)	0.99999958 (5)	0.001202 (2)	35.3 (3)
298	870 (2)	996 (1)	1.00000 (3)	0.000161 (5)	35.21(4)
308	860 (2)	994 (1)	0.9997 (7)	0.001128 (5)	35.3 (4)
318	851 (2)	990 (1)	1.00000 (2)	0.0015 (1)	35.9 (3)
338	833 (2)	981 (1)	1.0000 (4)	0.001794 (9)	35.6 (3)
358	813 (2)	969 (1)	1.0000 (1)	0.00592 (2)	35.1 (3)

methyl ester (organic) molecules and another containing $N_w = 2200$ water molecules. This is done since all the aqueous solutions of methyl esters exhibit a very high degree of immiscibility. [33–35] The dimensions L_x and L_y of all the simulation boxes used in this work are kept constant with $L_x = L_y = 4.0\,\text{nm}$. Initial lengths of the simulation boxes along the z-axis vary depending on the mixture considered. For the case of aqueous solutions of methyl acetate and methyl propionate, L_z varies from 20.8 to 21.8 nm, and from 24.3 to 26.1 nm, when temperature varies from 278 to 358 K, respectively. For the rest of mixtures, $L_z = 29.0$, 32.2, 36.0, and 39.9 nm for the methyl butyrate +, methyl valerate +, methyl hexanoate +, and methyl heptanoate + water mixtures, respectively. Once both simulation boxes have been equilibrated separately, an inhomogeneous biphasic simulation box is constructed assembling along the z direction the simulation box corresponding to the water-rich phase and two replicas of the organic-rich phase at both ends. Then, this biphasic simulation box is allowed to evolve at constant temperature and pressure until the two parallel explicit interfaces are fully equilibrated. The length and number of molecules used ensures that the two independent planar interfaces existing during simulations do not interact each other and that the three liquid bulk slabs (organic-rich, water-rich, and organic-rich liquid phases) are thick enough to ensure that equilibrium properties of each phase can be calculated correctly.

All MD simulations have been carried out using the GROMACS software package (version 4.6.1). [36] We use the Verlet leapfrog algorithm [37] with a time step of 0.001 ps. This time step value is chosen to ensure that the torsional potentials of the ester models are correctly calculated. Temperature and pressure are kept constant using a Nosé-Hoover [38, 39] thermostat and a Parrinello-Rahman [40] barostat with a relaxation time of 2 ps, respectively. In order to reduce the truncation and system size effects involved in the phase equilibrium and interfacial properties calculations, the cut-off radius is set equal to $r_c = 1.95\,\text{nm}$ for the methyl acetate + water mixture and 1.975 nm for the rest of the aqueous solutions. These elections correspond in all cases to a reduced cut-off radius with respect to the largest segment size of 5σ. It has been shown by several authors [41–43] that such a value provides a reasonable description for the interfacial properties. Note also that this cut-off radius is compatible with the dimensions L_x and L_y of all the simulation boxes used in this work, $L_x = L_y = 4\,\text{nm}$. This corresponds to a value $L_x = L_y = 10.13\sigma$. According to Chen [44], González-Melchor *et al.* [45], and Janeček [46], simulation results do not show a dependence of the interfacial tension on the surface area for systems with $L_x = L_y > 10\sigma$, as in this work. The long-range interactions due to coulombic forces are determined using the three-dimensional Ewald technique. Particularly, the real part of the coulombic potential is also truncated at $r_c = 1.95 - 1.975\,\text{nm}$. The Fourier term of the Ewald sums is evaluated using the particle mesh Ewald (PME) method [47]. The width of the mesh is 1 Å with a relative tolerance of 10^{-5} Å. Simulations of the homogeneous liquid systems are equilibrated during 10 ns. After this, the inhomogeneous systems are also equilibrated during 10 ns. After the systems reach equilibrium, the properties of the LL coexisting phases are obtained as appropriate averages during 50 ns. In order to estimate errors on the variables computed, the sub-blocks average method has been applied. [48] In such approach, the production period is divided into M independent blocks. The statistical error are then estimated from the standard deviation of the average $\bar{\sigma}/\sqrt{M}$, where $\bar{\sigma}$ is the variance of the block averages and M has been fixed in this work to $M = 10$.

The interfacial tension, γ, is obtained from the diagonal components of the pressure tensor using the mechanical route [49, 50] as,

$$\gamma = \frac{L_z}{2}\left[\langle P_{zz}\rangle - \frac{\langle P_{xx}\rangle + \langle P_{yy}\rangle}{2}\right] \tag{6.4}$$

In Eq. (6.4), the additional factor 1/2 comes from having two interfaces in the system, and L_z is the size of the simulation box in the z direction, defined along the longitudinal dimension across the interface.

6.5 Results

In this section, we present and discuss the LL phase behavior of aqueous solutions of methyl esters as obtained from MD simulation. Simulations are performed using the direct coexistence method in the anisotropic isothermal-isobaric or $NP_z\mathcal{A}T$ ensemble. We focus on the thermodynamic and structural properties, including density profiles, coexistence densities and compositions, and interfacial tension.

Fig. 6.1 shows the density profiles obtained by MD simulations of six methyl ester + water mixtures (from methyl acetate to methyl heptanoate) at atmospheric pressure and temperatures from 278 up to 358 K. For the sake of clarity, we only plot half of the profiles corresponding to one of the interfaces. The left side of the density profiles represents the organic-rich liquid phase and the right side the water-rich liquid phase. The inhomogeneous box is divided into 200 parallel slabs in the z-direction in order to study the density profiles. The molecular density profiles are obtained by assigning the position of each interacting site to the corresponding slab and constructing the molecular density from mass balance considerations.

An inspection of the density profiles of water across the interface indicates a monotonic increasing behavior when passing from the organic-rich liquid phase to the water-rich liquid phase. Particularly, water density profiles show the approximated traditional shape of the hyperbolic tangent function, without change in the shape of the profiles as temperature and molecular weight of the organic compound are increased. In addition to that, density of water does not vary with temperature at the organic-rich liquid phase. However, it slightly decreases as the temperature is increased at the water-rich liquid phase. The behaviour of water density in the organic-rich liquid phase, as well as that of the methyl esters density, clearly indicates a relatively low solubility of water in the organic phase.

The behaviour and structure of the density profiles of methyl esters observed in this work are similar to that exhibited by other mixtures, including aqueous mixtures of carbon dioxide [51] and methane [30]. They show an adsorption peak located at the organic-rich liquid phase next to the interface. This peak is usually related with the activity of the organic compound at the interface. Particularly interesting in this context is the LL interfacial behaviour of linear 1-alcohol + water homologous series mixtures. Methyl esters, although are clearly different compounds, present some functional similarities. They have a polar chemical group at the end of the quasi-linear molecular structure and an alkyl tail that increases in length as the molecular weight of the molecule becomes larger, as it happens in linear 1-alcohols. Algaba *et al.* [52] have recently shown by means of computer simulation that alcohol + water mixtures exhibit preferential adsorption of alcohols at the LL interface. However, the structure of the LL interface of aqueous solutions of alcohols is different than that of the methyl ester + water mixtures. According to the results presented by Algaba *et al.*, density profiles of alcohol molecules exhibit a more pronounced oscillatory behaviour across the LL interface. The profiles exhibit depressions (desorptions) and complementary peaks (adsorptions) directly related with the behaviour of the corresponding density profiles of water, indicating a self-organized structure of alcohols and water molecules near the interface. Particularly, these mixtures form bilayers of alcohols molecules oriented perpendicularly to the interface, together with a small accumulation (adsorption) of water molecules in the organic-rich phase at the LL interface. This is especially true as the molecular weight

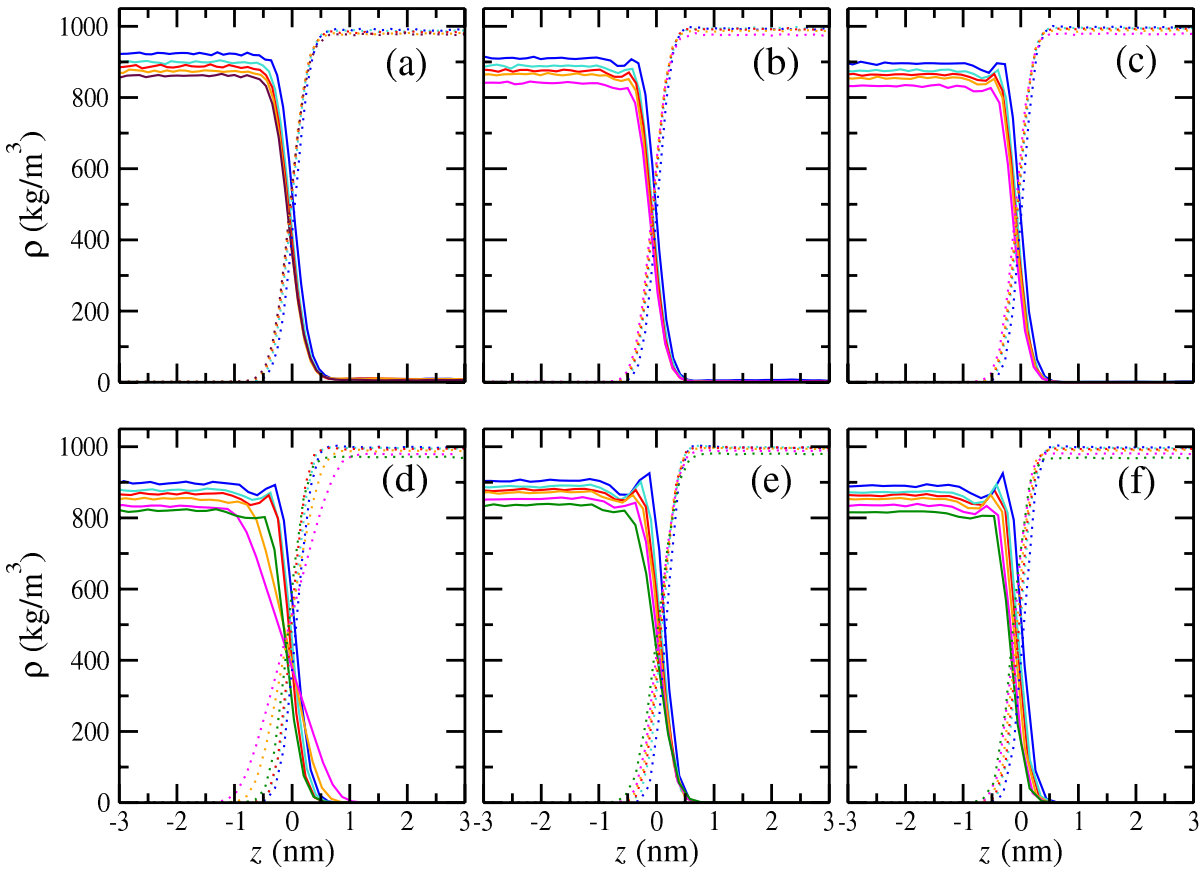

Figura 6.1: Simulated equilibrium density profiles, $\rho(z)$, across the LL interface of methyl esters (continuous curves) and water (dotted curves) as obtained from MD $NP_z\mathcal{A}T$ simulations of (a) methyl acetate + water, (b) methyl propionate + water, (c) methyl butyrate + water, (d) methyl valerate + water, (e) methyl hexanoate + water and (f) methyl-heptanoate + water, at 1 bar and 278 (blue), 298 (turquoise), 308 (red), 318 (orange), 328 (violet), 338 (magenta), and 358 K (green).

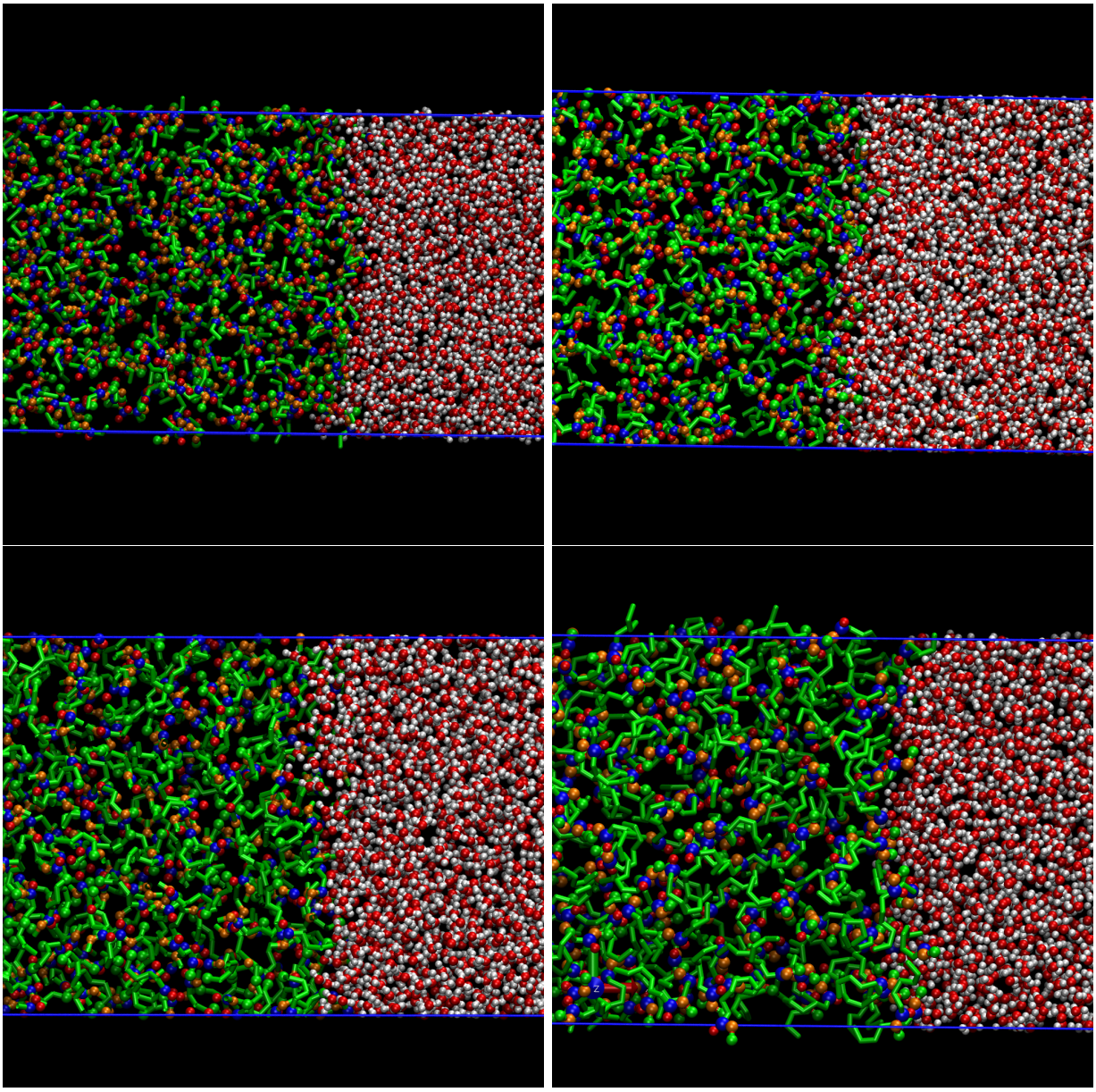

Figura 6.2: Snapshots of the LL interface obtained from MD $NP_z\mathcal{A}T$ simulations of the methyl butyrate + (top left), methyl valerate + (top right), methyl hexanoate + (bottom left), and methyl-heptanoate + water (bottom right) mixtures at 1 bar and 278 K. Green licorice representation corresponds to alkyl groups of methyl esters (CH3 and CH2 groups), orange, blue, and red spheres in the organic-rich liquid phase (van der Waals representation) correspond to the ester oxygen, carbonyl carbon, and carbonyl oxygen atoms of methyl esters, respectively, and red and white spheres (in the water-rich liquid phase) correspond to oxygen and hydrogen atoms in water molecules, respectively.

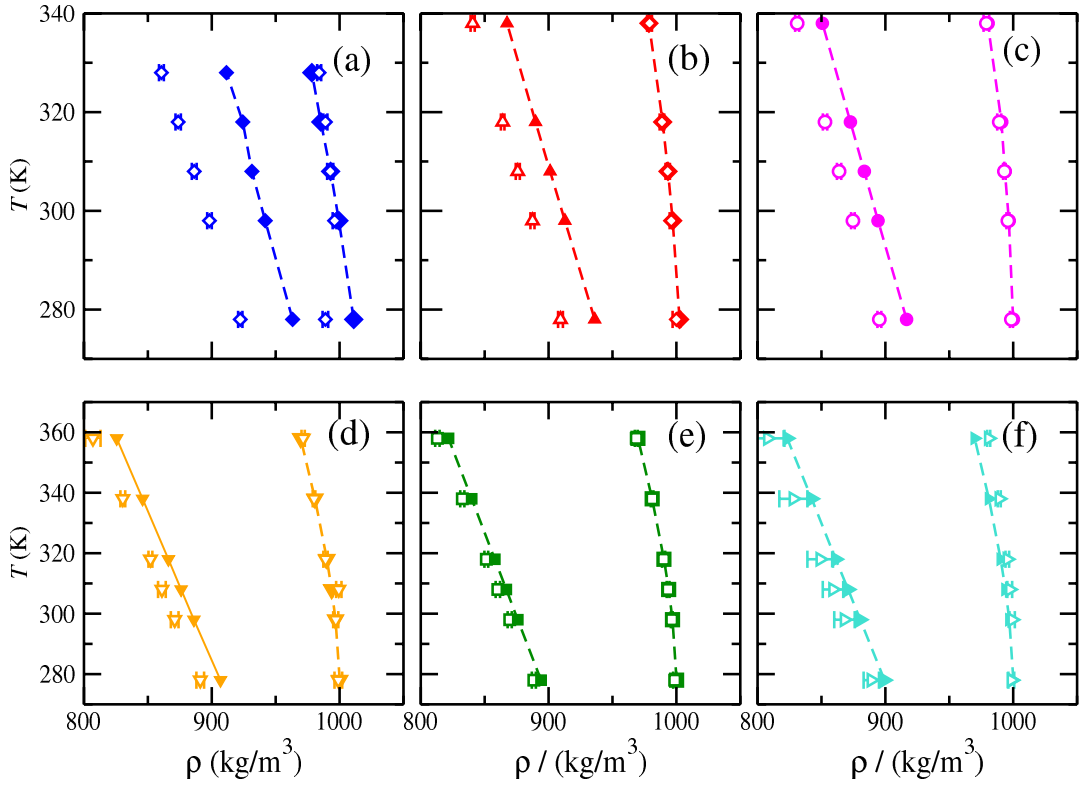

Figura 6.3: Tρ projection of the phase diagram of the (a) methyl-acetate + water (blue symbols), (b) methyl-propionate + water (red symbols), (c) methyl-butyrate + water (magenta symbols), (d) methyl-valerate + water (orange symbols), (e) methyl-hexanoate + water (green symbols) and (f) methyl-heptanoate + water (turquoise symbols) mixtures at 1 bar. Filled symbols and curves correspond to experimental data taken from the literature [8] and open symbols to MD $NP_z\mathcal{A}T$ simulation results obtained in this work.

of the alcohols increases. However, according to our results, methyl esters do not exhibit preferential orientation at the interface, even in the case of the methyl heptanoate + water mixture.

We have also calculated, but it is not shown here, the density profiles corresponding to the ester chemical group of the methyl ester molecules across the interface. These density profiles exhibit the same qualitative behaviour than density profile of methyl ester molecules presented in Fig. 6.1. The absence of preferential orientation at the interface described in the previous paragraph is also corroborate looking at the interface with the "eyes" of MD. Fig. 6.2 shows snapshots extracted from MD trajectories of the simulation of methyl butyrate +, methyl valerate +, methyl hexanoate +, and methyl heptanoate + water mixtures. As can been in all cases, there is no preferential orientation of the methyl esters molecules at the interface. It is useful to compare the snapshots presented in Fig. 6.2 with those corresponding to the first members of the alcohol + water homologous series, butan-1-ol +, pentan-1-ol +, hexan-1-ol +, and heptan-1-ol + water mixtures (see Fig. 2 of the work of Algaba *et al.* [52]).

We think the differences observed between the self-organization of alcohols and the non-preferential orientation of methyl ester across the interface are related with the different ability of alcohols and methyl esters forming hydrogen bonds with water and with the non-equivalent molecular architectures of both organic compounds. Linear 1-alcohols have a hydroxyl chemical group, –OH, that makes alcohols polar. This allows to form hydrogen bonds to another alcohol and to water molecules in aqueous solutions. Particularly, both oxygen and hydrogen atoms can be acceptor and donor atoms, respectively, for hydrogen bonding with water molecules. However, the configuration of oxygen atoms in the case of methyl esters is not as favorable as in the case of alcohols. Methyl esters do not have available hydrogen atoms to act as donor to form hydrogen bonds with water. In addition to that, the oxygen atom double-bonded to the carbon atom (carbonyl group), and especially the ester group (the oxygen bonded to the carbon of the carbonyl and methyl groups) are not particularly suited for hydrogen bonding. In other words, although these oxygen atoms could form hydrogen bonds with water molecules, the number of such bonds is small compared with the number of alcohol-water hydrogen bonds. Note that oxygen in methyl esters are not located at the end of the molecule, as in the case of the hydroxyl group in linear 1-alcohols. This also produces negative steric hindrance effects on hydrogen bonding. Finally, it is important to note that the alkyl chains of linear 1-alcohols promote the formation of ordered and packed layers at the water interface in aqueous solutions [52]. Contrary, the presence of the carbonyl groups in methyl esters produces difficulties to induce this packing, which is also prevented by the absence of a significant number of methyl ester-water hydrogen bonds at the interface.

From the information of the densities profiles of methyl esters and water is also possible to determine other interesting properties, including solubilities and coexistence densities. The coexistence densities can be calculated from the density profiles in the regions at which liquids are homogeneous, i.e., averaging the appropriate central homogeneous liquid slabs in each phase excluding the interfacial region. See the works of Algaba *et al.* [53, 54], Garrido *et al.* [31], and Mejía *et al.* [55] for further details. Coexistence densities of both phases as obtained from MD simulations are summarized in Table 6.5.

Fig. 6.3 shows the temperature-density or $T\rho$ projections of the phase diagram of aqueous solutions of methyl esters at atmospheric pressure. Liquid densities in both phases decrease as the temperature is increased. This behaviour is observed for the six mixtures considered. However, this trend is clearly marked in the case of the organic-rich liquid phase (left-side phase boundary in the figure) as compared

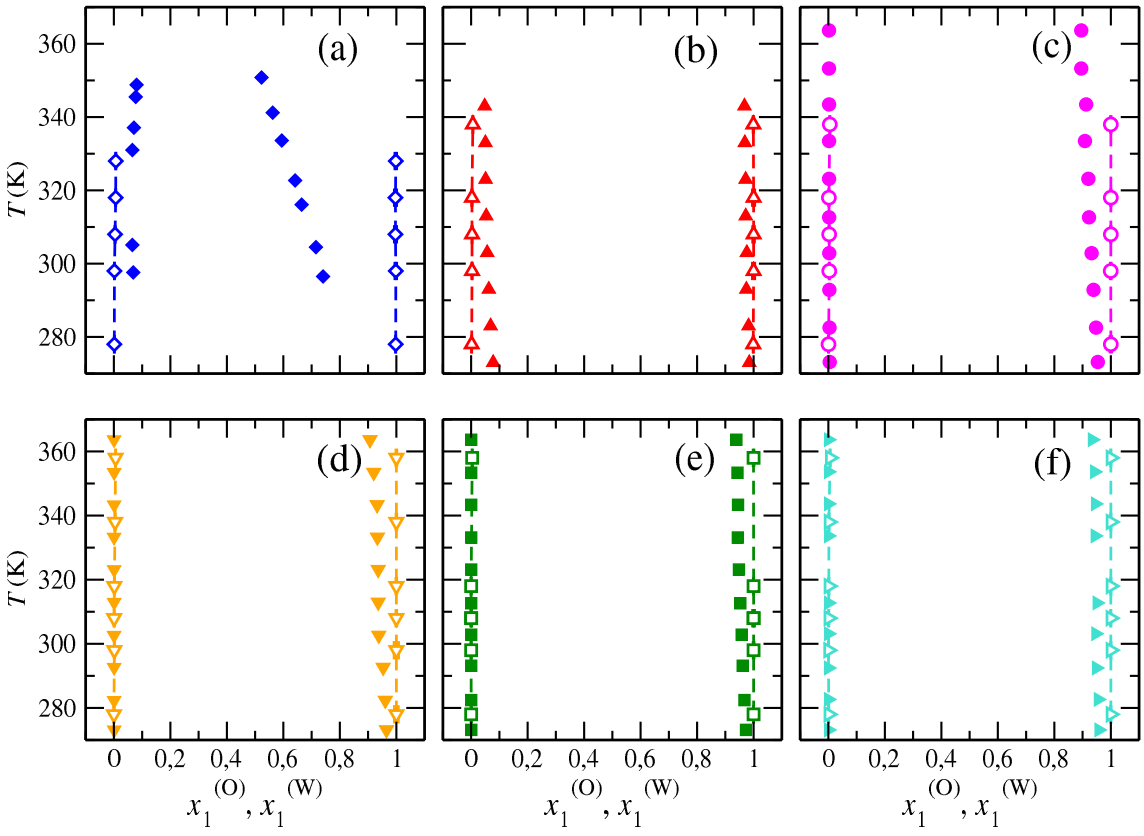

Figura 6.4: Tx projection of the phase diagram of the (a) methyl-acetate + water (blue symbols), (b) methyl-propionate + water (red symbols), (c) methyl- butyrate + water (magenta symbols), (d) methyl-valerate + water (or- ange symbols), (e) methyl-hexanoate + water (green symbols) and (f) methyl-heptanoate + water (turquoise symbols) mixtures at 1 bar. Filled symbols correspond to experimental data taken from the literature, [33–35] open symbols to MD $NP_z\mathcal{A}T$ simulations obtained in this work and dashed curves to the fitting of the experimental values. $x_1^{(O)}$ and $x_1^{(W)}$ are the molar fractions of methyl esters in the organic-rich and in the water-rich liquid phases, respectively.

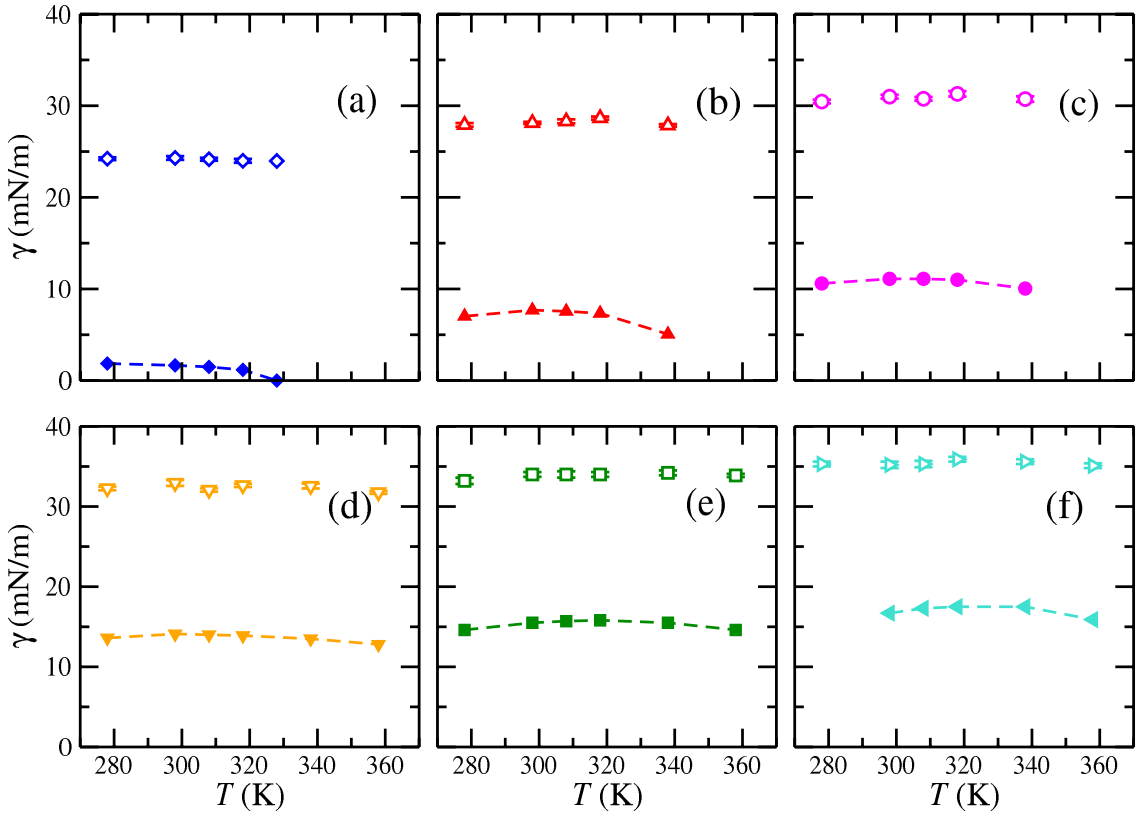

Figura 6.5: LL interfacial tension as a function of temperature of the (a) methyl acetate + water (blue symbols), (b) methyl propionate + water (red symbols), (c) methyl butyrate + water (magenta symbols), (d) methyl valerate + water (orange symbols), (e) methyl hexanoate + water (green symbols) and (f) methyl heptanoate + water (turquoise symbols) mixtures at 1 bar. Filled symbols correspond to experimental data taken from the literature, [8] open symbols to MD $NP_z\mathcal{A}T$ simulations obtained in this work, and dashed curves to the fitting of the experimental interfacial tension values to parabolic curves.

with the case of the aqueous phase. In that case, although liquid density also decreases, its value is nearly constant. It is also interesting to compare the evolution of the phase boundaries of the $T\rho$ projection of the phase diagram as the molecular weight of the methyl ester is increased from that of methyl-acetate up to methyl-heptanoate. As can be seen, the phase boundary corresponding to the water-rich liquid phase stays nearly unchanged in all the cases. Contrary, density values corresponding to the organic-rich phase decrease as the molecular weights of the esters increase. Predictions obtained from MD simulation are able to predict the experimental behaviour of the coexistence liquid densities with temperature and molecular weight presented by del Pozo and collaborators [8]. Particularly, liquid density of the water-rich phase is quantitatively described by the molecular models. However, predictions corresponding to the organic-rich liquid phase deserve a more detailed description. As can be seen, computer simulation results slightly underestimate the density for the mixtures with methyl acetate, methyl propionate, and methyl butyrate at all temperatures. Particularly, differences between simulation and experimental data are always bellow 5% (4.6% in the case of the mixture with methyl acetate). Nevertheless, simulations are able to account for quantitatively the experimental organic-rich liquid densities in the whole range of temperatures (deviations between experiments and simulation results are only equal to a 0.6% in the case of methyl heptanoate). The behaviour observed for coexistence liquid densities of aqueous solutions of methyl esters is very similar to that found for alcohol + water binary mixtures. This phenomenology can be easily explained in terms of three key ingredients: (1) unlike organic-water interactions; (2) solubilities of methyl esters in water; and (3) exclude volume effects. We recommend the reader the work of Algaba *et al.* [52] for further details.

As we have discussed previously, agreement between computer simulation predictions and experimental data taken from the literature for coexistence liquid densities is good except in the case of the mixtures containing the lighter methyl esters (methyl acetate, methyl propionate, and methyl butyrate). Molecular models used for water (TIP4P/2005) [22] and methyl esters (TraPPE) [15] are able to provide an accurate description of the vapour-liquid coexistence diagram of the real substances, including their interfacial properties, among many other thermodynamic and transport properties. According to our previous investigations [52], the main reason for discrepancies should be found in the use of the Lorentz-Berthelot combining rules for the unlike organic-water intermolecular interactions. Particularly, the largest differences between simulations and experiments occur when the molecular weight of the methyl esters is lower. According to results obtained in this work, in qualitative agreement with our previous work on alcohol + water mixtures, this happens since solubility of water in methyl-acetate, methyl-propionate, and methyl-butyrate is not as low as for heavier methyl esters. Consequently, there is an important number of unlike organic-water intermolecular interactions in the system not accounted for appropriately by the Lorentz-Berthelot combining rules. As the molecular weight of the organic compound increases, solubility of water in the organic-rich liquid phases decreases and the effective number of unlike interactions lowers. This improves the agreement between simulations and experiments. This behaviour is completely similar to what happens with aqueous solutions of alcohols modelled with the TIP4P/2005 model for water and TraPPE force fields for alcohols. We recommend the work of Algaba and collaborators [52] for a complete discussion of this issue.

We now consider the effect of temperature and molecular weight, at atmospheric pressure, of the organic compound on the temperature-composition or Tx projection of the phase diagram of aqueous solutions of methyl esters at atmospheric pressure. Fig. 6.4 shows the phase diagrams of the mixtures as obtained from MD simulations. As in the case of the $T\rho$ projections of the phase diagram, we have also included the corresponding experimental data taken from the literature. [33–35] This allows to assess if the molecular models for water (TIP4/2005) and methyl esters (TraPPE) are able to predict

accurately the LL composition of the mixtures. We have also included in Table 6.5 the molar fractions of the organic compounds in both liquid phases as obtained from MD simulations. As can be seen, the Tx projections of the mixtures are dominated by huge regions of LL immiscibility, for all the systems studied and at all the temperatures considered. According to our previous discussion, this behaviour is due to large unfavourable organic-water intermolecular interactions in the system. It is interesting to note that solubilities are practically constant as the temperature is increased in all cases. The only exception is the case of the the methyl acetate + water mixture in which solubilities increase, especially the solubility of water in the organic-rich liquid phase, as temperature is increased.

Molecular models for water and methyl esters are able to provide a good description of the composition of the mixtures in all cases, except for the methyl acetate + water system. Agreement between experimental data taken from the literature and predictions obtained from MD simulations is reasonably accurate, although simulations predict wider LL immiscibility regions in all cases. Particularly, results from MD simulations slightly overestimate the molar fractions of the methyl esters in the organic-rich liquid phase. Contrary, simulations are able to provide an accurate and quantitative agreement with experimental molar fractions of the methyl esters in the water-rich liquid phase. However, they slightly overestimate the molar fractions of the methyl propionate in the organic phase. In the case of the methyl acetate + water mixture, discrepancies between experiments and predictions from the MD simulations are larger, particularly in the case of the molar fraction of the methyl acetate in the organic-rich liquid phase. The reason of this lack of agreement is probably due to the presence of unlike interactions between methyl esters and water molecules that are not accounted for correctly using the standard Lorentz-Berthelot combining rules.

Finally, we analyze the ability of the TIP4P/2005 and TraPPE molecular models for predicting LL interfacial tensions of aqueous solutions of methyl esters. Results obtained from MD simulations are presented in Table 6.5 and Fig. 6.5. In addition to that, we have also included LL interfacial tensions measured in the laboratory [8] to check if models are able to describe the characteristic behaviour of the LL interfacial tension, as a function of temperature, for the systems considered. As can be seen, computer simulation are able to describe the parabolic behavior exhibited by the LL interfacial tension with the temperature of all methyl ester + water binary mixtures. Additionally, predictions from MD simulations capture the existence of a relative maximum value for the interfacial tension in each system, larger values of interfacial tension as the carbon chain length of methyl esters is increased, and the reduction of differences of interfacial tension, at constant temperature, as the molecular weight of methyl esters increases. Unfortunately, experimental values of interfacial tension are substantially overestimated by simulation predictions for all systems at all thermodynamic conditions. According to this, the accurate prediction of LL interfacial tensions for these type of systems continues being a computational challenge. In fact, Algaba *et al.* [52] have demonstrated that is not possible to predict accurately the anomalous behavior of LL interfacial tensions for alcohols (from pentan-1-ol up to heptan-1-ol) + water mixtures. Interfacial tension is a extremely sensitive property to the molecular and simulation details, such as the cutoff radius, box size, and number of particles, among others. Additionally, it was observed that MD simulations underestimate the density of the organic phase of the mixture, which impact the final value of the interfacial tension due to an underestimation of the organic density generate an over-prediction of the interfacial tension (i.e., $\gamma \propto \left(\rho^{(w)} - \rho^{(0)}\right)^4$)

Although the mixture model exhibits limitations for the quantitative prediction of this property, this is the first time the LL phase equilibria and interfacial tensions of methyl ester + water binary mixtures are determined from computer simulation. This work represents a first step to gain an understanding of the microscopic structure of LL interfaces from a molecular-based perspective.

6.6 Conclusions

We have determined the LL phase equilibria and interfacial properties of the methyl ester (from methyl acetate up to methyl heptanoate) + water binary mixtures at atmospheric pressure and temperatures from 278 to 358 K using MD molecular simulations. In particular, we combine isothermal-isobaric or $NP_z\mathcal{A}T$ simulations, the direct coexistence simulation technique and the well-known molecular models for water (TIP4P/2005) and methyl esters (TraPPE-UA).

We firstly analyze the density profiles of water and methyl esters molecules across the LL interface as a function of temperature for all methyl ester + water binary mixtures considered. Density profiles of water exhibit a monotonic behaviour when passing from one liquid phase to the other. Contrary, density profiles of methyl esters exhibit relative maxima, indicating an increasing preferential adsorption at the interface as the molecular weight of the organic compound increases. This phenomenon is less marked as the temperature is increased in all of cases due the thermal agitation. Contrary to what happens with other similar systems that exhibit LL immiscibility, as linear alcohol + water binary mixtures, do not observe preferential orientation of methyl esters perpendicular to the interface. In fact, the molecules do not show the formation of monolayers or bilayers or organic molecules as in the case of alcohols in aqueous solutions. This is probably due to the inability of methyl esters to form hydrogen bonds with water molecules.

From the information of density profiles of water and methyl esters, we determine the temperature-density, $T\rho$, and temperature-composition, Tx, projections of the phase diagram at atmospheric pressure. MD simulations show, with the molecular parameters of pure components and without any further adjustment, that mixtures exhibit large regions of LL immiscibility in all cases. Particularly, molecular models are able to provide a very good description of both phase envelopes, except for the methyl acetate + water system. In this case, simulations predict a wider phase separation, in densities and compositions, compared with experimental data taken from the literature. In the rest of mixtures, simulations predict accurate values of coexistence densities and compositions for the mixtures in the whole range of temperatures considered.

Finally, we consider the LL interfacial tension of the mixtures at atmospheric pressure. In particular, we use the virial route to calculate the normal and tangential components of the pressure tensor. Molecular models are able to predict the characteristic parabolic shape of the interfacial tension as a function of temperature. They also capture the existence of a relative maximum value for each system at a temperature that increases as the molecular weight of the organic molecule is increased. Unfortunately, experimental values of interfacial tension are substantially overestimated by our predictions in all cases. This is probably since unlike interactions between organic molecules and water are not accounted properly. Although TIP4P/2005 and TraPPE models exhibit limitations for predicting in a quantitative manner the experimental data, they are able to capture an important number of issues characteristics of these complex binary mixtures.

Conflicts of interest

The authors declare that they have no known competing financial interests or personal relationships that could have appeared to influence the work reported in this paper.

Acknowledgements

This work was financed by Spanish Ministerio de Economía, Industria y Competitividad (Grant No. FIS2017-89361-C3-1-P), Junta de Andalucía (Grant No. P20-00363), both co-financed by EU FEDER funds, and Universidad de Huelva. We also acknowledge the Centro de Supercomputación de Galicia (CESGA, Santiago de Compostela, Spain) for providing access to computing facilities. AM acknowledges funding from Fondecyt (Chile) through Grant 1190107.

Bibliography

[1] R. Luque, C. S. K. Lin, K. Wilson, and J. Clark, *Handbook of Biofuels Production*. Woodhead Pub. 2ed, 2016.

[2] P. P. Peralta-Yahya, F. Zhang, S. B. del Cardayre, and J. D. Keasling, "Microbial engineering for the production of advanced biofuels," *Nature*, vol. 488, pp. 320–328, 2012.

[3] D. Bolonio, M.-J. García-Martínez, M. Ortega, M. Lapuerta, J. Rodríguez-Fernández, and L. Canoira, "Fatty acid ethyl esters (faees) obtained from grapeseed oil: a fully renewable biofuel," *Renew. Energy*, vol. 132, pp. 278–283, 2019.

[4] R. M. Ceballos, *Bioethanol and Natural Resources: Substrates, Chem. & Eng. Systems.* CRC Press, 2017.

[5] N. D. D. Carareto, C. Y. C. S. Kimura, E. C. Oliveira, M. C. Costa, and A. J. A. Meirelles, "Flash points of mixtures containing ethyl esters or ethylic biodiesel and etanol," *Fuel*, vol. 96, pp. 319–326, 2012.

[6] T. J. Bruno, T. M. Loestead, J. R. Riggs, E. L. Jorgenson, and M. L. Huber, "Comparison of diesel fuel oxygenate additives to the composition-explicit distillation curve method. part 1: Linear compounds with one to three oxygens," *Energy Fuels*, vol. 25, pp. 2493–2507, 2011.

[7] A. T. Gros and R. O. Feuge, "Surface and interfacial tensions, viscosities, and other physical properties of some n-aliphatic acids and their methyl and ethyl esters," *J. Am. Oil Chem. Soc.*, vol. 29, pp. 313–317, 1952.

[8] I. del Pozo, M. Cartes, F. Llovell, and A. Mejía, "Densities and interfacial tensions for fatty acid methyl esters (from methyl formate to methyl heptanoate) + water demixed mixtures at atmospheric pressure conditions," *J. Chem. Thermodynamics*, vol. 121, pp. 121–128, 2018.

[9] S. Enders and K. Quitzsch, "Calculation of interfacial properties of demixed fluids using density gradient theory," *Langmuir*, vol. 14, p. 4606–4614, 1998.

[10] H. Renon and J. M. Prausnitz, "Local Compositions in Thermodynamic Excess Functions for Liquid Mixtures," *AIChE Journal.*, vol. 14, pp. 135–144, 1968.

[11] A. Mączyński, B-Wiśniewska-Goclowska, and A. Jezierski, "Iupac-nist solubility data series. 88. esters with water—revised and updated. part 1. c_2 to c_4 to esters," *J. Phys. Chem. Ref. Data*, vol. 38, pp. 1093–1127, 2009.

[12] A. Mejía. Personal communication.

[13] R. L. Scott and P. H. V. Konynenburg, "Static properties of solutions. van der waals and related models for hydrocarbon mixtures," *Discuss. Faraday Soc.*, vol. 49, pp. 87–97, 1970.

[14] P. H. V. Konynenburg and R. L. Scott, "Critical lines and phase equilibria in binary van der waals mixtures," *Phil. Trans.*, vol. A298, pp. 495–540, 1980.

[15] E. Feria, J. Algaba, J. M. Míguez, A. Mejía, P. Gómez-Álvarez, and F. J. Blas, "Vapour–liquid phase equilibria and interfacial properties of fatty acid methyl esters from molecular dynamics simulations," *Phys. Chem. Chem. Phys.*, vol. 22, pp. 4974–4983, 2020.

[16] G. M. Martin and J. I. Siepmann, "Transferable potentials for phase equilibria. 1. united-atom description of n-alkanes," *J. Phys. Chem. B*, vol. 102, pp. 2569–2577, 2001.

[17] B. Chen, J. J. Potoff, and J. I. Siepmann, "Monte carlo calculations for alcohols and their mixtures with alkanes. transferable potentials for phase equilibria. 5. united-atom description of primary, secondary, and tertiary alcohols," *J. Phys. Chem. B*, vol. 105, pp. 3093–3104, 2001.

[18] G. Kamath, J. Robinson, and J. J. Potoff, "Application of trappe-ua force field for determination of vapor–liquid equilibria of carboxylate esters," *Fluid Phase Equil.*, vol. 240, pp. 46–55, 2006.

[19] J. J. Potoff and J. I. Siepmann, "Vapor-liquid equilibria of mixtures containing alkanes, carbon dioxide, and nitrogen," *AIChE Journal.*, vol. 47, pp. 1676–1682, 2001.

[20] G. Kamath, F. Cao, and J. J. Potoff, "An improved force field for the prediction of the vapor-liquid equilibria for carboxylic acids," *J. Phys. Chem. B*, vol. 108, pp. 14130–14136, 2004.

[21] J. Stubbs, J. J. Potoff, and J. I. Siepmann, "Transferable potentials for phase equilibria. 6. united-atom description for ethers, glycols, ketones, and aldehydes," *J. Phys. Chem. B*, vol. 108, pp. 17596–17605, 2004.

[22] J. L. Abascal and C. Vega, "A general purpose model for the condensed phases of water: Tip4p/2005," *J. Chem. Phys.*, vol. 123, pp. 234505–1–234505–12, 2005.

[23] "http://chem-siepmann.oit.umn.edu/siepmann/trappe/index.html, (retrieved november, 2019)."

[24] H. J. C. Berendsen, J. R. Grigera, and T. P. Straatsma *J. Chem. Phys.*, vol. 91, pp. 6269–71, 1987.

[25] W. L. Jorgensen, J. Chandrasekhar, J. Madura, R. W. Impey, and M. Klein *J. Chem. Phys.*, vol. 79, no. 2, pp. 926–35, 1983.

[26] M. W. Mahoney and W. L. Jorgensen, "A five-site model for liquid water and the reproduction of the density anomaly by rigid, nonpolarizable potential functions," *J. Chem. Phys.*, vol. 112, p. 8910–8922, 2000.

[27] H. W. Horn, W. C. Swope, J. W. Pitera, J. D. Madura, T. J. Dick, G. L. Hura, and T. Head-Gordon *J. Chem. Phys.*, vol. 120, no. 20, pp. 9665–78, 2004.

[28] J. M. Míguez, D. González-Salgado, J. L. Legido, and M. M. Piñeiro, "Calculation of interfacial properties using molecular simulation with the reaction field method: Results for different water models," *J. Chem. Phys.*, vol. 132, pp. 184102–1–184102–5, 2010.

[29] C. Vega and E. D. Miguel, "Surface tension of the most popular models of water by using the test-area simulation method," *J. Chem. Phys.*, vol. 126, pp. 154707–1–154707–10, 2007.

[30] C. Miqueu, J. M. Míguez, M. M. Piñeiro, T. Lafitte, and B. Mendiboure, "Simultaneous application of the gradient theory and monte carlo molecular simulation for the investigation of methane/water interfacial properties," *J. Phys. Chem. B*, vol. 115(31), pp. 9618–9625, 2011.

[31] J. M. Garrido, H. Quinteros-Lama, M. M. J, F. J. Blas, and M. M. Piñeiro, "On the physical insight into the barotropic effect in the interfacial behavior for the $h_2o + co_2$ mixture," *J. Phys. Chem. C*, vol. 123, pp. 28123–28130, 2019.

[32] J. M. Míguez, J. M. Garrido, F. J. Blas, H. Segura, A. Mejía, and M. M. Piñeiro, "Comprehensive characterization of interfacial behavior for the mixture $co_2 + h_2o + ch_4$: Comparison between atomistic and coarse grained molecular simulation models and density gradient theory," *J. Phys. Chem. C*, vol. 118, pp. 24504–24519, 2014.

[33] J. Rayman. PhD thesis, University of Budapest, 1906.

[34] A. Skrzecz, "Mutual solubility of water and n-alkyl acetates," *Pol. J. Chem.*, vol. 54, pp. 1101–1104, 1980.

[35] R. Stephenson and J. Stuart, "Mutual binary solubilities: Water - alcohols and water - esters," *J. Chem. Eng. Data*, vol. 31, pp. 56–70, 1986.

[36] D. van der Spoel, E. Lindahl, B. Hess, G. Groenhof, A. E. Mark, and H. J. Berendsen, "Gromacs: Fast, flexible, and free," *J. Comput. Chem.*, vol. 26, no. 16, pp. 1701–1718, 2005.

[37] M. A. Cuendet and W. F. V. Gunsteren, "On the calculation of velocity-dependent properties in molecular dynamics simulations using the leapfrog integration algorithm," *J. Chem. Phys.*, vol. 127, pp. 184102–1–184102–9, 2007.

[38] S. Nosé, "A molecular dynamics method for simulations in the canonical ensemble," *Mol. Phys.*, vol. 52, pp. 255–268, 1984.

[39] W. G. Hoover, "Canonical dynamics: Equilibrium phase-space distributions," *Phys. Rev. A*, vol. 31, pp. 1695–1697, 1985.

[40] M. Parrinello and A. Rahman, "Polymorphic transitions in single crystals: A new molecular dynamics method," *J. Appl. Phys.*, vol. 52, pp. 7182–7190, 1981.

[41] G. Galliero, M. M. Piñeiro, B. Mendiboure, C. Miqueu, T. Lafitte, and D. Bessieres, "Interfacial properties of the mie n-6 fluid: Molecular simulations and gradient theory results," *J. Chem. Phys.*, vol. 130, pp. 104704–1–104704–10, 2009.

[42] G. Galliero, "Surface tension of short flexible lennard-jones chains: Corresponding states behavior," *J. Chem. Phys.*, vol. 133, pp. 074705/1–074705–7, 2010.

[43] J. M. Míguez, M. M. Piñeiro, and F. J. Blas, "Influence of the long-range corrections on the interfacial properties of molecular models using monte carlo simulation," *J. Chem. Phys.*, vol. 138, pp. 034707–1–034707–11, 2013.

[44] L.-J. Chen *J. Chem. Phys.*, vol. 103, pp. 10214–10216, 1995.

[45] M. González-Melchor, P. Orea, J. López-Lemus, F. Bresme, and J. Alejandre, "Stress anisotropy induced by periodic boundary conditions," *J. Chem. Phys.*, vol. 122, pp. 094503–1–094503–8, 2005.

[46] J. Janeček, "Effect of the interfacial area on the equilibrium properties of lennard-jones fluid," *J. Chem. Phys.*, vol. 131, pp. 124513–1–124513–9, 2009.

[47] U. Essmann, L. Perera, M. L. Berkowitz, T. Darden, H. Lee, and L. G. Pedersen, "A smooth particle mesh ewald method," *J. Chem. Phys.*, vol. 103, pp. 8577–8593, 1995.

[48] H. J. C. Berendsen, J. P. M. Postma, W. F. V. Gunsteren, A. D. Nola, and J. R. Haak, "Molecular dynamics with coupling to an external bath," *J. Chem. Phys.*, vol. 81, pp. 3684–1–3684–8, 1984.

[49] H. Hulshof, "Ueber die oberflachenspannung," *Ann. Phys. (Berlin)*, vol. 4, pp. 165–186, 1901.

[50] E. A. Müller, A. Ervik, and A. Mejía, "A guide to computing interfacial properties of fluids from molecular simulations," *Living J. Comp. Mol. Sci.*, vol. 2, pp. 21385–1–21385–27, 2021.

[51] T. Lafitte, B. Mendiboure, M. M. Piñeiro, D. Bessieres, and C. Miqueu, "Interfacial properties of water/co_2: a comprehensive description through a gradient theory-saft-vr mie approach," *J. Phys. Chem. B*, vol. 114, pp. 11110–11116, 2010.

[52] J. Algaba, J. M. Míiguez, Gómez-Álvarez, A. Mejía, and F. J. Blas, "Vapour–liquid phase equilibria and interfacial properties of fatty acid methyl esters from molecular dynamics simulations," *J. Phys. Chem. B*, vol. 124, pp. 8388–8401, 2020.

[53] J. Algaba, J. M. Garrido, J. M. Míguez, A. Mejía, A. I. M.-V. Bravo, and F. J. Blas, "Interfacial properties of tetrahydrofurane and carbon dioxide mixture from computer simulation," *J. Phys. Chem. C*, vol. 122, pp. 16142–16153, 2018.

[54] J. Algaba, M. Cartes, A. Mejía, J. M. Míguez, and F. J. Blas, "Phase equilibria and interfacial properties of the tetrahydrofuran + methane binary mixture from experiment and computer simulation," *J. Phys. Chem. C*, vol. 123, pp. 20960–20970, 2019.

[55] A. Mejía, M. Cartes, G. Chaparro, E. Feria, F. J. Blas, J. M. Míguez, J. Algaba, and E. A. Müller, "Phase equilibria and interfacial properties of selected methane + n-alkane binary mixtures," *J. Mol. Liq.*, vol. 431, pp. 116918–1–116918–13, 2021.

Capítulo 7

Resumen y Conclusiones

El objetivo de este trabajo es el estudio del equilibrio de fase y las propiedades interfaciales de mezclas binarias compuestas por substancias de interés industrial mediante simulación molecular. Para llevar a cabo todas las simulaciones se ha utilizado una combinación de técnicas de dinámica molecular utilizando el programa GROMACS (versión 4.6.5) y la metodología de coexistencia directa, que permite simular explícitamente la coexistencia entre dos fases en equilibrio termodinámico, y por tanto, determinar las propiedades interfaciales de los sistemas bajo estudio, incluyendo energías libres interfaciales.

En primer lugar se han considerado mezclas de alcanos, de diferente peso molecular, con metano. Para esta primera parte, se han utilizado modelos simplificados en los que las diferentes unidades monoméricas empleadas son sitios tipo *coarse-grained*, que permiten predecir el comportamiento real de mezclas con gran precisión. Esto es posible debido a la propia naturaleza de los modelos simplificados, que permiten simular un menor número de unidades monoméricas sin perder calidad en las predicciones obtenidas. La principal razón para estudiar mezclas de alcanos desde esta perspectiva es que permite poner a punto las técnicas de dinámica molecular necesarias para llevar a cabo las simulaciones haciendo uso de la técnica de coexistencia directa.

Una vez que se adquiere la experiencia necesaria, con el consiguiente éxito en la descripción del comportamiento de fase e interfacial de mezclas de alcanos lineales con metano, se ha procedido al modelado y estudio mediante técnicas similares de modelos moleculares más realistas. En particular, se ha abordado el estudio de disoluciones acuosas de ésteres metílicos, compuestos orgánicos formados por cadenas de hidrocarburos cuasi lineales de gran importancia energética y medioambiental. Como paso previo al estudio de las mezclas con agua, se han seleccionado y modelado ésteres puros aprovechando los modelos TraPPE-UA propuestos por Siepmann y colaboradores. En particular, la elección de modelos ha seguido la filosofía del uso de parámetros transferibles, es decir, utilizar parámetros moleculares de otros compuestos para modelar los ésteres metílicos sin necesidad de llevar a cabo ningún ajuste con resultados experimentales. De este modo, los resultados obtenidos para compuestos puros son predicciones puras obtenidas mediante la combinación inteligente de parámetros moleculares tomados de la literatura y el uso de la simulación molecular.

Una vez comprobado que los modelos propuestos permiten predecir el equilibrio de fase y las

propiedades interfaciales de ésteres metílicos puros, en excelente acuerdo con datos experimentales tomados de la literatura, se ha procedido a extender el estudio de las propiedades termodinámicas, con especial énfasis en las propiedades interfaciales de disoluciones acuosas de ésteres metílicos. Al igual que en el caso del estudio llevado a cabo con los compuestos puros, se hace uso extensivo de la transferibilidad de los parámetros moleculares y modelos para la descripción de sus mezclas con agua. En este caso, el agua se ha modelado utilizando posiblemente el mejor modelo rígido no polarizable que existe en la bibliografía, el modelo TIP4P/2005 propuesto originalmente por el grupo del Prof. Carlos Vega de la Universidad Complutense de Madrid. Al igual que en el caso de los sistemas puros, se han comparado las predicciones obtenidas mediante simulación con datos experimentales tomados de la literatura.

Para finalizar este preámbulo, conviene destacar que todos los resultados obtenidos durante el trabajo de tesis doctoral han sido publicados en distintas revistas internacionales situadas todas ellas en el primer cuartil (Q1) del campo correspondiente. Seguidamente se resumen las principales conclusiones obtenidas en las diferentes partes de la tesis.

- En el **Capítulo 4** se ha estudiado el equilibrio de fase y el comportamiento interfacial de mezclas binarias metano + n-alcano (n-decano, n-dodecano, n-tetradecano y n-hexadecano) en un amplio rango de presiones, desde los 0.1 hasta los 30 MPa a 334.15 K. Para el estudio mediante simulación molecular, llevado a cabo en GROMACS, se han empleado modelos *coarse-grained* en los que las unidades monoméricas que forman las cadenas moleculares y el metano interaccionan a través de un potencial de interacción de Mie. También se ha obtenido el equilibrio de fase de las mezclas utilizado la versión de potencial variable (*Variable Range*) Mie dentro del contexto de la Teoría Estadística de Fluidos Asociantes o SAFT (del inglés *Statistical Associating Fluid Theory*), conocida en la literatura como SAFT-VR Mie. Además, se ha combinado con el formalismo de la Teoría del Gradiente o SGT (del inglés *Square Gradient Theory*) para predecir el comportamiento interfacial de las mezclas a través de una ruta teórica alternativa. No obstante, conviene destacar que esta tesis se ha centrado fundamentalmente en la obtención del comportamiento termodinámico de los sistemas mediante simulación molecular. Finalmente, el estudio se ha completado con la determinación experimental del equilibrio de fase y las propiedades interfaciales de las mismas mezclas en la laboratorio del Prof. Mejía en la Universidad de Concepción (Chile). En particular, para la determinación de todas las propiedades se han utilizados diferentes equipos, densímetros para la determinación de densidades de las fases involucradas y tensiómetros para la mediación de tensiones interfaciales líquido-vapor de las mezclas metano + n-alcano.

  El estudio ha arrojado un importante número de conclusiones relevantes que permiten explicar el comportamiento macroscópico obtenido en el laboratorio a través de las prediciones teóricas y las obtenidas mediante dinámica molecular. Uno de los principales resultados obtenidos es el comportamiento de la tensión interfacial líquido-vapor de todos los sistemas, que disminuye monotónicamente a medida que aumenta la presión del sistema o disminuye el peso molecular del n-alcano de la mezcla. También se ha constatado un aumento de la densidad de la fase vapor (rica en metano) y una disminución de la densidad de la fase líquida (rica en alcano), como es de esperar ya que las mezclas presentan comportamiento crítico a altas presiones. Haciendo uso de una de las características más relevantes de la simulación molecular mediante la técnica de la coexistencia directa, se ha investigado el comportamiento de la densidad de cada uno de los componentes de las mezclas a lo largo de la interfase, o dicho de otro modo, el comportamiento de los perfiles de la densidad de los alcanos y el metano. Se ha observado, en acuerdo con las predicciones independientes de las teoría del gradiente y SAFT-VR Mie, una importante

actividad en la interfase líquido-vapor de todos los sistemas. En particular, se ha observado una adsorción preferencial del componente más volátil de la mezcla (metano) en la interfase, que se hace más importante a medida que el peso molecular del n-alcano aumenta. También se observa, para una mezcla dada, una tendencia similar cuando la presión del sistema aumenta. Este comportamiento no es monotónico, sino que existe un valor máximo de la presión a partir del cual la adsorción se vuelve una función decreciente con la presión, es decir, existe una saturación en la adsorción del metano en la interfase. Este comportamiento se ha cuantificado determinando las correspondientes isotermas de adsorción relativa de Gibbs en todos los casos. Al igual que en el resto de propiedades, las predicciones de las simulaciones están en excelente acuerdo con los resultados proporcionados por la teoría SAFT-VR Mie + SGT, y lo que es más importante, con los resultados experimentales obtenidos en el laboratorio. No obstante, se aprecian diferencias entre los resultados de las simulaciones y las predicciones teóricas debido a la propia naturaleza de la teoría empleada. Aunque la ecuación de estado SAFT-VR Mie es muy precisa, continúa siendo una ecuación analítica, y desde la perspectiva del comportamiento crítico de estos sistemas, una ecuación clásica que no predice correctamente el comportamiento del sistema en las proximidades del punto crítico. Sería preciso un tratamiento no clásico, que involucraría el uso de teorías del grupo de renormalización, que se encuentra fuera de los objetivos planteados en esta tesis doctoral.

- En el **Capítulo 5**, una vez que se han puesto a punto todas las técnicas necesarias para la determinación de propiedades de equilibrio de fase e interfaciales mediante la técnica de la coexistencia directa en modelo sencillos, se ha hecho uso de ellas para predecir el comportamiento interfacial de sustancias más complejas desde el punto de vista molecular. Como paso previo, se ha determinado el equilibrio de fase y las propiedades interfaciales de ésteres metílicos de bajo peso molecular, desde el metil acetato hasta el metil heptanoato. Para ello, se ha utilizado el banco de parámetros transferibles propuestos por Siempann y su grupo de investigación, conocidos genéricamente como modelos TraPPE-UA. Estos parámetros se pueden utilizar de manera transferible, esto es, sin ajustes adicionales, para describir otras moléculas que contienen los mismos grupos químicos funcionales. Esta forma de proceder, que permite predecir el comportamiento de compuestos moleculares más complejos, se puede entender como una contribución de grupos termodinámica a nivel molecular. Antes de realizar las correspondientes simulaciones, se ha realizado un estudio exhaustivo de los parámetros disponibles para hacer la mejor elección posible. De este modo, los modelos propuestos de ésteres metílicos son capaces de predecir de la forma más precisa, no solo el equilibrio de fase líquido-vapor sino también sus propiedades interfaciales más relevantes. En particular, se ha hecho uso de parámetros para describir alcanos, alcoholes primarios, ácidos carboxílicos y dióxido de carbono, entre otros para la definición de todas las interacciones moleculares entre ésteres metílicos. Como en el capítulo anterior, se ha hecho uso del programa de simulación GROMACS para resolver las ecuaciones de la dinámica molecular, una vez definido el modelo a utilizar. De acuerdo a la regla de las fases de Gibbs, dado que es preciso similar la coexistencia entre dos fases de un compuesto puro, se han llevado a cabo las simulaciones en el colectivo canónico o NVT.

  El estudio llevado a cabo en este capítulo ha permitido obtener una valiosa información que permite describir el comportamiento microscópico de la interfase líquido-vapor de ésteres metílicos puros en función de la temperatura. Al igual que en el capítulo anterior, las predicciones obtenidas se han comparado con datos experimentales tomados de la literatura para verificar la bondad de los modelos propuestos. Para cada sistema molecular, se ha obtenido el comportamiento de

los perfiles de la densidad, así como un importante número de propiedades termodinámicas de equilibrio, incluyendo las densidades de coexistencia en las fases líquido y vapor, las presiones de vapor, entalpías y entropías interfaciales, en función de la temperatura. A partir de esta información, se ha analizado cómo varían la densidad y temperatura crítica de los ésteres metílicos a medida que aumenta el peso molecular de los mismos. Atención especial merece el comportamiento de la tensión interfacial líquido-vapor de los ésteres metílicos, como función de la temperatura y del peso molecular de los mismos. Aunque la tensión superficial se puede medir experimentalmente en la mayoría de sistemas, a temperaturas superiores a los 360 K los ésteres metílicos se vuelven térmicamente inestables y se producen microburbujas en los densímetros y tensiómetros utilizados para su determinación. En la práctica, esto provoca la imposibilidad de medir con la precisión deseada esta propiedad a altas temperaturas. Y es precisamente en estas condiciones en las que la simulación molecular juega un papel esencial en la predicción del comportamiento termodinámico e interfacial de sistemas complejos. Dado que la inestabilidad térmica no se produce durante las simulaciones, es posible extender el estudio a temperaturas arbitrarias. Si, como sucede en este caso, los modelos son capaces de predecir el comportamiento a bajas temperaturas, es posible predecir valores de tensiones interfaciales a altas temperaturas con suficiente confianza. Este es precisamente el escenario que se produjo durante este trabajo. Por ello, las predicciones obtenidas para el comportamiento de la tensión interfacial líquido-vapor de estos compuestos son relevantes, siendo este el primer trabajo publicado en la literatura que predice este comportamiento para estos sistemas. Estos resultados son aun más valiosos si se tiene en cuenta que han sido obtenidos a partir de parámetros moleculares optimizados para otras moléculas diferentes y sin llevar a cabo ningún ajuste de ningún tipo, lo que pone de manifiesto el poder predictivo del uso conjunto de modelos moleculares y la simulación molecular.

- En el **Capítulo 6**, una vez que en la sección previa se han elegido los modelos adecuados para describir las principales características de los ésteres metílicos puros, con especial énfasis en el equilibrio de fase y muy particularmente en las propiedades interfaciales, se presentan los resultados obtenidos para el estudio de sus disoluciones acuosas. Para ello, como se ha mencionado al comienzo de estas conclusiones, se hace uso del modelo de agua rígido no polarizable más utilizado hoy en día, el modelo TIP4P/2005. De acuerdo a la filosofía seguida a lo largo de todo el estudio doctoral, se hace uso de las reglas de Lorentz-Berthelot para describir las interacciones cruzadas en las mezclas éster metílico + agua. Esto permite obtener el comportamiento de estos sistemas sin necesidad de ajustes adicionales con datos experimentales tomados de la literatura. En particular, se ha determinado el comportamiento de las mezclas homólogas desde metil acetato + hasta metil heptanoato + agua, a presión atmosférica y un rango de temperaturas comprendido entre los 278 y 358 K. Para ser consistente con la regla de las fases de Gibbs para sistemas formados por componentes que exhiben coexistencia entre dos fases, se han llevado a cabo simulaciones de dinámica molecular mediante el método de coexistencia directa a través del colectivo isotérmico-isobárico o NPT.

  Los resultados más notables obtenidos en este estudio comprenden, en primer lugar, el análisis de la variación de la densidad de cada uno de los compuestos de las mezclas éster metílicos + agua a través de la interfase líquido-líquido (perfiles de la densidad), en función de la temperatura para cada una de las mezclas consideradas. Se ha observado que los perfiles asociados a los ésteres metílicos exhiben adsorción selectiva importante a medida que disminuye la temperatura. Este comportamiento solo se observa para mezclas que contienen ésteres metílicos de alto peso molecular. Asociado a los máximos relativos en los perfiles de la densidad, también se observan

mínimos relativos a medida que nos alejamos de la interfase. En contraposición a lo que ocurre en el caso de disoluciones acuosas de alcoholes lineales primarios, los perfiles de la densidad del agua muestran un comportamiento crecimiento monótono al pasar de la fase orgánica a la acuosa. Este comportamiento está directamente relacionado con el hecho de que no se observa ordenación preferencial de las moléculas de ésteres metílicos en la interfase, a diferencia de lo que ocurre con mezclas de alcoholes de alto peso molecular con agua, debido a que los ésteres metílicos son incapaces formar puentes de hidrógeno con el agua. Esto contrasta claramente con la arquitectura más favorable para este tipo de interacciones específicas en el caso de los alcoholes lineales primarios, que les permite incluso formar bicapas moleculares con una orientación preferencial a lo largo de la interfase (perpendicular a la misma) y una organización compleja a su alrededor. Se ha determinado además las densidades y composiciones de coexistencia para todas las mezclas consideradas, en función de la temperatura (diagramas temperatura-densidad y temperatura-composición, a presión constante). Los resultados de simulación confirman, en acuerdo con la información experimental disponible en la literatura, que estas disoluciones exhiben grandes regiones de inmiscibilidad líquido-líquido en todos los casos. En particular, los modelos moleculares predicen con excelente acuerdo con los datos experimentales los diagramas de coexistencia temperatura-densidad y temperatura-composición, a excepción del metil acetato. Las simulaciones indican que los modelos para la disolución acuosas de metil acetato predicen una separación de fase mayor que la experimental, tanto para densidades como composiciones. Este resultado posiblemente se deba a que las interacciones cruzadas, predichas a través de las reglas de Lorentz-Berthelot, no son descritas con la precisión deseadas. Finalmente, ha sido posible determinar las tensiones interfaciales, a presión atmosférica, de todos los sistemas estudiados. Los modelos propuestos permiten predecir, sin necesidad de ningún ajuste, la forma parabólica de la tensión interfacial en función de la temperatura, observándose el máximo exhibido por los datos experimentales. En particular, los modelos son capaces de predecir, al menos cualitativamente, del aumento del valor máximo de la tensión interfacial a medida que el peso molecular del componente orgánico aumenta. Desafortunadamente, las predicciones obtenidas mediante simulación sobrestiman los valores experimentales en todos los casos. Esto se debe probablemente a que la interacción entre las distintas moléculas no se ha tenido en cuenta correctamente a través de las reglas de Lorentz-Berthelot. Un intento de mejorar las predicciones obtenidas podría ser posible tratando de mejorar las reglas de mezclas, aunque esto se encuentra fuera de los objetivos planteados de esta tesis doctoral. No obstante, merece la pena mencionar que este trabajo constituye el primer estudio llevado a cabo por simulación para determinar el comportamiento interfacial de disoluciones acuosas de ésteres metílicos.

Parte IV

Anexo: Trabajos Publicados Derivados de la Tesis Doctoral

Phase equilibria and interfacial properties of selected methane + n-alkane binary mixtures

Autores/as: A. Mejía, M. Cartes, G. Chaparro, E. Feria, J. M. Míguez, J. Algaba y F. J. Blas

Publicado en: Journal of Molecular Liquids, 116918 (2021).

DOI: 10.1016/j.molliq.2021.116918

Factor de impacto de la revista en el año de publicación: 6.165

Rank: 4/37, en Physics/Atomic/Molecular & Chemical (Q1)

Journal of Molecular Liquids 341 (2021) 116918

Contents lists available at ScienceDirect

Journal of Molecular Liquids

journal homepage: www.elsevier.com/locate/molliq

Phase equilibria and interfacial properties of selected methane + n-alkane binary mixtures

Andrés Mejía [a,*], Marcela Cartes [a], Gustavo Chaparro [a], Esther Feria [b], Felipe J. Blas [b], José Manuel Míguez [b], Jesús Algaba [c], Erich A. Müller [c]

[a] Departamento de Ingeniería Química, Universidad de Concepción, Concepción, Chile
[b] Laboratorio de Simulación Molecular y Química Computacional, CIQSO-Centro de Investigación en Química Sostenible and Departamento de Ciencias Integradas, Universidad de Huelva, 21007 Huelva, Spain
[c] Department of Chemical Engineering, Imperial College London, South Kensington Campus, London SW7 2AZ, UK

ARTICLE INFO

Article history:
Received 7 April 2021
Revised 26 June 2021
Accepted 1 July 2021
Available online 5 July 2021

Keywords:
Methane + n-alkane binary mixtures
Tensiometry
Interfacial properties

ABSTRACT

Experimental determination, theoretical modeling, and molecular simulation have been combined to describe the bulk phase equilibria (*i.e.*, pressure, liquid, and vapor saturated mass densities) and interfacial properties (*i.e.*, interfacial concentration, adsorption, and interfacial tension) for methane + n-decane, n-dodecane, n-tetradecane and n-hexadecane binary mixtures at 344.15 K and in a pressure range between 0.1 and 30 MPa. Experimental determinations are carried out using a combined apparatus that includes a high-pressure vibrating tube densimeter and a high-pressure pendant drop tensiometer. The theoretical approach is based on the van der Waals gradient theory coupled to the Statistical Associating Fluid Theory of Variable Range employing a Mie potential (SAFT-VR-Mie) equation of state, where the fluids are described as Coarse Grained (CG) atoms. Molecular dynamics simulation for the same systems based on the CG Mie potential are reported. The three approaches are able to indepen independently predict phase equilibrium and interfacial properties, showing a very good agreement amongst themselves. For the systems and conditions studied here, the vapor mass density increases; the liquid mass density and interfacial tensions decrease as the pressure increases, and with a fixed temperature and pressure, the liquid mass density and interfacial tensions increase as the n-alkane molecular chain length increases. It is observed that methane is adsorbed along the interfacial region, whereas the n-alkanes (n-decane, n-dodecane, n-tetradecane, n-hexadecane) do not exhibit surface activity. The relative Gibbs adsorption of methane increases significantly with pressure until it reaches a maximum denoting the adsorption saturation limit. It is also observed that the adsorption of methane only slightly increases with the chain length of the n-alkane.

1. Introduction

The phase and interfacial behavior of n-alkane mixtures have received continuous attention in applied thermodynamics. Their description and accurate prediction are key in the petroleum and oil refining industries, gas condensate recovery, liquefaction of natural gas, oil transportation, and recently have become relevant within the context of environmental control.[1] Particularly interesting are the asymmetric mixtures of methane with alkanes of high molecular weight that display a fascinating but complex behavior. They exhibit large departures from ideality, mainly caused by the differences in the molecular size of the components of the mixture, and also show several types of phase and interfacial behavior. Specifically, methane + n-alkane up to n-pentane mixtures are completely miscible in the liquid phase (with only vapor–liquid equilibria, VLE), and are described as Type I in the van Konynenburg and Scott classification.[2] From methane + n-hexane onwards, the phase behavior is complemented by the appearance of three-fluid phase line (*i.e.*, vapor-liquid–liquid equilibria, VLLE) near to the critical point of methane. This VLLE causes that the VLE critical line be separated into two branches: one of them initiates at the critical point of methane ascending up to the upper critical end point (UCEP) of the VLLE, and the second one from the lower critical end point (LCEP) of the VLLE with a maximum in the pressure up to the critical point of n-hexane. For the case of methane + n-heptane mixture, the VLLE is interrupted by another three-phase line: solid n-heptane + L+V (SLVE).

* Corresponding author.
E-mail address: amejia@udec.cl (A. Mejía).

https://doi.org/10.1016/j.molliq.2021.116918
0167-7322/

Vapour-liquid phase equilibria and interfacial properties of fatty acid methyl esters from molecular dynamics simulations

Autores/as: E. Feria, J. Algaba, J. M. Míguez, A. Mejía, P. Gómez-Álvarez y F. J. Blas

Publicado en: Physical Chemistry Chemical Physics, 22(9), 4974-4983 (2020)

DOI: DOI 10.1039/C9CP06397H

Factor de impacto de la revista en el año de publicación: 3.676

Rank: 8/37, en Physics/Atomic/Molecular & Chemical (Q1)

PCCP

ROYAL SOCIETY OF CHEMISTRY

PAPER

Cite this: *Phys. Chem. Chem. Phys.*, 2020, **22**, 4974

Vapour–liquid phase equilibria and interfacial properties of fatty acid methyl esters from molecular dynamics simulations

Esther Feria,[a] Jesús Algaba,[a] José Manuel Míguez,[a] Andrés Mejía,[b] Paula Gómez-Álvarez[a] and Felipe J. Blas *[a]

Received 26th November 2019,
Accepted 8th February 2020

DOI: 10.1039/c9cp06397h

rsc.li/pccp

We have determined the phase equilibria and interfacial properties of a methyl ester homologous series (from methyl acetate to methyl heptanoate) using direct simulations of the vapour–liquid interfaces. The methyl esters are modelled using the united atom approach in combination with transferable parameters for phase equilibria (TraPPE) force fields for alkanes, alkenes, carbon dioxide, ethers, and carboxylic acids in a transferable way. This allows us to take into account explicitly both dispersive and coulombic interactions, as well as the repulsive Pauli-exclusion interactions. Simulations are performed in the *NVT* or canonical ensemble using molecular dynamics. Vapour–liquid surface tension is determined using the virial route, *i.e.*, evaluating the normal and tangential components of the pressure tensor along the simulation box. We have also calculated density profiles, coexistence densities, vapour pressures, surface entropies and enthalpies, and interfacial thickness as functions of temperature, as well as the normal boiling temperatures and the critical temperatures, densities, and pressures for each member of the series. Special attention is paid to the comparison between experimental data taken from the literature and our results obtained using molecular dynamics simulations. We also analyze the effect of increasing the molecular weight of the methyl esters (at fixed temperature) on all the properties considered, with special emphasis on phase equilibria envelopes and surface tension. The TraPPE force fields transferred from other molecules and chemical families are able to predict very accurately the experimental vapour–liquid phase envelopes of methyl esters. We also compare the results obtained from simulations of the surface tension, with experimental data taken from the literature. To our knowledge, this is the first time that vapour–liquid phase equilibria and interfacial properties, and particularly surface tension, of this methyl ester homologous series are obtained using computer simulation.

1 Introduction

Current environmental regulations and energy directives recommend and promote an increase, of at least 10%, the use of renewable fuels for transport by 2020, and also to dramatically reduce the transportation emission levels by 2030.[1] These initiatives have been motivated to reduce greenhouse gas emissions, where transportation contributes 34% of the total emissions. One of the most ground-breaking alternatives to accomplish these targets is to replace (partially or totally) fossil-fuels with biofuels (fuels produced from natural renewable sources), where one of the most recently emerging biofuels is biodiesel. Biodiesels are considered to be the third (or fourth) generation of biofuels[2] as they are renewable, biodegradable, non-toxic, produce less carbon dioxide than fossil fuels, and also they can replace petroleum diesel and be used either in their neat form or blended with fossil diesel inside of compression ignition engines without any extensive engine modification. In general terms, biodiesel can be obtained from a group of mono-alkyl esters[3] that, depending on the alcohol (methanol or ethanol) used for the transesterification process, become fatty acid methyl esters (FAMEs) or fatty acid ethyl esters (FAEEs), respectively. From a technical viewpoint, the use of FAMEs as a fuel is more developed than FAEEs[4,5] for efficient use.

Despite the novel use of FAMEs as diesel fuel, systematic research concerning the characterization of interfacial properties (*e.g.*, the interfacial concentration of species, the interfacial thickness, the superficial enthalpy and entropy, and surface or interfacial tension) of pure FAMEs and mixtures containing FAMEs is very limited. For the case of pure short chain FAMEs

[a] *Laboratorio de Simulación Molecular y Química Computacional, CIQSO-Centro de Investigación en Química Sostenible and Departamento de Ciencias Integradas, Universidad de Huelva, 21007 Huelva, Spain. E-mail: felipe@uhu.es*
[b] *Departamento de Ingeniería Química, Universidad de Concepción, POB 160-C Concepción, Chile*

Molecular dynamics of liquid–liquid equilibrium and interfacial properties of aqueous solutions of methyl esters

Autores/as: E. Feria, J. Algaba, J. M. Míguez, A. Mejía y F. J. Blas

Publicado en: Physical Chemistry Chemical Physics, 24, 5371-5382 (2022)

DOI: DOI: 10.1039/D1CP05346A

Factor de impacto de la revista en el año de publicación: 3.676

Rank: 8/37, en Physics/Atomic/Molecular & Chemical (Q1)

PCCP

ROYAL SOCIETY OF CHEMISTRY

PAPER

View Article Online
View Journal

Cite this: DOI: 10.1039/d1cp05346a

Molecular dynamics of liquid–liquid equilibrium and interfacial properties of aqueous solutions of methyl esters

Esther Feria,[a] Jesús Algaba,[b] José Manuel Míguez,[a] Andrés Mejía[c] and Felipe J. Blas *[a]

Received 22nd November 2021,
Accepted 3rd February 2022

DOI: 10.1039/d1cp05346a

rsc.li/pccp

In this work, the liquid–liquid phase equilibria and interfacial properties of methyl ester + water binary mixtures are determined at atmospheric pressure and from 278 to 358 K combining the direct coexistence technique and molecular dynamics simulations. Methyl esters are modelled using new parametrizations based on the united atom TraPPE model force field proposed recently by us [E. Feria, J. Algaba, J. M. Míguez, A. Mejía, P. Gómez-Álvarez and F. J. Blas, *Phys. Chem. Chem. Phys.*, 2019, **22**, 4974–4983] that are able to predict the vapour–liquid interfacial properties of pure methyl esters with high accuracy. In the case of water, we consider the well-known TIP4P/2005 model, the most popular rigid and non-polarizable model to describe the interfacial properties of pure water. The simulations are performed using the direct coexistence technique in the isothermal–isobaric or NP_zAT ensemble in combination with molecular dynamics. We obtain density profiles, temperature–densities and temperature–composition projections of the phase diagrams, and interfacial tensions. The liquid–liquid interfacial tension is calculated from the normal and tangential components of the pressure tensor according to the mechanical virial route. We pay attention particularly to the ability of the molecular models in predicting the experimental behavior of the systems. Simulation results are able to account for the liquid–liquid phase equilibria of these binary mixtures, in good agreement with the experimental data taken from the literature. Unfortunately, experimental values for interfacial tensions are substantially overestimated by predictions from computer simulations in all cases. To our knowledge, this is the first time that the liquid–liquid phase equilibrium and interfacial properties of methyl ester + water mixtures have been predicted from computer simulations.

1 Introduction

Biodiesel is considered a clean, renewable, and eco-friendly alternative to reduce the use and production of diesel from fossil fuel sources. The main advantages are that biodiesel can be used as a liquid fuel in diesel engines without any extensive modification, and it can be used in pure form or blended with petroleum diesel in any percentage, where the most common blend is 20% biodiesel and 80% petroleum diesel. Biodiesel can be produced by reacting an alcohol (or bioalcohol) with a group of mono-alkyl esters, which are obtained from vegetable oil, animal fat, or recycled cooking grease. Depending on the alcohol (methanol or ethanol) used in the transesterification reaction route, it is possible to obtain Fatty Acid Methyl Esters (FAMEs) or Fatty Acid Ethyl Esters (FAEEs), respectively.[1,2,3] Both FAMEs and FAEEs are good substitutes for petroleum-based diesel, moreover, FAEEs are more ecosystemic and renewable than FAMEs as ethanol can also be obtained from a renewable source (*e.g.* food crops, waste vegetables, algae, fruits, root vegetables, wood waste, cellulose, forest waste, *etc.*).[1,2,4]

Unfortunately, the production of biodiesel based on FAEEs has not yet been sufficiently developed for efficient use.[5] On the other hand, the production and technical use of FAMEs are mature techniques but the evaluation of its environmental impact is limited as the thermophysical properties needed to describe the phase and interfacial behavior of FAMEs in contact with water are undetermined, especially in the case of interfacial properties. Interfacial properties, such as interfacial tension, surface activity, and wettability of these aqueous mixtures at liquid–liquid (LL) equilibrium, are key properties

[a] *Laboratorio de Simulación Molecular y Química Computacional, CIQSO-Centro de Investigación en Química Sostenible and Departamento de Ciencias Integradas, Universidad de Huelva, Huelva 21007, Spain. E-mail: felipe@uhu.es*
[b] *Department of Chemical Engineering, Imperial College London, South Kensington Campus, London SW7 2AZ, UK*
[c] *Laboratorio de Cohesión, Departamento de Ingeniería Química, Universidad de Concepcion, POB 160-C, Correo 3, Chile*